Optimal Phasor Measurement Unit Placement for Enhancement of Static and Dynamic Security Assessment in Power Systems

Optimal Phasor Measurement Unit Placement for Enhancement of Static and Dynamic Security Assessment in Power Systems

電力系統の静的および動的セキュリティ評価増強のための
同期位相計測装置の最適配置

Yoshiaki Matsukawa

ACADEMIC DISSERTATION
A dissertation presented for the degree of Doctor of Engineering

Department of Engineering
Graduate School of Engineering
Kyushu Institute of Technology
Japan

March 2020

電力系統の静的および動的セキュリティ評価増強のための同期位相計測装置の最適配置

松川　義明

（学生番号：17595501）

指導教員　渡邊政幸　准教授

博士学位論文

九州工業大学　工学府　工学専攻　電気電子工学領域

2020 年　3 月

Yoshiaki Matsukawa
Kyushu Institute of Technology
Department of Engineering
Tobata, Kitakyushu Fukuoka, Japan
p349532y@mail.kyutech.jp

THE DOCTORAL DISSERTATION SUPERVISOR AND CHAIR OF DOCTORAL DISSERTATION APPROVAL COMMITTEE:

Masayuki Watanabe, Dr. Eng.
Associate Professor, Department of Electrical and Electronic Engineering
Faculty of Engineering, Kyushu Institute of Technology
Tobata, Kitakyushu, Fukuoka, Japan

THE MEMBERS OF DOCTORAL DISSERTATION APPROVAL COMMITTEE:

Yasunori Mitani, Dr. Eng.
Professor, Department of Electrical and Electronic Engineering
Faculty of Engineering, Kyushu Institute of Technology
Tobata, Kitakyushu, Fukuoka, Japan

Tsuyoshi Hanamoto, Dr. Eng.
Professor, Department of Biological Functions Engineering
Graduate School of Life Science and Systems Engineering, Kyushu Institute of Technology
Wakamatsu, Kitakyushu, Fukuoka, Japan

Mochimitsu Komori, Dr. Eng.
Professor, Department of Electrical and Electronic Engineering
Faculty of Engineering, Kyushu Institute of Technology
Tobata, Kitakyushu, Fukuoka, Japan

The committees have examined the dissertation entitled “Optimal Phasor Measurement Unit Placement for Enhancement of Static and Dynamic Security Assessment in Power Systems” presented by Yoshiaki Matsukawa, a candidate for the degree of Doctor of Engineering and hereby certify that it is worthy of acceptance.

Preface

Loss of electricity by the whole or major part of power system blackout triggers interruption of use of electric appliances, internet disconnection, traffic interruption. In power systems, the state are changing by many reasons such as load increment, line switching, disturbances and so on, and it could be moved toward the stability boundary. Recent power system state tends to be easily changed and be hardly understood due to a huge penetration of Renewable Energy Sources (RESs). Preventive/corrective security control actions are performed to avoid the blackout and make the system state far away from the boundary. However, if the pre-stage security assessment cannot be accurately performed, the following security actions may be misconducted.

Concerning above situations, Phasor Measurement Unit (PMU) has been installed on power systems to provide very accurate information including voltage/current phasor measurements, which are able to execute State Estimation (SE) accurately. SE is the first step of understanding the system state which gives the whole power system state to the security assessment input. However, PMU is expensive device so that the optimal number and placement in power systems should be considered not to affect the system planning cost.

On consideration of optimal PMU placement, several issues lie down in power systems. PMU cost: increasing the number of placed PMUs makes the power system planning cost suffered, thus minimization of PMU cost is required. SE accuracy: particularly assessing estimation error of SE for the static security assessment which is affected by the power flow condition and measurement propagation is necessary because the recent system is pretty uncertain and unpredictable. Static security assessment using estimated state vector: because almost all PMU placement researchers ignores how SE error affects the static security assessment, the relationship between PMU placement and latter actual security assessment should be investigated. Dynamic security: in power system security control, not only static security but also dynamic security is important. Thus, optimal PMU placement considering both of static and dynamic security is keenly required. This research work includes approaches to solving all above issue in terms of placing PMUs optimally. Chapters will be unfolded one by one to solve each issue in order to finally propose the optimal PMU placement method considering PMU device cost, static/dynamic security assessment.

In Chapter 4, Multi Objective Optimal PMU Placement (MOOPP) problem considering minimization of PMU device cost with the PMU current channel selection and maximization of SE accuracy through different power flow scenarios named CCS-MOOPP is proposed. By solving CCS-MOOPP, cost-effective Pareto solutions are obtained which can mitigate the impact on the system planning cost by eliminating redundant current channels. In Chapter 5, measurement uncertainty propagation in the PMU pseudo measurement is considered by classical uncertainty propagation theory. It is implemented in the OPP problem: named CCS-MOOPP/U.

By solving this problem as well as Chapter 4, the realistic SE error assessment is achieved. Inclusion of consideration of measurement uncertainty propagation in PMU pseudo measurement not to degrade the merit of installation of PMUs is proved to be eventually effective. In Chapter 6, considering the voltage security assessment using estimates obtained by SE through optimally placed PMUs, Critical Boundary Index (CBI) is calculated as a static voltage security index. Investigation on the single load increment test showed that a mixed measurement situation makes CBI calculation error bigger. For optimally obtained PMU placements, discarding of PMU estimated value is suggested not to degrade the merit of PMUs. By those analysis, this chapter bridges between OPP and actual static security assessment. Chapter 7 extends OPP's target to Dynamic Vulnerability Assessment (DVA). This chapter's proposals include the novel clustering method for the fast coherent area partition, OPP for DVA and MOOPP considering both of static and dynamic security assessment. Firstly, a novel clustering algorithm is proposed to partition a power systems into the number of fast coherent areas for DVA. Secondly, OPP problem for DVA named OPP-DVA is proposed. OPP-DVA places PMUs to cover as many areas as possible to estimate DVA index. As the final form of MOOPP problem in this research work, CCS-MOOPP/U-S&D considering PMU device cost minimization, static SE accuracy maximization and DVA enhancement, which is possible to consider both regions of security assessment. To sum up all results of works, this research thesis can contribute to enhance static and dynamic security assessment accuracy by optimally placing PMUs considering PMU placement cost based on maximization of merit of PMUs, in terms of avoiding power system blackouts.

Acknowledgements

Much of outcomes, information and insight presented in this dissertation were achieved through a long time research and study conducted by the author on power system engineering over the last 9 years in Hiroshima Institute of Technology (2011-2015) and Kyushu Institute of Technology (2015-2020).

This dissertation would not have been possible without the support of so many people during the author's study. First and foremost, the author wishes to extend the sincerest and the biggest gratitude to his supervisor, Assoc. Prof. Dr. Masayuki Watanabe who is very helpful, patient and enthusiastically offered invaluable assistance, support and guidance. Without his knowledge and guidance, this research would not have been successful. The author also expresses his deep gratitude to Prof. Dr. Yasunori Mitani, Prof. Dr. Tsuyoshi Hanamoto and Prof. Dr. Mochimitsu Komori who served as his supervisory committee members, for their continuous support, guidance and comments, during the period of his study. The author extends many thanks and appreciation to Assoc. Prof. Ir. Dr. Mohammad Lutfi Othman (Universiti Putra Malaysia, Malaysia) for partial supervision, innovative ideas and supports and Assoc. Prof. Ir. Dr. Noor Izzri Abdul Wahab (Universiti Putra Malaysia, Malaysia) for his technical advice and innovative ideas. The author also wants to thank Dr. Thongchart Kerdphol (Kyushu Institute of Technology) for technical guidance, fruitful discussions and cooperative research works. The author also wants to thank Mr. Hibiki Takahashi and Mr. Yoshihide Nakamura (Kyushu Institute of Technology) as laboratory members for spending invaluable study period together, sharing research ideas and several cooperative research works in the laboratory. Also, the author represents a big gratitude to laboratory secretaries Mrs. Miki Tokumori and Mrs. Aiko Toyoshima for managing paperwork and supporting the laboratory members. The author also expresses his gratitude to Assoc. Prof. Mr. Nicholas James Kemp (Kyushu International University) for proofreading the author's articles.

It is pleasure to acknowledge the scholarships the author received during PhD program: Power Academy research grant for PhD student.

The author would like to express his heartfelt thanks and appreciation to all of his colleagues, students and staffs at Kyushu Institute of Technology as well as the great nation of Japan. Finally, the author offers his deepest personal gratitude to his wife, parents and family for the strength that keeps him standing and believing that this research would be possible, more interest and successful.

Yoshiaki Matsukawa

March 2020

Contents

List of Figures

List of Tables

List of Acronyms

AAP	Adaptive Affinity Propagation
AI	Artificial Intelligence
ANN	Artificial Neural Network
BCS	Best Compromised Solution
BESS	Battery Energy Storage System
BILP	Binary Integer Linear Programming
BOI	Bus Observability Index
BPSO	Binary Particle Swarm Optimization
BS	Bisecting Search
CB	Circuit Breaker
CBI	Critical Boundary Index
CCS-MOOPP	Current Channel Selectable Multi Objective Optimal PMU Placement
CCS-MOOPP/U	Current Channel Selectable Multi Objective Optimal PMU Placement based on Uncertainty propagation
CCS-MOOPP/U-S&D	Current Channel Selectable Multi Objective Optimal PMU Placement based on Uncertainty propagation considering Static and Dynamic security assessment
CI	Computational Intelligence
CMDS	Classical Multi-Dimensional Scaling
COI	Center-Of-Inertia
CR	Cover Rate
CT	Current Transformer
CWT	Continuance Wavelet Transform
DOE	Department Of Energy
DPSO	Discrete Particle Swarm Optimization
DVA	Dynamic Vulnerability Assessment
DWT	Discrete Wavelet Transform
EA	Evolutionary Algorithm

FCM	Fuzzy *C*-Means
FFT	Fast Fourier Transform
FVSI	Fast Voltage Stability Index
GA	Genetic Algorithm
GIS	Geographic Information System
GPS	Global Positioning System
HC	Hierarchical Clustering
HSE	Hybrid State Estimation
HVDC	High Voltage Direct Current
ICT	Internet and Communication Technology
IEC	International Electrotechnical Commission
IEEE	Institute of Electrical and Electronics Engineers
ILP	Integer Linear Programming
ISO	Independent System Operator
KCL	Kirchhoff's Current Law
LCPI	Line Collapse Proximity Index
LMI	Liner Matrix Inequalities
MCS	Monte Carlo Simulation
MISO	Midwest Independent System Operator
MOEA/D	Multi Objective Evolutionary Algorithm on Decomposition
MOOPP	Multi Objective Optimal PMU Placement
MOPSO	Multi Objective Particle Swarm Optimization
NASPI	North America Synchro-Phasor Initiative
NE	New England
NERC	North American Electric Reliability Council
NHC	Non-Hierarchical Clustering
NSGA-II	Non-dominated Sorting Genetic Algorithm-II
OLTC	On Load Tap Changers
OPF	Optimal Power Flow
OPP	Optimal PMU Placement
OPP-DVA	Optimal PMU Placement for Dynamic Vulnerability Assessment

PCA	Principle Component Analysis
PDC	Phasor Data Concentrator
PDM	Power Dynamic Management
PMU	Phasor Measurement Unit
PSE	Phasor State Estimation
PSO	Particle Swarm Optimization
PSS	Power System Stabilizer
PT	Potential Transformer
RES	Renewable Energy Source
RNI	Ratio of Non-dominated Individuals
RNN	Recurrent Neural Network
RTU	Remote Terminal Unit
SA	Simulated Annealing
SAIDI	System Average Interruption Duration Index
SAIFI	System Average Interruption Frequency Index
SC	Subtractive Clustering
SCADA	Supervisory Control And Data Acquisition
SE	State Estimation
SI	Swarm Intelligence
SORI	System Observability Redundancy Index
SPCS	Synchro-Phasor Communication System
SPEA	Strength Pareto Evolutionary Algorithm
SPS	Special Protection Scheme
SVC	Static Var Compensator
TCSC	Thyristor Controlled Series Compensator
TEP	Transmission Expansion Planning
TS	Tabu Search
TSO	Transmission System Operator
TVE	Total Vector Error
UC	Unit Commitment
UCTE	Union for the Coordination of Transmission of Electricity

UPQC	Unified Power Quality Control
VCPI	Voltage Collapse Proximity Index
VLSI	Voltage Stability Load Index
VSI	Voltage Stability Index
WADC	Wide Area Damping Controller
WAMPAC	Wide Area Monitoring, Protection And Control
WAMS	Wide Area Measurement System
WASI	Wide Area Severity Index
WLS	Weighted Least Square
WSCC	Western System Coordinating Council
ZIB	Zero Injection Bus

1 Introduction

1.1 BACKGROUND AND MOTIVATION

Since power systems have been established and become larger to enhance the reliability and the economic performance by inter-connection, there have been always concern about the cascading blackout. In the history of power systems, there have been some instances of power blackout so far. The USA-Canada power system widespread blackout of August 2003 is one of the most notorious blackout event among them, eventually impacted the economics with a net loss about USD 6 billion by power supply loss about 61,800 MW [1]. This cascading event has begun in misunderstanding of the power system state by no update of State Estimation (SE) of Midwest Independent System Operator (MISO) as the reliability coordinator. In this time, the power system analyst turned off the automatic SE and the control, and updated the state manually, hence the several events such as generator or transmission line outage occurred after that were not recognized by the system operator. Finally these events resulted in the widespread blackout by the chain reaction collapse. This big event reminds us of importance of the power system monitoring and correct understanding of the state for avoiding the cascaded blackouts.

Recently, the power system state has been getting more uncertain, unpredictable and vulnerable because of a huge penetration of Renewable Energy Source (RES) which outputs unstable power generation and the electricity market deregulation that coexisting many player can sell electric power resulting in more congested transmission line with irregular power flow variation. These facts indicate that the power system in recent are threatened to fall easily into the blackout compared to the previous simple system, the importance of power system monitoring has been getting more significant.

On the other hand, nowadays, because of the significantly developed Internet and Communication Technology (ICT), the Wide Area Measurement System (WAMS) with Phasor Measurement Unit (PMU) by its fast and large data communication and transmission has become the promising technology for accurate and constant monitoring of the power system [2]. PMU is the key apparatus in WAMS which is able to measure the voltage and current phasor data synchronized by Global Positioning System (GPS). Measurement of the phase angle by GPS time synchronization enables to determine the phase reference of the measured sinusoidal voltage signal at distant measuring points. Before the PMU has been installed in power systems in 1980's, collection of measurement data such as active power, reactive power, voltage magnitude and frequency has been conducted by traditional measurements called Remote Terminal Unit (RTU) in monitoring system based on Supervisory Control And Data Acquisition (SCADA). At that time, the concept of synchrophasor measurement was proposed [3], however, it had not been realized as a form of PMU since GPS was not really developed. In 1993, the official use of GPS has been declared and the concept of PMU was introduced by

Phadke et al. [4]. Thereafter, PMUs have been introduced in power systems in some countries such as USA, Europe, China and so on, with applications to SE, adaptive relay, oscillation control [5].

Since the PMUs have been installed in power systems, there have been many contributions by research articles, and many issues have been discussed by researchers in universities, electric makers and utilities. Among them, SE supported by PMU is one of the most important issues. SE that assigns a value to unknown system state variable (voltage phasor of power system bus) based on measurements including an error from the meters is very important for system state understanding and online modeling [6]. Conventionally, SE has been executed using measured data obtained by RTU, which is solving the nonlinear measurement equation mostly by Weighed Least Square (WLS) to obtain state vector. This method takes several iterations and the accuracy is not really good. However, by applying PMU to SE, state vector can be obtained by solving the linear measurement equation with pretty much higher accuracy since it is directly solvable by the direct observation of voltage phasor amount by PMU [7]. In order to monitor a power system for avoiding cascading blackout by preventive/corrective security control actions, accurate understanding of the system state by SE using measurement data obtained by PMU is indispensable in recent power systems.

In 1986, Phadke et al. has established the concept of Phasor State Estimation (PSE) which only uses PMU data as the measurement vector. However, the PMU cost was not concerned in the article [7]. The average overall costs per unit of typical PMU installed at transmission level substation range between USD 40,000 and USD 180,000 including the costs of procurement, installation, and commissioning [8]. For only the device, it is reported that a PMU itself is about USD 20,000 and a current measurement channel cost is about USD 3,000 as of 2016 [9]. These facts indicate that it is impossible to place PMUs to all buses if the number of system buses gets bigger, in perspective of realistic power system operation and planning. Therefore, the Optimal PMU Placement (OPP) problem has been discussed for over a couple of decades, begun in the article by Baldwin et al. [10]. In general definition of OPP is a problem to find the set of PMUs placed with a minimum number while it satisfies arbitrarily equality/inequality constraints. Normally, in order to carry out PSE, the feasible set of PMU placements needs to make the system observable (numerical/topological observability, explained in Chapter 3). In OPP, once PMU is placed at a bus, the adjacent buses become observable (pseudo measurements). In accordance with the pseudo measurements and observability constraint, the OPP problem which minimizes the number of PMUs by covering the power system observability given as a combinatorial optimization problem, has been proven as the Non-deterministic Polynomial time (NP) complete class problem by polynomial-time reduction from the planar 3-satisfiability problem [11]. In these days, there are a lot of research articles about OPP problem because of its significance, even some review and taxonomy papers have been published [12-14]. In such circumstance, OPP for SE is quite trending topic in power system studies.

1.2 RESEARCH OBJECTIVE AND CONTRIBUTIONS

This book designs the novel OPP formulation and solving it by a metaheuristic optimization method. In recent studies of OPP problem, maximization of SE reliability for PMU observation network, enhancement of SE accuracy, the PMU current channel allocation have been required while the number of placed PMUs is minimized. Minimization of the number of PMUs is generally basic concept of OPP established by Baldwin et al. [10], in addition, enhancement of the robustness of PMU observation network or the actual SE accuracy are studied. Since power systems are built in the nature, its topology can be changed by unscheduled line outage or planned line outage, resulting in the loss of a observability. In another case, power systems go out of being observable caused by the PMU device outage. The robustness of PMU network can be improved by placing many more PMUs to cover such concerns treated by N–1 or N–1–1 criteria [15] – [19]. These redundancy indices are called Bus Observability Index (BOI) or System Observability Redundancy Index (SORI) [19]. However, most of studies enhancing BOI and SORI only takes into account the graph theory based topological observability of the system, ignoring the actual SE accuracy. Moreover, redundant placement of PMUs quite raises the total placement costs, those strategy are not realistic. On the other hand, a few of studies about enhancement of actual SE accuracy have been conducted so far [20]. As power system uncertainty and unpredictability by RES which outputs the unstable generation are concerned, we shall look at the improvement of SE accuracy for many power flow cases in OPP problem. Also, there are two SE methods in OPP: PSE which only uses PMU for the measurement vector and Hybrid State Estimation (HSE) which combines the RTU and PMU for the measurement vector [21]. Traditionally, since SE has been done in power systems using RTUs, HSE installs PMUs into the already-made measurement network condition based on RTUs. Thus, HSE can relatively reduce the number of PMUs. In addition, two-stage type HSE overlaps the PMU measurement vector on the state vector previously estimated by RTUs [21]. This means there is no necessity to make it robust by PMUs if the RTU measurement network is robust enough for the loss of observability. Therefore, this research employs HSE for the cost performance.

In the PMU components installed at a substation, there are a voltage measurement channel and current measurement channels. For the conventional OPP problem research, generally PMUs as units only are optimally placed in a power system, there is no consideration on the current channel placement: the current channels are allocated for all incident lines to the bus that the PMU is placed. For PMU placement cost minimization in this case, the total placement cost including the PMU and voltage channel and the current measurement channels may increase when the system scale gets larger that resulting in not economic performance. Su and Chen proposed to limit the number of current measurement channels in OPP [22], however, it cannot contribute to the appropriate current channel selection. This research formulates the flexible current channel selection method in OPP, given by hierarchical structure representation in the augmented decision variables [23]. By this formulation, appropriate redundant current channel elimination is realized, resultantly reduces the total PMU placement cost.

Considering minimization of the total PMU placement cost and SE error, both objectives are being in the trade-off relationship each other. It indicates that a

objective can be improved while the other one is suffered to be deteriorated. The same thing is true of the minimization of the PMU placement cost and maximization of BOI or SORI in the past research [15] and [17]. Let the OPP problem which has multiple objective be called Multi Objective Optimal PMU Placement (MOOPP) problem. There are several approaches for multi objective optimization. If weighted sum method is employed, it is possible to obtain single solution by giving weight coefficients to both objectives. However, it is quite difficult to obtain the solution which the decision maker (power system operator/planner) actually hopes to get, and to set the appropriate weight coefficients for the objective functions. On the other hand, it is effective to obtain Pareto optimal solutions that are optimal in the wider sense that no rather solution in the search space are superior to them when all objectives are considered [24]. Pareto solutions in multi objective optimization are evaluated with dominance by Pareto's law whereas the solution in single objective optimization is evaluated with the absolute fitness. Hence, this research obtained the multiple Pareto solutions using evolutionary multi objective optimization method, Non-dominated Sorting Genetic Algorithm-II (NSGAII) [25]. As a result of optimization by NSGA-II, Current-Channel-Selectable (CCS) MOOPP which is formulated by the augmented decision variable via the hierarchical structure representation obtained better dominant Pareto solutions compared to the conventional MOOPP which ignores the current channel selectability.

In OPP, there are two types of measurement method to obtain the state vector. Those are called the direct measurement and pseudo measurement. The former one is to obtain voltage phasor at a bus by PMU voltage measurement channel. The latter one is to obtain voltage phasor using the measurements such as current phasor and voltage phasor already obtained at another bus. In case of use of pseudo measurement many times (pseudo measurement obtained by another pseudo measurement), there is a concern about measurement uncertainty propagation [26]. It may make the SE error larger depending on the number of pseudo measurements and the path of pseudo measurement and the targeted system characteristics. Therefore, this research involves measurement uncertainty propagation in HSE of the CCS-MOOPP problem and evaluates it, not to degrade the merit of PMU.

This thesis book also designs considerations on the power system security control after obtained the state vector by HSE, realized by placed PMUs in CCS-MOOPP. There have been some research articles about Voltage Stability Index (VSI) calculation using state vector estimated by SE. Understanding of VSI updated by SE can be the way to a secure system operation to avoid voltage collapse in recent power systems. Tang et al. proposed an adaptive load shedding method based on both frequency and voltage stability assessment using PMUs [27]. Although the authors established a novel load shedding method based on voltage stability assessment by modal analysis, the basic assumption is that the number of PMUs is sufficient. This assumption makes the planning cost of power systems tremendously expensive if the system scale is larger. Makasa and Venayagamoorthy considered voltage stability assessment based on an optimal PMU placement [28]. However, the authors did not consider the SE error of pseudo measurement which may result in bigger SE errors. Having the literature reviews, the VSI and the power system SE by optimal PMU placement have not yet been bridged. In this research, calculation of Critical Boundary Index (CBI) [29] as line-based VSI is carried out using estimated state by an optimally placed set of PMUs. The result showed that

the calculation of CBI based on HSE by the obtained set of PMUs is more accurate compared to use of RTUs alone. Additionally, in the mixed measurement condition (PMUs and RTUs), phenomenon that the use of state vector estimated through different estimators makes the CBI estimation error bigger, is found in the process of CBI calculation, and it might even worsen the SE error than the use of RTUs only. Hence in that case, discarding the state vector estimated by PMUs and use of state vectors obtained through same measurements are suggested.

As another consideration of OPP, this research also focused on the OPP for Dynamic Vulnerability Assessment (DVA) [30]. In the power system corrective control, DVA is the important action as an input of power system corrective control action, by giving the vulnerability symptom of the power system to the system operator. The power system vulnerability assessment has been done in off-line or on-line basis. However, PMU has developed the real time DVA realized by its practical capability to update the synchronized voltage phasor data in real time order [30]. To widen the PMU's availability in WAMS, the PMU placement should be assessed considering both of the static security assessment by static SE and the dynamic security assessment by DVA. Following the work by Cepeda et al. [31], DVA begins from the power system coherent area basis, and it is normally given by fast coherency in the DVA region. This thesis book designs a novel method of the fast coherent area identification by Hierarchical Clustering (HC), called HC-max. HC-max employs calculation of a criterion to evaluate the clustering precision by the point biserial correlation coefficient, on both of the number of clusters and the cluster linkage methods. HC-max is statistically superior to other non-hierarchical clustering methods in terms of point biserial correlation coefficient. After the identification of the fast coherent areas, OPP is assessed with an evaluation function to estimate the Center-Of-Inertia (COI) based area frequency by bus frequency signal obtained by placed PMUs. As a result of optimization by the exhaustive search, the optimal PMU placements tend to be placed at buses of the generator or neighborhoods which have high dynamic observability.

This research work finally proposes MOOPP problem minimizing the PMU device cost and maximizing SE accuracy for static security assessment which is subject to DVA index bound as the extreme form of OPP problem in this thesis book. This optimization problem can consider both the static and dynamic observability while mitigating the PMU device cost. By above those works conducted in each chapters to build the final form of MOOPP, this thesis book contributes to the reliable and cost-effective power system operation and planning in order to avoid power system blackouts.

1.3 Optimization and Machine Learning in Power Systems

This research employs metaheuristic optimization and machine learning techniques for the OPP problem, such as NSGA-II and HC-max. The main advantages of optimization techniques are the ability to deal with complex problems that conventional method cannot solve. In power system studies, optimization and machine learning techniques have been applied for solving problems because of its complexity and gigantic scale. Also in many cases, the optimization function is non-convex and indifferentiable, or combinatorial. Hence, stochastic optimization such

as metaheuristic optimization is more popular rather than the deterministic optimization. In online or real time power system operation, machine learning technique can be applied. Moreover, metaheuristic optimization is sometimes used for tuning of the parameters of supervised machine learning. A brief survey of the metaheuristic optimization and machine learning methods, and the application in power systems are given as follows:

Genetic Algorithm (GA)

GA is the most well-known Evolutionary Algorithm (EA) based on a natural selection laws and Darwin's evolutionary principle of survival of the fittest, developed step by step from 1950 and the fundamental is finally established by Holland in 1975 [32]. In GA, represented solutions called individuals evolve toward the global optima through genetic operators such as selection, crossover and mutation. Since GA is a stochastic optimization method, the initial population is randomly generated in each iteration. In the selection operation, evaluation of each solution by fitness function that assesses how good the solution is following the objective function, and individuals are selected with higher fitness value. Evolution of solution is fastened by crossover and mutation. To avoid trapping in the local minima, several types of improved GA have been invented. In power system application, GA is applied to the OPP of course [33], also to the parameter optimization of the Unified Power Quality Conditioner (UPQC) [34] and Power System Stabilizer (PSS) [23] for power system control, Unit Commitment (UC) problem [35] and Transmission Expansion Planning (TEP) [36] problem for power system planning, etc.

Particle Swarm Optimization (PSO)

PSO invented by Kennedy and Eberhart belongs to the category of Swarm Intelligence (SI) in the Computational Intelligence (CI) technique [37]. Communication among individuals locally/globally is the characteristic of SI, and this stimulates the emergence that results in the good search. PSO operates particles moving in searching space with the position and the velocity. The position and the velocity are updated by the local best and the global best position of particles to find the global optima in the searching space. PSO's convergence speed is pretty high since a particle finds a good position once, the others rapidly follow it. Since PSO is generally continuous optimization method, Discrete PSO (DPSO) and Binary PSO (BPSO) have been proposed for discrete optimization problems. The application in power systems is wide ranging: the OPP problem [38], parameter tuning problems of power system controllers such as PSS [39], Thyristor Controlled Series Compensator (TCSC) [40], Static Var Compensator (SVC) [41], planning problems in power systems such as black-start restoration [42], UC [43] and so on.

Simulated Annealing (SA)

SA is inspired from annealing method in metal engineering proposed by Kirkpatrick et al. [44]. SA develops a single solution by transition toward the global optimum with a small perturbation. Before SA, a typical single point search method called hill climbing was the representative searching method. Hill climbing tends to get easily stuck on a local optimum since it accepts the solution better than the present. SA overcame this point by introduction of solution transition probability with cooling schedule in annealing. Systematically SA is a single point search

method, not like GA or PSO as multi-point search methods, application of SA combined with another method is suggested to enhance the solution searching performance. Baldwin et al. applied SA combined with Bisecting Search (BS) to the OPP problem [10]. There have been several SA application to the power system planning problems: reactive power planning [45], Optimal Power Flow (OPF) problem [46], power system decomposition problem [47], and so on.

Artificial Neural Network (ANN)

ANN is a basic and trending supervised leaning method in machine learning which is inspired from the neuron behavior. Development of ANN has begun with the first systematic study by McCulloch and Pitts [48], and nowadays it draws attention as breaking-through Artificial Intelligence (AI) technique by its capability to learn or to approximate well any arbitrary nonlinear functions [49]. Because of advancement of computation performance in hardware/software, ANN has got popular in solving engineering problems. ANN consists of the number of nonlinear activation function, composed of input, output and one or more hidden layers. Input signal received by the input layer propagates with transition through layer by layer, then the output is obtained [49]. In ANN, learning of weights between each layer is significant, and it is optimization problem that minimizes the error between ANN output and the learning data. This process can be carried out by descent method, backpropagation, metaheuristics such as GA and PSO. Especially in power systems, ANN well fits together with power system online or real-time operation problem, such as adaptive PSS tuning [50], optimum power allocation in Battery Energy Storage System (BESS) [51], forecasting of photovoltaics output [52].

Cluster Analysis

In unsupervised learning, clustering analysis is the most frequently used for data grouping in accordance with the relationship among the data [53]. There are systematically two major types for clustering technique: Hierarchical Clustering (HC) and Non-Hierarchical Clustering (NHC). In HC, data objects are clustered according to their distance each other with certain distance metric and linkage. The objects are clustered in series from a pair of objects which has the minimum distance, and the process will finish until all objects are clustered into one cluster. Finally HC builds a dendrogram that how objects are clustered. By cutting the dendrogram at a certain height, the number of cluster can be determined. NHC partitions objects into clusters by evaluation function that assesses the goodness of the clustering. Since most of the NHC methods employs searching from a set of random initial points, the clustering result may vary in every trial [53]. Clustering fits well together with power system partition problems such as power system buses partitioning by Fuzzy *C*-Means (FCM) [54], *K*-means method [55] for power system coherent area grouping.

1.4 DISSERTATION OUTLINE

This book is separated into 8 chapters and appendices. Chapter 1 provides research background by significance of OPP, objective and contributions of this thesis, introduction on the significance of CI and AI techniques such as optimization and machine learning methods and their applications in power system studies.

Chapter 2 gives the general concept of PMU, power system monitoring principle, and other applications of PMU in power system studies. Firstly, fundamentals of power system monitoring and the system security control is given. After that, a concept of synchrophasor measurement technology and its applications in power system is described.

Chapter 3 presents an introduction of the OPP problem which is the main topic of this thesis book with the literature review. The principle of SE is also given in this chapter, categorized into conventional SE (SCADA SE), HSE and PSE, with the power system observability realized by RTU and PMU through an appropriate placement.

Chapter 4 proposes a novel MOOPP formulation which considers the PMU current channel allocation called CCS-MOOPP realized by the hierarchical structure representation, in order to reduce the total placement cost. The result of numerical simulation solving by NSGA-II is shown as comparison of the obtained Pareto front in both CCS-MOOPP and the conventional MOOPP. The simulation employed the IEEE modified New England 39-bus (NE 39-bus) and 57-bus test systems as the target systems, the significance of proposed method is confirmed by behavior of the PMU current channel selection on the target system. To propose single solution to the decision maker (system operator), the Best Compromised Solution (BCS) is selected from a set of Pareto solutions using fuzzy membership function. By performing SE and checking the SE accuracy statistically for the BCS, the SE accuracy is successfully improved by placing PMUs while reducing average PMU device cost.

Chapter 5 formulates CCS-MOOPP considering influence of measurement uncertainty propagation in PMU pseudo measurements. Since measurement uncertainty may propagate in case of use of PMU pseudo measurement, iterative use of pseudo measurement may cause a big error in HSE. Therefore, the consideration of measurement uncertainty propagation is included in CCS-MOOPP by a certain formulation in three types of pseudo measurement. As the result of numerical simulation in modified NE 39-bus solving by NSGA-II, proposed method can mitigate the impact of measurement uncertainty propagation by optimally placing PMUs considering the pseudo measurement with the number of use of it and the path to obtain it.

Chapter 6 investigates the possibility of advanced static voltage security assessment using estimated voltage phasor by SE for voltage security. Since optimal PMU placement can be obtained by CCS-MOOPP, its result can be expanded to the security control. After obtaining a set of optimal PMU placements, single placement is selected as the BCS, and CBI is calculated by the estimated voltage phasor in HSE with the obtained PMU placement. Obviously the estimation accuracy of CBI in use of voltage phasor obtained by PMU measurement is better than RTU. However, in HSE that is mixed measurement environment, CBI as line VSI estimation accuracy gets worse when a pair of voltage phasor estimated by different measurement device because line VSI may use the phase difference between two buses taken by subtraction of amounts having different error order. This investigation proves that it is better to discard the voltage phasor obtained by

PMU in case of CBI estimation by mixed measurements not to degrade the merit of installing PMU into power systems.

Chapter 7 expands the possibility of MOOPP to the perspective of corrective security controls. Since the MOOPP only focuses on static SE for static security assessment, there is no consideration on observation of dynamics of a power system. Focusing on the PMU's ability that can measure the synchronized voltage/current phasor with high resolution, a novel formulation of MOOPP including the dynamic observability constraint in DVA is designed in this chapter. In the OPP for DVA, a novel clustering analysis method called HC-max is proposed and compared with other NHC methods. After the confirmation of clustering precision, CCS-MOOPP constrained by mitigated dynamic observability. By this formulation, OPP that considers both of static and dynamic security assessment is discussed.

Chapter 8 concludes the whole results from the proposed OPP problem. Finally, appendices including test power system data, hardware/software information and computation time in this research are revealed.

1.5 SUMMARY

This chanter provides research background by significance of OPP, objective and contributions of this thesis, introduction on the significance of CI and AI techniques such as optimization and machine learning methods and their applications in power system studies.

1.6 REFERENCES

[1] U.S.-Canada Power System Outage Task Force, Final Report on the August 14, 2003 Blackout in the United States and Canada: Causes and Recommendations, 2004.

[2] H. Bevrani, M. Watanabe, and Y. Mitani, *Power System Monitoring and Control*, 1st ed., John Wiley & Sons, USA, Chapter 1, pp. 1-5, 2014.

[3] A. G. Phadke, J. S. Thorp, and M. G. Adamiak, A new measurement technique for tracking voltage phasors, local system frequency, and rate of change of frequency, *IEEE Transactions on Power Apparatus and Systems*, vol. 102, no. 1, pp. 73-77, 1983.

[4] A. G. Phadke, Synchronized phasor measurements in power systems, *IEEE Computer Applications in Power*, vol. 6, no. 2, pp. 10-15, 1993.

[5] Y. Mitani, Power system observation by using synchronized phasor measurements as a smart device, *IEEJ Transactions on Power and Energy*, vol. 130, no. 9, pp. 791-794, 2010. (in Japanese)

[6] A. Monticelli, *State Estimation in Electric Power Systems – A Generalized Approach*, 1st ed., Kluwer Academic Publishers, USA, Chapter 1, pp.1-13, 1999.

[7] A. G. Phadke, J. S. Thorp, and K. J. Karimi, State estimation with phasor measurements, *IEEE Transactions on Power Systems*, vol. 1, no. 1, pp. 233-238, 1986.

[8] U. S. Department of Energy, *Factors Affecting PMU Installation Costs*, 2014.

[9] M. Ghamsari-Yazdel and M. Esmaili, Reliability-based probabilistic optimal joint placement of PMUs and flow measurements, *International Journal of Electric Power and Energy Systems*, vol. 78, pp. 857-863, 2016.

[10] T. L. Baldwin, J. S. Thorp, and K. J. Karimi, Power system observability with minimal phasor measurement placement, *IEEE Transactions on Power Systems*, vol. 8, no. 2, pp. 707-715, 1993.

[11] D. J. Brueni and L. S. Heath, The PMU placement problem, *SIAM Journal of Discrete Math*, vol. 19, no. 3, pp. 744-761, 2005.

[12] N. M. Manousakis, G. N. Korres, and P. S. Georgilakis, Taxonomy of PMU placement methodologies, *IEEE Transactions on Power Systems*, vol. 27, no. 2, pp. 1070-1077, 2012.

[13] N. M. Manousakis, G. N. Korres, and P. S. Georgilakis, Optimal placement of phasor measurement units: a literature review, *16th International Conference on Intelligent System Application to Power Systems* (ISAP 2011), Hersonisso, Greece, 2011.

[14] M. Nazari-Heris and B. Mohammadi-Ivatloo, Applocation of heuristic algorithms to optimal PMU placement in electric power systems: an updated review, *Renewable and Sustainable Energy Reviews*, vol. 50, pp. 214-228, 2015.

[15] K. Jamuna and K. S. Swarup, Multi-objective biogeography based optimization for optimal PMU placement, *Applied Soft Computing Journal*, vol. 12, no. 5, pp.1503-1510, 2012.

[16] F. Aminifar, A. Khodaei, M. Fotuhi-Firuzabad, and M. Shahidehpour, Contingency-constrained PMU placement in power networks, *IEEE Transactions on Power Systems*, vol. 25, no. 1, pp. 516-523, 2010.

[17] B. Milosevic and M. Begovic, Nondominated sorting genetic algorithm for optimal phasor measurement placement, *IEEE Transactions on Power Systems*, vol. 18, no. 1, pp. 69-75, 2003.

[18] O. Gomez, M. Rios, and G. Anders, Reliability-based phasor measurement unit placement in power systems considering transmission line outage and channel limits, *IET Generation, Transmission and Distribution*, vol. 8, no. 1, pp. 121-130, 2014.

[19] D. Dua, S. Dambhare, R. K. Gajbhiye, and S. A. Soman, Optimal multistage scheduling of PMU placement: an ILP approach, *IEEE Transactions on Power Delivery*, vol. 23, no. 4, pp. 1812-1820, 2008.

[20] S. Ogawa and H. Mori, Application of moment matching method to optimal allocation of PMUs in state estimation, *IEEJ Transactions on Power and Energy*, vol. 138, no. 2, pp. 121-130, 2018.

[21] J. James and S. Bindu, Hybrid state estimation including PMU measurements, *International Conference on Control, Communication and Computing*, Trivandrum, India, 2015.

[22] C. Su and Z. Chen, Optimal placement of phasor measurement units with new considerations, *2010 Asia-Pacific Power and Energy Engineering Conference* (APPEEC 2010), Chengdu, China, 2010.

[23] K. Hongesombut, Y. Mitani, and K. Tsuji, Simultaneous tuning of power system stabilizers based on a combined method of a Micre-GA, HGA and minimum phase control, *IEEJ Transactions on Power and Energy*, vol. 122, no.12, pp. 1270-1279, 2002.

[24] E. Zitzler and L. Thiele, Multiobjective evolutionary algorithms: a comparative case study and the strength Pareto approach, *IEEE Transactions on Evolutionary Computation*, vol. 3, no. 4, pp. 257-271, 1999.

[25] K. Deb, S. Pratab, S. Agarwal, and T. Meyarivan, A fast and elitist multi-objective genetic algorithm: NSGA-II, *IEEE Transactions on Evolutionary Computation*, vol. 6, no. 2, pp. 182-197, 2002.

[26] ISO-IEC-OMIL-BIPM, Guide to the Expression of Uncertainty in Measurement, JCGM, Sèvres, France, 1992.

[27] J. Tang, J. Liu, F. Ponci, and A. Monti, Adaptive load shedding based on combined frequency and voltage stability assessment using synchrophasor measurements, *IEEE Transaction on Power Systems*, vol. 28, no. 2, pp. 2035-2047, 2013.

[28] K. J. Makasa and G. K. Venayagamoorthy, On-line voltage stability load index estimation based on PMU measurements, *2011 IEEE PES General Meeting* (IEEE PES GM 2011), Detroit, MI, USA, 2011.

[29] M. Furukakoi, O. B. Adewuyi, M. S. S. Danish, A. M. Howlader, T. Senju, and T. Funabashi, Critical Boundary Index (CBI) based on active and reactive power deviations, *International Journal of Electrical Power and Energy Systems*, vol. 100, pp. 50-57, 2018.

[30] J. C. Cepeda and J. L. Rueda, *Introduction: The Role of Wide Area Monitoring Systems in Dynamic Vulnerability Assessment*, In *Dynamic Vulnerability Assessment and Intelligent Control: For Sustainable Power Systems*, J. L. Rueda-Torres and F. Gonzalez-Longatt (eds.), 1st ed., pp. 1-19, Wiley IEEE press, USA, 2018.

[31] J. C. Cepeda, J. L. Rueda, I. Erlich, and D. G. Colomé, Probabilistic approach-based PMU placement for real-time power system vulnerability assessment, *2012 3rd IEEE PES Innovative Smart Grid Technologies Europe* (ISGT Europe 2012), Berlin, Germany, 2012.

[32] J. H. Holland, *Adaptation in Natural and Artificial Systems*, MIT press, USA, 1992.

[33] F. J. Marin, F. Garcia-Lagos, G. Joya, and F. Sandoval, Genetic algorithms for optimal phasor measurement units in electrical networks, *IEEE Electronics Letters*, vol. 39, no. 19, 2003.

[34] C. Benachaiba, O. Abdelkhalek, S. Dib, and M. Haidas, Optimization of parameters of the unified power quality conditioner using genetic algorithm method, *Information Technology and Control*, vol. 36, no. 2, pp. 242-245, 2015.

[35] S. A. Kazarlis, A. G. Bakirtzis, and V. Petridis, A genetic algorithm solution to the unit commitment problem, *IEEE Transactions on Power Systems*, vol. 11, no. 1, pp. 83-92, 1996.

[36] A. R. Abdelaziz, Genetic algorithm-based power transmission expansion planning, *7th International Conference on Electronics, Circuits and Systems* (ICECS 2000), Jounieh, Lebanon, 2000.

[37] J. Kennedy and R. Eberhart, Particle swarm optimization, *International Conference on Neural Networks* (INCC '95), Perth, WA, Australia, 1995.

[38] M. Hajian, A. M. Ranjbar, T. Amraee, and B. Mozafari, Optimal placement of PMUs to maintain network observability using a modified BPSO algorithm, *International Journal of Electrical Power and Energy Systems*, vol. 33, no. 1, pp. 28-34, 2011.

[39] Z. Qing, W. Huang, and S. Jiao, Optimizing power system parameters using hybridized differential evolution and particle swarm optimization, *2013 9th International Conference on Natural Computation* (ICNC 2013), Shenyang, China, 2013.

[40] S. K. Rautray, S. Choudhury, S. Mishra, and P. K. Rout, A particle swarm optimization based approach for power system transient stability enhancement with TCSC, *Procedia Technology*, vol. 6, pp. 31-38, 2012.

[41] S. A. Jumaat, I. Musirin, M. M. Othman, and H. Mokhlis, Optimal location and sizing of SVC using particle swarm optimization technique, *2011 1st International Conference on Informatics and Computational Intelligence* (ICI 2011), Bandung, Indonesia, 2011.

[42] Y. Liu and X. Gu, Reconfiguration of network skeleton based on discrete particle-swarm optimization for black-start restoration, *2006 IEEE PES General Meeting* (IEEE PES GM 2006),

[43] V. S. Pappala, I. Erlich, Power systems optimization under uncertainties: a PSO approach, *2008 IEEE Swarm Intelligence Symposium* (SIS 2008), St. Louis MO, USA, 2008.

[44] S. Kirkpatrick, C. D. Gelatt, and M. P. Vecchi. Optimization by simulated annealing, *Science*, vol. 220, no. 4598, pp. 671-680, 1983.

[45] Y. L. Chen and Y. L. Ke, Multi-objective var planning for large-scale power systems using projection-based two-layer simulated annealing algorithms, *IEE Proceedings-Generation, Transmission and Distribution*, vol. 151, no. 4, pp. 555-560, 2004.

[46] C. A. Roa-Sepulveda and B. J. Pavez-Lazo, A solution to the optimal power flow using simulated annealing, *International Journal of Electrical Power and Energy Systems*, vol. 25, no. 1, pp. 47-57, 2003.

[47] H. Mori and K. Takeda, Parallel simulated annealing for power system decomposition, *IEEE Transactions on Power Systems*, vol. 9, no. 2, pp. 789-795, 1994.

[48] W. W. McCulloch and W. Pitts, A logical calculus of the ideas immanent in nervous activity, *The Bulletin of Mathematical Biophysics*, vol. 5, no. 4, pp. 115-133, 1943.

[49] M. Fathi and H. Bevrani, *Optimization in Electrical Engineering*, 1st ed., Supringer Nature AG, Switzerland, Chapter 7, pp. 137-168, 2019.

[50] P. Tulpule and A. Feliachi, Online learning neural network based PSS with adaptive training parameters, *2007 IEEE PES General Meeting* (2007 IEEE PES GM), Tampa, FL, USA, 2007.

[51] T. Kerdphol, Y. Qudaih, M. watanabe, and Y. Mitani, RBF neural network-based online intelligent management of a battery energy storage system for stand-alone microgrids, *Energy, Sustainability and Society*, vol. 6, no. 5, pp. 1-16, 2016.

[52] M. Abuella and B. Chowdhury, Solar power forecasting using artificial neural network, *47th Annual North American Power Symposium* (NAPS 2015), Charlotte, NC, USA, 2015.

[53] L. Kauuman and P. J. Rousseeuw, *Finding Groups in Data*, 1st ed., John Wiely & Sons, USA, Chapter 1, pp. 1-63, 1990.

[54] I. Kamwa, A. K. Pradhan, G. Joos, and S. R. Samantaray, Fuzzy partitioning of a real power system for dynamic vulnerability assessment, *IEEE Transactions on Power Systems*, vol. 24, no. 3, pp. 1356-1365, 2009.

[55] D. Sharma, K. Thulasiraman, D. Wu, and J. N. Jiang, A network science-based k-means++ clustering method for power systems network equivalence, *Computational Social Networks*, vol. 6, no. 4, 2019.

2 PMU-Based Power System Monitoring and Control

2.1 Introductions of Power System Monitoring and Security Controls

2.1.1 Fundamental of Power System Monitoring

The power system operator needs to let a power system stays away from instability to keep provide electricity, with a certain electric power quality. The quality of electric power includes maintenance of voltage, frequency, and less number of outage. To keep power system stay healthy, power supplier is responsible to maintain voltage and frequency in a certain range in accordance with a grid code applied by the International Electrotechnical Commission (IEC) or the Institute of Electrical and Electronics Engineers (IEEE) [1], also outage should be prevented in terms of reliability indices as System Average Interruption Duration Index (SAIDI) and System Average Interruption Frequency Index (SAIFI) [2]. In power system operation, security state is managed by constant monitoring with security assessment and following security control that minimizes the spreading of influence of power system events such as load increment, generator dispatch, disturbances by short circuit or ground fault, and so on. Operating security states of a power system and control strategies are categorized by Kundur [3] as follows:

Normal State

All values such as voltage, frequency and power flow stay within the nominal range, there is no overloaded power equipment.

Alert State

The security level falls below a certain limit of adequacy by some reasons. In this state, all system variables are still within the acceptable range and all constraints are satisfied. However, if this state is left without any security controls, the security state would be developed into the next state: an emergency state, by single outage. The system can be restored to the normal state by preventive control actions.

Emergency State

By severe contingency in the alert state, the system security state is placed in the emergency state. Some power equipment are overloaded and exceed short-term emergency ratings, and voltage at many buses is low. The system is still intact and may be restored to the alert state by conducting emergency control actions.

Extreme Emergency State

Generally, security control actions are taken when the security state is the alert state or emergency state. If those actions are not made in time or not

successfully done, the system enters the severest state called the extreme emergency state. During this state, partial or total service interruption occurs.

Restorative State

The restorative state is the system condition in which control actions are being taken to reconnect all the facilities and to restore system load. The system transits from this state to either the alert state or the normal state, depending or the system conditions.

2.1.2 Preventive Security Control

Preventive security control actions are taken before the system gets a severe state by postulate or unpostulated disturbances. Hence, preventive control is initiated in the alert state to bring back the power system state the normal state. Practically, generation rescheduling, network switching, reactive compensation, load curtailment etc. are type of preventive control [4]. Fig. 2.1 shows a clear diagram of the operating states and transitions for power systems adapted from article by Fink and Carlsen [5]. Basically, preventive security control is initiated referring to the static security assessment of the power system.

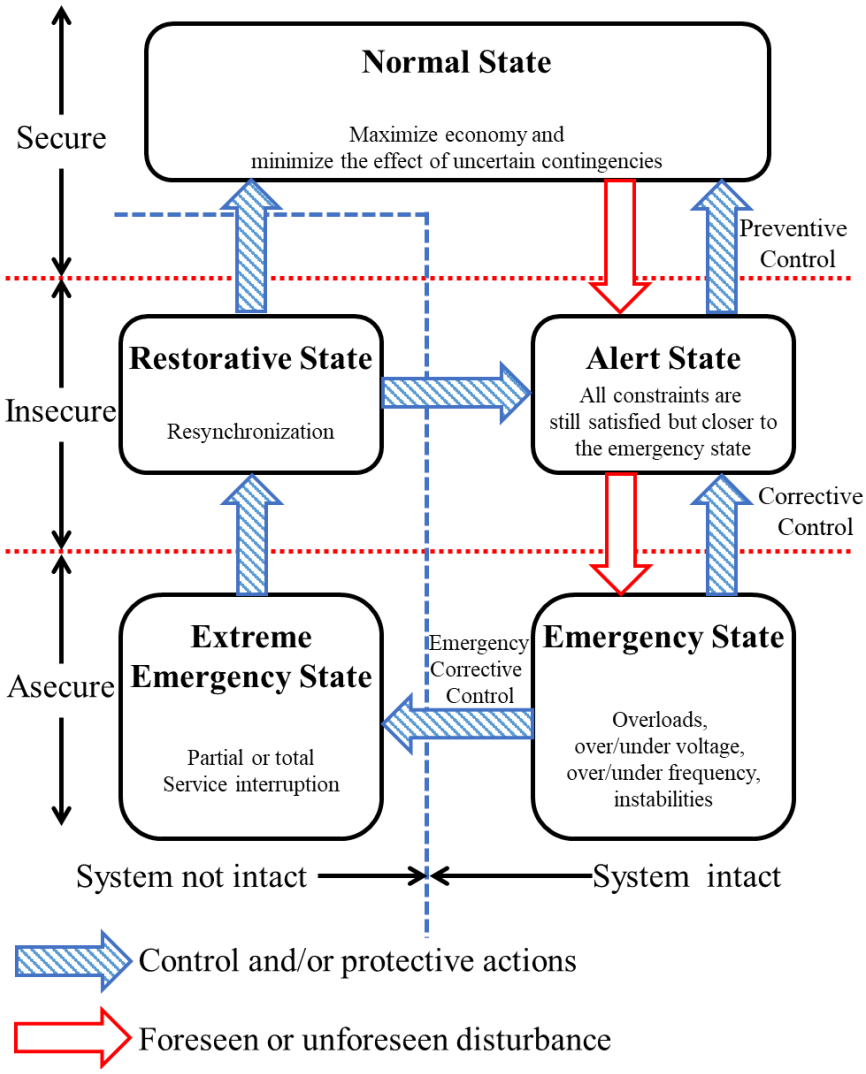

Fig. 2.1 The operating states and transitions for power systems.

2.1.3 Corrective Security Control

Corrective control actions are executed when power system is in the emergency state. From the emergency state, the state may transit to either the alert state or the extreme emergency state by the corrective control. The system may be restored to the alert state by corrective control actions such as: fault clearing, excitation control, fast-valving, generation tripping, generation run-back, High Voltage Direct Current (HVDC) modulation, load curtailment and so on. As aforementioned, the system enters partial or total cascading outage when security control actions could not conduct the system to more securer state. In this case, emergency corrective control schemes such as loads shedding and controlled system separation are aimed at saving the system as much as possible from a widespread blackout [3][4]. Basically, corrective security control needs to refer to the result of dynamic security assessment of the power system.

2.2 SYNCHRONIZED MEASUREMENT TECHNIQUE

2.2.1 General Description of PMU

In power systems, their representative quantities are voltage (V), current (I), active power (P), reactive power (Q), frequency (f) and phase angle (θ). Conventionally, those information except phase angle is collected by RTU. The system state vector represented by voltage phasor is obtained indirectly via power flow calculation or nonlinear SE using measurement data of RTUs. There is no problem in calculation of phase difference between two buses in short distance by measuring voltage at both buses at the same timing. However, it will be problem in case of distant places that power systems are generally formed. To calculate phase angle, the reference phase angle must be calculated precisely, time synchronization of the phase angle at distant multi-measurement points is required. It is obviously impossible to perform time synchronization by independent clock at each measurement point because for example, in 60 Hz AC waveform, 1 cycle is 16.7 ms i.e. the precision about less 2 digits than 16.7ms is required to obtain phase angle accurately. Under such circumstances, appearance of the GPS satellite enabled synchronized phasor measurement, and following invention of the PMU utilizing GPS allowed direct measurement of voltage/current phasor. Also, PMU's data sampling rate is above 30 Hz whereas the RTU is about 0.2-0.5 Hz.

The phasor representation of sinusoids is briefly described [6]. A pure sinusoidal quantity is given by:

$$x(t) = X_m \cos(\omega t + \varphi) \tag{2.1}$$

where, ω is the frequency of the signal in radians per second, φ is the phase angle in radians and X_m is the peak amplitude of the signal. The effective value of the input signal is $X_m/\sqrt{2}$. Recall that the effective value quantities are particularly useful in calculating active and reactive power in AC circuit. Equation (2.1) can be also written as follows:

$$x(t) = \mathrm{Re}\left\{X_m e^{j(\omega t+\varphi)}\right\} = \mathrm{Re}\left[\left\{e^{j(\omega t)}\right\} X_m e^{j\varphi}\right]. \tag{2.2}$$

The sinusoid of (2.1) is represented by a complex number X known as its phasor representation as follows:

$$x(t) \leftrightarrow X = \left(X_m/\sqrt{2}\right)e^{j\varphi} = \left(X_m/\sqrt{2}\right)[\cos\varphi + j\sin\varphi]. \tag{2.2}$$

A sinusoid and its phasor representation are depicted in Fig. 2.2.

Fig. 2.3 shows a block diagram of PMU function. A PMU generally used for power system monitoring in a substation performs anti-aliasing filtering and A/D conversion for analog signal obtained from Current Transformer (CT) and Potential Transformer (PT). After filtering and conversion, obtained digital information is synchronized referring a pulse signal from GPS receiver and converted to the phasor representation. Through this procedure, voltage and current phasor quantities are finally obtained.

Fig. 2.4 shows a general architecture of WAMS that is composed of the PMUs, Phasor Data Concentrator (PDC) and the Synchro-Phasor Communication System (SPCS) [7]. In WAMS, decentralized PMUs are digital signal processing units that can calculate the voltage phasor at the buses and the current phasor at the incident transmission lines, time-stamped by GPS synchronization. RTU may participate to WAMS as another meter to collect data. In the upper hierarchy, there are PDC and super PDC which collect data from different PMUs with identical time tags, to create archival files of data for future retrieval, use and available application tasks with appropriate speed and latency[6]. SPCS plays a role to pass the obtained data from PMUs to PDCs, or PDCs to super PDCs. The data transfer methods in SPCS are classified into two categories: wired and wireless. The wired communication methods such as the power line and the fiber optic cable communications, offer high reliability, huge capacity and protection against interference. In contrast, the wireless communication methods which include microwave, cellular and the satellite communications, provide rapid deployment, low installation and maintenance costs and access to remote geographic locations as the advantage [7].

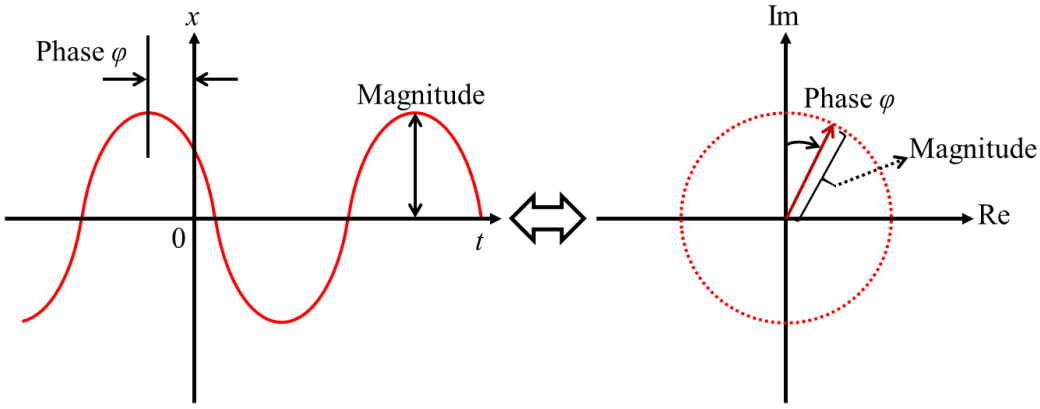

Fig. 2.2 A measured sinusoidal wave and its phasor representation [3].

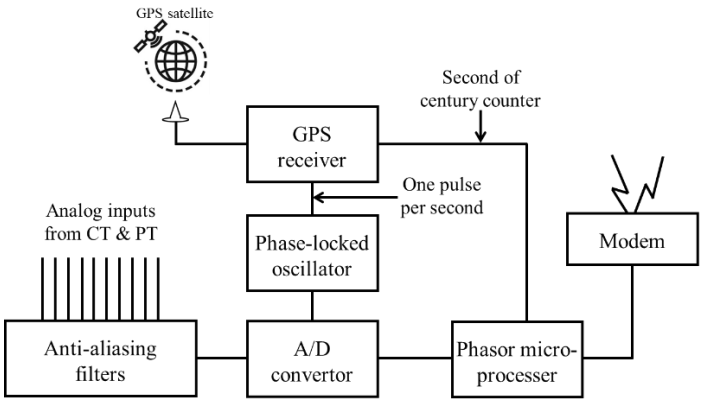

Fig. 2.3 The PMU function block diagram [3].

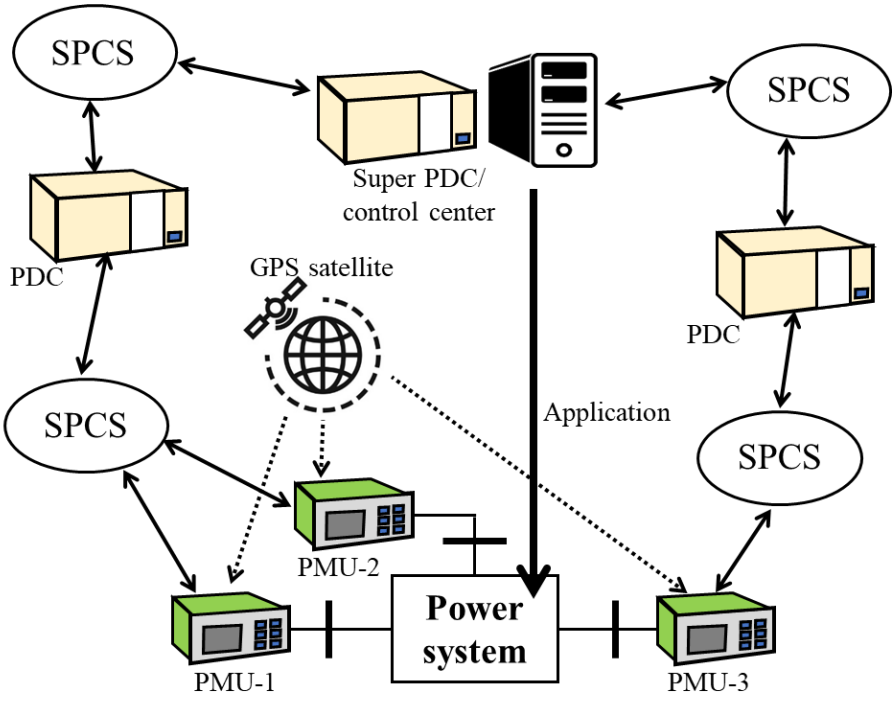

Fig. 2.4 The general architecture of WAMS [7].

2.2.2 PMU Applications in Power Systems

There are many ways to apply PMUs to power systems. The main topic of this thesis book is OPP problem for SE and enhancement of following security control action's accuracy. In this section, not only SE application but also other fields of PMU application in power systems are briefly introduced. Firstly, its application is majorly classified into the offline application, the online and real time application.

2.2.2.1 Offline Applications

Analysis and assessment of power systems based on PMU data in offline time range are wide-ranging. For offline analyses, they are performed using PMU data log based on the past events, and are intended to establish secure operating ranges for real time/online applications and validation of simulation models and parameters for operations and planning tasks [8].

Post Disturbance Analysis

High-resolution PMU measurement data is ideal for tracing a disturbance phenomenon in the transient region and power oscillation after the disturbance as the steady state region. By disturbance analyses based on PMU measurement data, power system hidden vulnerability may be revealed that could not be detected in simulation using model which may not exactly reflect the real system, or measurement data using RTUs. Based on the analyzed data, some countermeasures e.g. PSS tuning and control actions, can be taken for disturbances [8].

Model Validation

Generators, other controllers and system topology are significant elements in power systems, these need to be represented as correctly as possible on a power system simulation. Placing PMUs and obtaining the precise data of the components enable validating difference between simulation model and measured data which is nearer to the actual power system's behavior. By reflecting it to the simulation model, responses of generators and controllers can be improved [8].

Offline Controller Design

PMU's synchronized phase angle difference can be used for Wide Area Damping Controller (WADC) as the input signal, to damp the inter-area oscillation mode. Since the inter-area oscillation is a swing of the whole system, global oscillation signals caught by PMUs placed at some substations are quite useful for mitigating the inter-area oscillation. Matsukawa et al. proposed optimal PSS and WADC coordinated design using PMUs placed at the generator buses, considering PMU the transport delay [9]. Chompoobutrgool and Vanfretti proposed a novel concept called "dominant path" for effective design of WADC using PMU signals [10]. These approaches are mostly intended to perform robust controller tuning as those are offline design.

Pattern Recognition and Correlation Analysis

Because PMUs store measurement data and estimated other amounts to a data server, those quantities may be used for big data analysis. Hence, PMUs may be used as the event logger in power systems. By analyzing such data via certainly homogeneous big data analysis method, some useful information to detect future unknown events could be identified, which potentially gives a significant support to the power system operation. The application is mostly for protection or event detection by machine learning methods, formulating the pattern recognition as a classification problem. Klingsmith et al. extracted useful features from collected PMU data by applying unsupervised clustering methods both HC and NHC [11]. Tokel et al. applied ANN for fault detection and classification considering PMU data transfer delay, in several fault type [12].

2.2.2.2 Online and Real Time Applications

Owing to PMU's data sampling rate, the measured data and/or estimated data are appropriate to online and real time power system operation. For those analysis and action initiation, instant data updating and validation are required. The online system operation needs to respond within few seconds whereas the real time system operation requires within a second or millisecond order, and sometimes such severe time delay might not be accepted.

Situational Awareness and Visualization

Situational awareness provides wide area system information that is understandable to a system operator. By visualization of system information using measurement data obtained by PMUs allocated in some places, the system operator can sensuously catch what is going on the system, and understand the potential of the whole system. Phase information is deeply connected with the transfer of electric power, it is suitable to be used in system state transition monitoring. Since the visualization is performed based on the geographical information, there have been several projects of power system visualization in real power systems using PMU measurement data through Geographical Information System (GIS) [13].

State Estimation

Compared to the traditional SE, SE supported by PMU can realize the more accurate state estimation. SE is the main topic of this thesis book, the detail will be given in the Chapter 3.

Small Signal Stability Evaluation

Using PMU measurement signals, the inter-area oscillation mode which was difficult to be monitored conventionally has become available to be understood, and measurement-based online stability monitoring in recent vulnerable power system is of importance. The inter-area oscillation mode is the most dominant, the most unstable and poor damping mode in the small signal stability region. Hence its online/real time assessment based on PMU measurement data is key to grasp the small signal stability in a power system. The inter-area oscillation is low frequency oscillation mode under 1 Hz, it can be extracted by some filtering techniques such as Fast Fourier Transformation (FFT) or Discrete Wavelet Transformation (DWT) and so on[14], from the raw voltage phase difference data of PMUs. Khairudin and Mitani applied FFT-Continuous Wavelet Transform (CWT) which is parameter free method to small signal stability assessment in both of simulation model and real system [15]. Despa et al. applied FFT filtering which uses FFT and inverse FFT to Malaysia and Singapore interconnected power system and assessed its stability by eigenvalues from the extracted oscillations [16]. Senesoulin et al. proposed estimation of dominant power oscillation mode by long short term memory Recurrent Neural Network (RNN) using PMU measurement data for the sake of real time applications [17].

Online Controller Design

In recent power system, the power system state suddenly changes because of a lot of installation of RES. Hence, measurement-based online tuning of power system controller has drawn attention in the researchers and utility operators. Related to the model validation, in designing controllers online, accurate system modeling is also very important. Hence, PMU signal is used for controller design to damp inter-area low-frequency oscillations with some uncertainties in power systems. Watanabe et al. used PMU signal to identify an approximate model, and based on the identified model, designed PSS by applying Linear Matrix Inequality (LMI) approach [18]. Wang at el. established a method to construct the dynamic state Jacobian matrix and system state matrix based on PMU ambient voltage phase angle signals and estimated the eigenvalues accurately [19]. Both methods have a

potential to design controllers in online time span basis including the system uncertainty which the offline model based design is unable to consider.

System Protection

PMU based less time delay, high resolution data can be applied to the system protection field [20]. In system protection, the out of step relays are used for mitigating the influence of disturbance in the power system by separating some generators selectively. By placing PMUs to substations and directly monitor the voltage phase angle, it is able to activate protection relays accurately, the system stability level can be enhanced [21]. From North American Electric Reliability Council (NERC) planning standard, Special Protection Scheme (SPS) is designed to detect abnormal system conditions and take preplanned, corrective actions to acceptable system performance [22]. In modern power systems, especially the protection scheme supported by PMUs are called Wide Area Monitoring, Protection and Control (WAMPAC).

2.2.3 Frontiers of PMU Installation in the World

In power systems all over the world, PMUs have been installed into the substations of the systems for monitoring and control of the wide area system across utilities, states and countries.

Europe

In the European power systems, PMUs are distributed in some substations in whole systems: about 20 PMUs for NORDEL power systems including Norway, Sweden, Finland and Denmark, 50 PMUs for the Union for the Coordination of Transmission of Electricity (UCTE) AC power systems. All PMUs are connected to the individual Transmission System Operator (TSO) data concentrators and in addition there are links between several TSO's data concentrators for exchanging information of strategic PMUs at international level [23]. In those systems, measurement data by installed PMUs are used for voltage stability monitoring, system damping assessment via oscillation analysis and so on [23].

North America

In the North American power systems, significance of PMU has been discussed since 2003 New York cascaded blackout. Nowadays, PMU is the main important topic in the concept of smart grid, North American Synchro-Phasor Initiative (NASPI) has been established for development of the sophisticated software and system toward PMU installation. NASPI conducts PMU placement, the measured data sharing, application development and research activities, via joint projects cooperated by utilities, consultants, electric makers, universities and national research institutes. Those projects are commercially supported by US Department Of Energy (DOE) and NERC. In 2012, about 500 PMUs are installed into the systems, about more 1,500 PMUs are added to the systems as of 2015 [24]. Fig. 2.5 shows the PMU installation map as of 2017 in North American power system referring NASPI. Obtained PMU data set is used for oscillation detection, fault location determination, voltage stability monitoring, frequency monitoring, static/dynamic SE and so on.

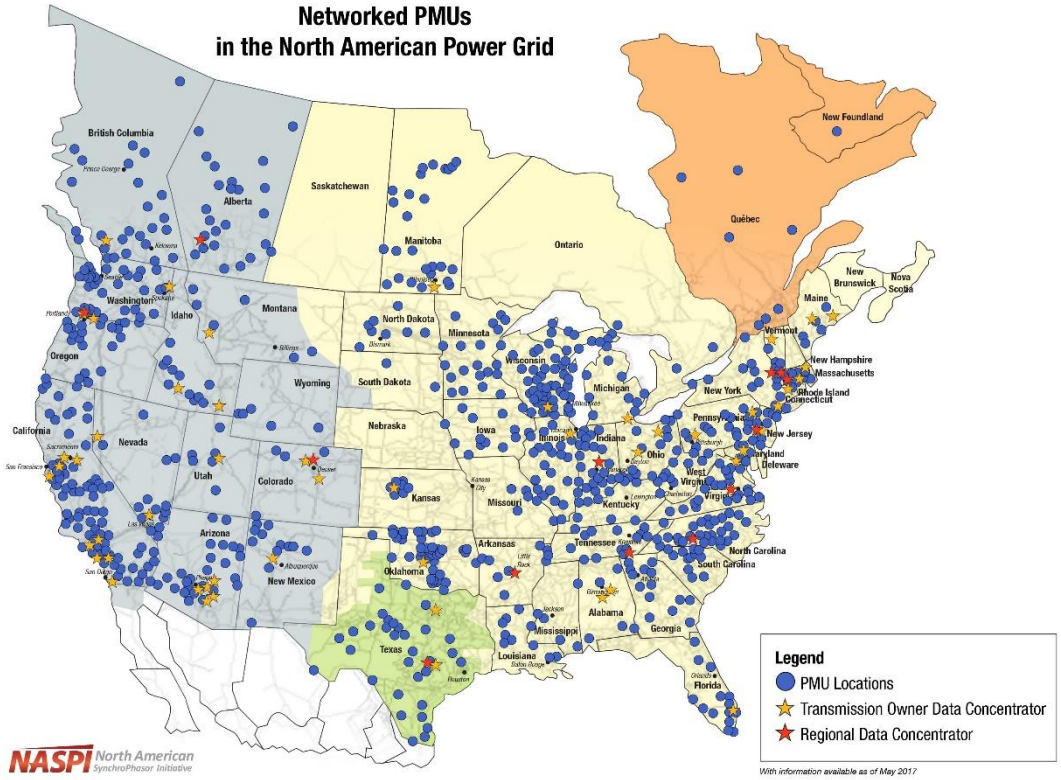

Fig. 2.5 The PMU installation map in North America as of March 2017.

China

China has a huge inter-connected mesh like power system as well as North America, research on PMU is also active. As of 2013, approximately 2,400 PMUs sets had been deployed in power grids in China, covering all 500 kV substations in the country [25]. The use applications are frequency and voltage monitoring, online oscillation monitoring, fault analysis, disturbance identification, model validation and so on. Using placed PMUs, not only use offline and application in power system planning, but also use online and application in power system online/real time operation are conducted in Chinese power systems. Hence, the trend of PMU/WAMS system application has been switching from offline to online, and from monitoring to control. However, the huge amount of measured and stored data by PMU/WAMS system remains far from being fully exploit to meet all smart grid requirements. Some researcher say that the combining PMU/WAMS with big data technology offers an important opportunity to extend their combined applications further [25].

Australia

Australia has a longitudinal power system which is situated in eastern coast side inter-connected with the southeastern populated area. Because of the form of the power system, inter-area oscillation is a primary issue in Australia. Independent System Operators (ISO) called NEMMCO and PowerLink coordinately construct Power Dynamic Management (PDM) as a measurement network, and conduct monitoring of such a poor damped oscillation [26].

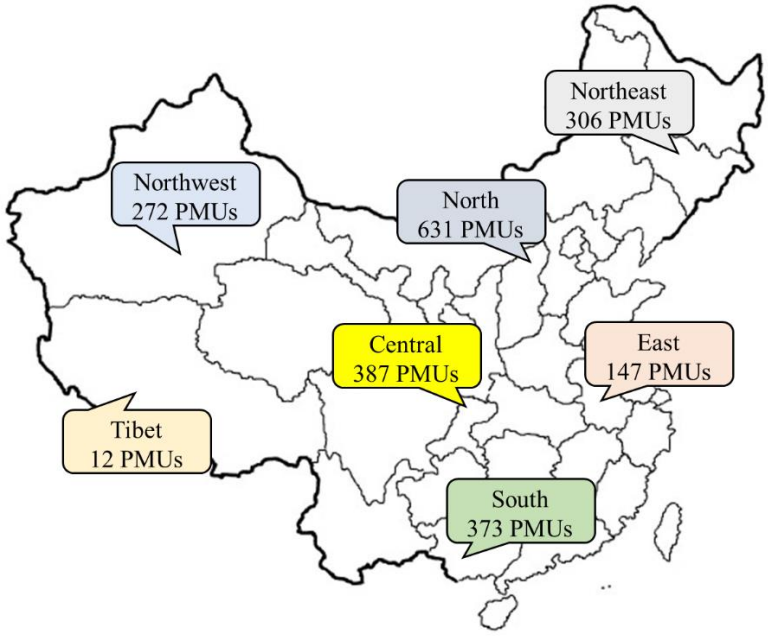

Fig. 2.6 The PMU installation map in China as of March 2013 [25].

Japan

In Japan, its longitudinal power system is not that big as continental countries, so that the number of installed PMUs is fewer. Tohoku electric Power Co., Inc. placed PMUs in substations of the main grid. Thereafter, they conducted oscillation monitoring between Tokyo and Tohoku area based on 100 V outlet PMUs, cooperating with a university and an electric manufacturer [26]. Recently, a power system under the jurisdiction of Kansai Electric Power Co., Inc. has installed power system phenomenon logger using PMUs which stores data for analyzing the system characteristics after voltage or frequency fluctuation, and regional system behavior. This logger is not intended to be used for constant system monitoring and online control actions, used for offline analysis and assessment of the system characteristics [26]. In Japan, instead constant system monitoring and online/real time control in real systems are not that active, creation of a new value via the offline analysis using PMUs have been led by universities and utilities. Among them, Campus WAMS consists of 100 V level PMUs is significant. Fig. 2.7 shows PMUs placement map in Japan's Campus WAMS. Mitani et al. conducted comparison of the monitored voltage phase angle difference in Campus WAMS PMUs and 500 kV substation level PMUs, and both showed similar oscillation behavior indicating Campus WAMS usefulness [27]. Hence, the voltage phase angle data obtained by Campus WAMS is used for offline power system model validation, system equitable inertia estimation and so on with a certain filtering technique.

2.3 SUMMARY

In this chapter, the fundamental of power system monitoring and security controls, general description of PMU, PMU application field in power systems and frontiers of PMU installation in real systems all over the world.

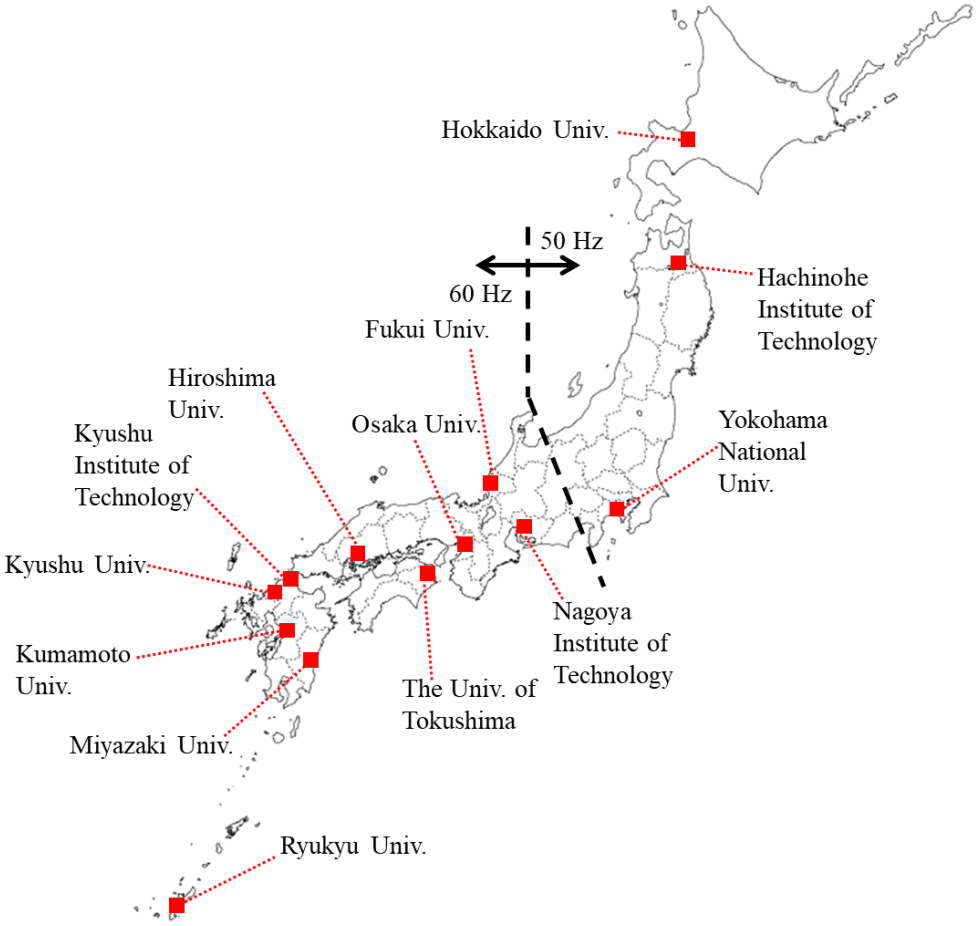

Fig. 2.7 The PMU placement map in Campus WAMS in Japan [29].

2.4 REFERENCES

[1] J. Arrillaga, N. R. Watson, and S. Chen, *Power System Quality Assessment*, 1st ed., John Wiley & Sons, UK, Chapter 2, pp. 19-48, 2000.

[2] Council of European Energy Regulators (CEER), CEER Benchmarking Report 6.1 on the Continuity of Electricity and Gas Supply, 2018.

[3] P. Kundur, *Power System Stability and Control*, 1st ed., McGraw-Hill, USA, Chapter 1, pp. 3-16, 1993.

[4] L. Wehenkel, D. Ruiz-Vega, D. Ernst, and M. Pavella, *Preventive and Emergency Control of Power Systems* In *Real-Time Stability in Power Systems: Techniques for Early Detection of the Risk of Blackout*, S. C. Savulescu (ed.), 2nd ed., pp. 199-232, Wiley IEEE press, USA, 2014.

[5] L. H. Fink and K. Carlsen, Operating under stress and strain, *IEEE Spectrum*, vol. 15, no. 3, pp. 48-53, 1978.

[6] A. G. Phadke and J. S. Thorp, *Synchronized Phasor Measurements and Their Applications*, 1st ed., Supringer, USA, Chapter 1, pp. 3-27, 2008.

[7] B. Appasani and D. K. Mohanta, A review on synchrophasor communication system: communication technologies, standards and applications, *Protection and Control of Modern Power Systems*, vol. 3, no. 1, pp. 1-17, 2018.

[8] J. H. Chow (ed.), L. Beard, M. Patel, P. Quinn, A. Silverstein, D. Sobajic, and L. Vanfretti, Guidelines for Siting Phasor Measurement Units, *NASPI RITT Report*, 2011.

[9] Y. Matsukawa, H. Takahashi, M. Watanabe, and Y. Mitani, Optimal placement and tuning approach for design of power system stabilizers and wide area damping controllers, *IFAC Workshop on Control Applications of Optimization* (IFAC CAO 2018), Yekaterinburg, Russia, 2018.

[10] Y. Chompoobutrgool and L. Vanfretti, Using PMU signals from dominant paths in power system wide-area damping signal, *Sustainable Energy, Grids and Networks*, vol. 4, no. 1, pp. 16-28, 2015.

[11] E. Klinginsmith, R. Barella, X. Zhao, and S. Wallace, Unsupervised clustering on PMU data for event characterization on smart grid, *5th International Conference on Smart Cities and Green ICT Systems* (SMARTGREENS 2016), Rome, Italy, 2016.

[12] H. A. Tokel, R. A. Halaseh, G. Alirezaei, and R. Mathar, A new approach for machine learning-based fault detection and classification in power systems, *2018 IEEE PES Innovative Smart Grid Technologies* (ISGT 2018), Washington DC, USA, 2018.

[13] M. P. Razanousky, S. Lee, and L. Min, Real-time applications of phasor measurement units (PMU) for visualization, reactive power monitoring and voltage stability protection, *The New York State Energy Research and Development Authority* (NYSERDA) final report, 2010.

[14] H. Bevrani, M. Watanabe, and Y. Mitani, *Power System Monitoring and Control*, 1st ed., John Wiley & Sons, USA, Chapter 3, pp. 26-41, 2014.

[15] Khairudin and Y. Mitani, Synchrophasor measurement based small signal stability assessment using FFT-CWT approach in Japan-Campus-WAMS, *5th IEEE PES Innovative Smart Grid Technologies 2014* (IEEE PES ISGT 2014), Istanbul, Turkey, 2014.

[16] D. Despa, Y. Mitani, M. Watanabe, and C. Li, PMU based monitoring and estimation of inter-area power oscillation for Singapore-Malaysia interconnection power system, *2010 International Power Engineering Conference* (IPEC 2010), Singapore, 2010.

[17] F. Senesoulin, K. Hongesombut, and S. Dechanupaprittha, Estimation of dominant power oscillation mode using LSTM-RNN based on synchrophasor data, *2019 IEEE International Conference on Environment and Electrical Engineering and 2019 IEEE Industrial and Commerical Power Systems Europe* (EEEIC / I&CPS Europe), Genova, Italy, 2019.

[18] M. Watanabe, M. Yamashita, and Y. Mitani, Wide area measurements based robust power system controller design, *18th Power Systems Computation Conference* (PSCC 2014), Wroclaw, Poland, 2014.

[19] X. Wang, J. Bialek, and K. Turitsyn, PMU-based estimation of dynamic state Jacobian matrix and dynamic system state matrix in ambient conditions, *IEEE Transactions on Power Systems*, vol. 33, no. 1, pp. 681-690, 2017.

[20] M. L. Othman, I. Aris, and N. I. A. Wahab, Modeling and simulation of industrial numerical distance relay aimed at knowledge discovery in resident event report, *Simulation: Transactions of Society for Modeling and Simulation International*, vol. 90, no. 6, pp. 660-686, 2014.

[21] M. G. Adamiak, A. P. Apostolov, M. M. Bergovic, C. F. Henville, K. E. Martin, G. L. Michel, A. G. Phadke, and J. S. Thorp, Wide area protection – technology and infrastructures, *IEEE Transactions on Power Delivery*, vol. 21, no. 2, pp. 601-609, 2006.

[22] M. Begovic, D. Novosel, D. Karlsson, C. Henville, and G. Michel, Wide-area protection and emergency control, *IEEE PES Power Systems Conference and Exposition* (IEEE PES PSCE 2004), New York, NY, USA, 2004.

[23] W. Sattinger, Application of PMU measurements in Europe TSO approach and experience, *2011 IEEE Trondheim PowerTech*, Trondheim, Norway, 2011.

[24] P. Overholt, D. Ortiz and A. Silverstein, Synchrophasor technology and the DOE: exciting opportunities lie ahead in development and deployment, *IEEE Power and Energy Magazine*, vol. 13, no. 5, pp. 14-17, 2015.

[25] C. Lu, X. Wu, and H. Sun, Advancing China's smart grid: phasor measurement units in a wide-area management system, *IEEE power and Energy Magazine*, vol. 13, no. 5, pp. 60-71, 2015.

[26] Y. Mitani, Power system observation by using synchronized phasor measurements as a smart device, *IEEJ Transactions on Power and Energy*, vol. 130, no. 9, pp. 791-794, 2010. (in Japanese)

[27] Y. Mitani, T. Kudo, A. Satake, and K. H. Basri, Monitoring the wide area power system dynamics by phasor measurement units based on Campus WAMS strategy, *19th IFAC World Congress*, Cape Town, South Africa, 2014.

3 Optimal PMU Placement Problem and State Estimation

3.1 Power System State Estimation

3.1.1 Static State Estimation

Electric power is indispensable in our life, and is provided by utility with a certain level of the security. In recent power systems, the system operation which is possibly close to the stability limit due to a lot of installation of RES forces the system planning and operation consider to improve the security level. To implement and initiate the aforementioned security control actions in the Chapter 2, SE which gives inputs to the security control actions is indispensable technique. From the past to the present, static SE has been performed in power systems to understand the system state i.e. complete and consistent power system network representation, for the following security control actions [1]. Static SE provides snapshots of the power system state assigned from the measurement data involving errors which are obtained by meters installed at the system substations, and its significance has been recognized with the concept of WAMS in smart grid.

Fig. 3.1 shows adopted and edited conceptual SE process based on some articles and books, considering the theory and the practice [1][2][3]. There are two types of information obtained by meters: analog measurements and Circuit Breaker (CB) status. The former provides the telemetered values of power system quantities

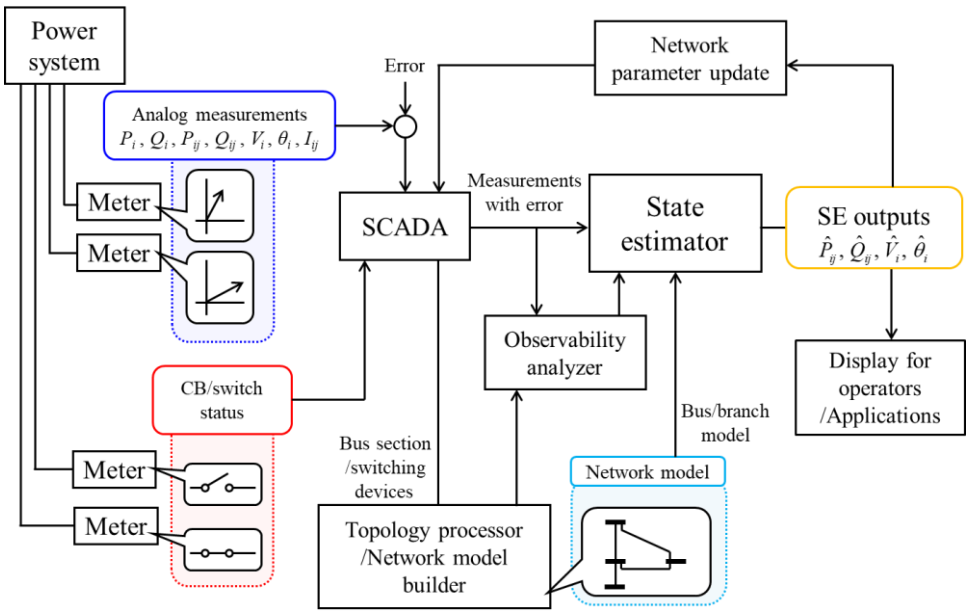

Fig. 3.1 Theoretical and practical SE process.

such as power flows, power injections, voltage magnitudes, phase angles and current magnitudes. The latter indicates the bus connection information represented by close/open states. SCADA system aggregates these values and gives each network function. SE is performed on a bus/branch model of the same type that is used in power flow calculations. The topology processer (network model builder) transforms the bus-section/switching-devices model which is the physical level representation into the bus/branch network model [1]. Observability analyzer determines whether the measurements are sufficient to carry out the SE. The observability analysis is executed on voltages at bus-sections and flows in switching devices, and if their values can be computed from the available measurements, they are considered to be observable [1]. Finally, the system state is obtained by SE using the processed measurements and results from the topology processer. The estimated system state may be used for OPF, security assessment, fault analysis, stability analysis, etc., depending on the systems operation policy [2][3]. If the estimated network model has a redundant meter coverage, bad data processing may be performed and the corrected network model is given through the network parameter update function block [1][3].

The origin of general SE can be traced to WLS and its attempt to obtain a correct state of measurements including the random error of the system. Its practical application has begun with prediction of a suborbital flight of a military missile, satellite orbit and so on. In a similar way, the power system is the time varying system, SE has been practically applied as of 1969 introduced by Schweppe et al. [4]. In this chapter, theoretical methods of power system SE and the surrounding necessities as power system observability and measurement types, and single/multi objective OPP formulation considering accuracy improvement of static SE are introduced.

3.1.1.1 Conventional State Estimation

Conventional SE also known as SCADA SE has been the still major methodology in the power system SE. SCADA SE is introduced with the simple WLS problem. SCADA SE estimates the state vector by the measurement vector consists of measured bus voltage magnitudes, active/reactive power injections and active/reactive power flows, collected by RTUs. There is no phasor measurements in SCADA SE since every quantity is collected without time synchronization. The state vector includes the voltage magnitudes and phase angles at all buses may be represented by rectangular coordinates. For given set of measurements, the measurement equation is given by [5]:

$$\mathbf{z} = \mathbf{h}(\mathbf{x}) + \boldsymbol{\varepsilon} \tag{3.1}$$

where $\mathbf{z}$ is a measurement vector, $\mathbf{x}$ is a state vector, $\mathbf{h}(\mathbf{x})$ is a nonlinear function with regard to the state vector, $\boldsymbol{\varepsilon}$ is a measurement error vector. Assume that errors are independent and identically distributed with zero mean, that is:

$$E\{\boldsymbol{\varepsilon}\} = 0,\ E\{\boldsymbol{\varepsilon}\boldsymbol{\varepsilon}^T\} = \mathbf{R} \tag{3.2}$$

where operator $E\{\cdot\}$ is the expectation value of $\cdot$, $\mathbf{R}$ is a covariance matrix of measurement error. $\mathbf{R}$ is represented by:

$$\mathbf{R} = \begin{bmatrix} \sigma_1^2 & 0 & \cdots & 0 \\ 0 & \sigma_2^2 & \ddots & \vdots \\ \vdots & \ddots & \ddots & 0 \\ 0 & \cdots & 0 & \sigma_{nm}^2 \end{bmatrix} \tag{3.3}$$

where σ_k is standard deviation of the kth measurement error, nm is the number of measurements. In order to find the optimal solution that holds the minimum measurement error, WLS equation is constructed as follows:

$$J(\mathbf{x}) = [\mathbf{z} - \mathbf{h}(\mathbf{x})]^T \mathbf{R}^{-1} [\mathbf{z} - \mathbf{h}(\mathbf{x})] . \tag{3.4}$$

Here, $\mathbf{h}(\mathbf{x})$ is the nonlinear function for $\mathbf{x}$, (3.1) is linearly-approximated as $\mathbf{h}(\mathbf{x})$ about $\mathbf{x}_k$, the value of $\mathbf{x}$ at the last iteration,

$$\mathbf{h}(\mathbf{x}) = \mathbf{h}(\mathbf{x}_k) + \mathbf{H}(\mathbf{x} - \mathbf{x}_k) \tag{3.5}$$

where, $\mathbf{H}$ is a Jacobian matrix calculated by taking first partial derivatives of the elements of $\mathbf{h}$ respect to the components of $\mathbf{x}$ evaluated at $\mathbf{x}_k$. Here, the linearized observation equation is as follows:

$$\Delta\mathbf{z} = \mathbf{H}\Delta\mathbf{x} + \boldsymbol{\varepsilon} \tag{3.6}$$

where,

$$\Delta\mathbf{x} = \mathbf{x} - \mathbf{x}_k , \tag{3.7}$$

$$\Delta\mathbf{z} = \mathbf{z} - \mathbf{h}(\mathbf{x}_k) . \tag{3.8}$$

From (3.6), (3.7) and (3.8), the linearized WLS equation which minimizes the measurement error is represented as follows:

$$J(\Delta\mathbf{x}) = [\Delta\mathbf{z} - \mathbf{H}\Delta\mathbf{x}]^T \mathbf{R}^{-1} [\Delta\mathbf{z} - \mathbf{H}\Delta\mathbf{x}] . \tag{3.9}$$

WLS method finds the optimal solution which holds the minimum estimation error of $\Delta\hat{\mathbf{x}}$ by minimizing (3.9) that is square error of the difference between the measurement values and the estimated values, assuming that the variance of measurement errors of meters are weights. The estimation value $\Delta\hat{\mathbf{x}}$ is the residue of estimated state vector obtained by iterative calculation of following equation:

$$\Delta\hat{\mathbf{x}} = (\mathbf{H}^T \mathbf{R}^{-1} \mathbf{H})^{-1} \mathbf{H} \mathbf{R}^{-1} \Delta\mathbf{z} . \tag{3.9}$$

In (3.9), by the iterative calculation, k+1th estimation value is given as follows:

$$\hat{\mathbf{x}}_{k+1} = \mathbf{x}_k + \Delta\hat{\mathbf{x}}_k . \tag{3.10}$$

To finish the iterative calculation, a convergence criterion φ is introduced. WLS obtains the estimation value as of satisfaction of following condition:

$$\max\left|\Delta\hat{\mathbf{x}}\right| \le \varphi \,. \tag{3.11}$$

A simple demonstration of SCADA SE is given as follows using IEEE Western System Coordinating Council (WSCC) 9-bus test system. The system detailed data is given in Appendix A. The single line diagram is shown in Fig. 3.2 with RTU meters placement. Here, to proceed SCADA SE in an actual example, calculation of elements of **R** is required i.e. standard deviation (standard uncertainty) is introduced. Given that the maximum measurement uncertainty is provided by the meter manufactures, the standard uncertainty in a measurement can be expressed in

$$u(\mathbf{p}(k)) = \frac{\Delta\mathbf{p}(k)}{\sqrt{3}} \tag{3.12}$$

where $\Delta\mathbf{p}(k)$ is a maximum uncertainty specified by the device manufacturer in the measurement $\mathbf{p}(k)$. Here, the probability distribution of measurement uncertainty is assumed as uniform distribution [6]. The standard uncertainty of measurement $\mathbf{p}(k)$ can be approximated by the standard deviation:

$$u(\mathbf{p}(k)) = \sigma_{\mathbf{p}(k)} \,. \tag{3.13}$$

Then, **R** can be constructed by (3.3) [7]. Note that the measurement uncertainties have zero mean and are independent. The maximum measurement uncertainties are given in Table 3.1 referring to an article by Valverde et al. [8]. In this demonstration, meters are placed to satisfy the numerical observability given in the later section.

The demonstration employs Newton-Raphson power flow calculation method and sets its results for the true value of the state vector. Since the state vector consists of bus voltage magnitudes and bus voltage phase angles, the WLS equation (3.4) is represented as follows:

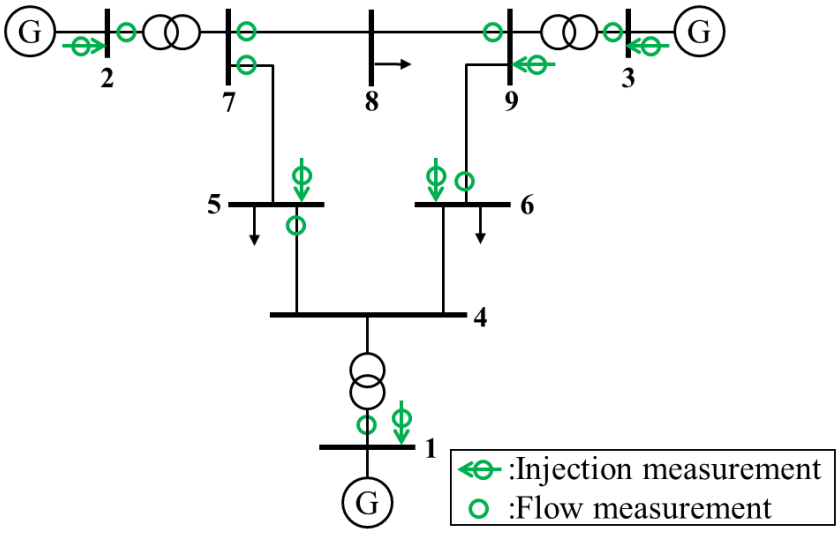

Fig. 3.2 WSCC 9-bus test system single line connection diagram with RTUs.

Table 3.1 Measurement uncertainties for conventional measurement quantities.

Quantity	Maximum Measurement Uncertainty
Voltage magnitude	0.2 %
Power injection	2 %
Power flow	2 %

$$J\left(\begin{bmatrix}\mathbf{V}\\ \boldsymbol{\theta}\end{bmatrix}\right)=\left[\begin{pmatrix}\begin{bmatrix}\mathbf{V}\\ \mathbf{z_P}\\ \mathbf{z_Q}\end{bmatrix}\end{pmatrix}-\mathbf{h}\left(\begin{bmatrix}\mathbf{V}\\ \boldsymbol{\theta}\end{bmatrix}\right)\right]^T\mathbf{R}^{-1}\left[\begin{pmatrix}\begin{bmatrix}\mathbf{V}\\ \mathbf{z_P}\\ \mathbf{z_Q}\end{bmatrix}\end{pmatrix}-\mathbf{h}\left(\begin{bmatrix}\mathbf{V}\\ \boldsymbol{\theta}\end{bmatrix}\right)\right] \tag{3.14}$$

where $\mathbf{V}$, $\boldsymbol{\theta}$, $\mathbf{z_P}$ and $\mathbf{z_Q}$ are vectors for bus voltages, bus voltage phase angle difference from the reference phase angle, active power injection/flow measurements, and reactive power injection/flow measurements, respectively. Taking through the same path from (3.4) to (3.9), the linearized iterative equation is given by follows:

$$\begin{bmatrix}\Delta\mathbf{V}\\ \Delta\boldsymbol{\theta}\end{bmatrix}=(\mathbf{H}^T\mathbf{R}^{-1}\mathbf{H})^{-1}\mathbf{H}^T\mathbf{R}^{-1}\begin{bmatrix}\Delta\mathbf{V}\\ \Delta\mathbf{z_P}\\ \Delta\mathbf{z_Q}\end{bmatrix} \tag{3.15}$$

where the operator Δ works as (3.7) and (3.8). Then $\mathbf{R}$ is constructed as (3.3) by putting measurement standard deviations calculated by (3.12) into corresponding positions of the matrix. Measurement Jacobian $\mathbf{H}$ is built by derivative calculations. Giving the SE convergence criterion $\varphi=1.0\times10^{-4}$, SCADA SE is carried out. Fig. 3.3 shows the convergence of $\max|\Delta\hat{\mathbf{x}}|$. The maximum value of estimated state residue converged at 3rd iteration judged by (3.11). Fig. 3.4 (a) and (b) show the errors of both bus voltage magnitudes and angles. These figures show error between

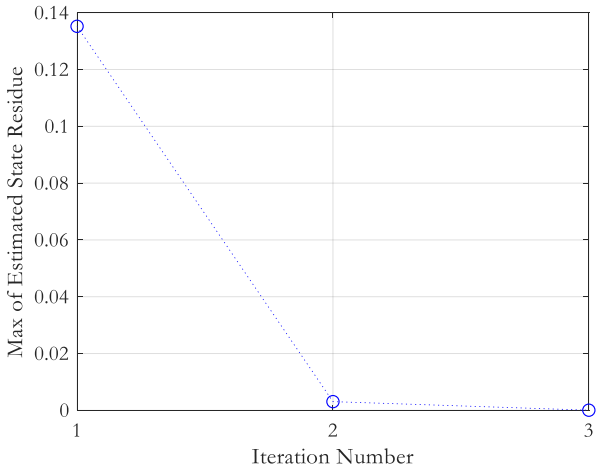

Fig. 3.3 Convergence of $\max|\Delta\hat{\mathbf{x}}|$.

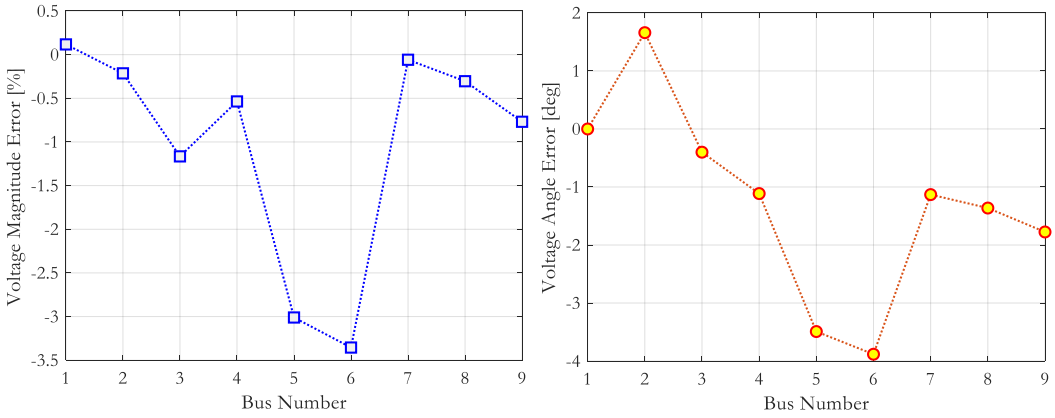

(a) Voltage magnitude (b) Voltage angle

Fig. 3.4 Estimation error of voltage magnitude and angle.

true value and estimated value obtained by SCADA SE. In this case, the reference bus is set to bus 1, and its phase angle is set to 0 deg. It is assumed that the RTU voltage magnitude meter is placed at bus 1 and its reference angle is ideally obtained since bus 1 is the slack bus.

3.1.1.2 Phasor State Estimation

PSE only consists of PMUs as the measurement device. Also, PSE is linear SE and does not require the iterative calculation because the relationship between the measurement vector which include voltage/current phasor and the state vector through Jacobian matrix is linear. The observation equation (3.1) can be written by linear form as follows [5]:

$$\mathbf{z} = \mathbf{H}\mathbf{x} + \boldsymbol{\varepsilon}\,, \tag{3.16}$$

As well as SCADA SE, the measurement error covariance **R** is constructed by (3.3), the state vector can be obtained as follows:

$$\hat{\mathbf{x}} = (\mathbf{H}^T\mathbf{R}^{-1}\mathbf{H})^{-1}\mathbf{H}^T\mathbf{R}^{-1}\mathbf{z}\,. \tag{3.17}$$

(3.17) is simply solved by substitution of the corresponding values. Compared to SCADA SE. In linear SE, the solution is obtained in a single iteration, the risk of divergence in the presence of bad data can be avoided if the measurement redundancy is sufficient.

A simple demonstration of PSE is given in this section. Fig. 3.5 shows a simple 4 bus test system just made for this example. Let the line admittance of line *i*-*j* y_{ij}, and shunt admittance of bus *i* y_{i0}, considering π-type transmission model. According to the linear observation equation, the elements of Jacobian matrix, state, measurement and error vector are represented by follows:

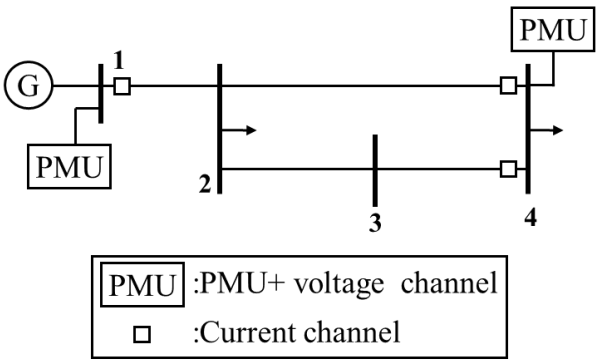

Fig. 3.5 A 4-bus test system for PSE and meter placement.

$$\begin{bmatrix} V_1 \\ V_4 \\ I_{12} \\ I_{42} \\ I_{43} \end{bmatrix} = \begin{bmatrix} 1 & 0 & 0 & 0 \\ 0 & 0 & 0 & 1 \\ y_{12}+y_{10} & -y_{12} & 0 & 0 \\ 0 & -y_{24} & 0 & y_{24}+y_{40} \\ 0 & 0 & -y_{34} & y_{24}+y_{40} \end{bmatrix} \begin{bmatrix} V_1 \\ V_2 \\ V_3 \\ V_4 \end{bmatrix} + \begin{bmatrix} \varepsilon_{V_1} \\ \varepsilon_{V_4} \\ \varepsilon_{I_{12}} \\ \varepsilon_{I_{42}} \\ \varepsilon_{I_{43}} \end{bmatrix} \tag{3.18}$$

where the subscripts of the ε indicates the measurement error of the corresponding measurement quantity. V, I and y as complex values are simplified on the equation. Now the state vector is 4×1 vector, the Jacobian matrix is 5×4 matrix, the measurement and the error vectors are 5×1 vectors. Bus 2 has redundant measurement. In PSE, the measurement error is very small, measurement error vector may be ignored. However, in frequent use of pseudo measurements, because measurement uncertainty propagation may occur, it is necessary to be assessed. The Jacobian matrix includes mixed elements, (3.16) can be also written as follows [5]:

$$\mathbf{z} = \begin{bmatrix} \mathbf{I} \\ \mathbf{yA} + \mathbf{y_s} \end{bmatrix} \mathbf{x} + \boldsymbol{\varepsilon} \ , \tag{3.19}$$

where **A** is matrix includes only zeros or positive/negative ones. **y** is the line admittance matrix, $\mathbf{y_s}$ is the shunt admittance matrix.

3.1.1.3 Hybrid State Estimation

Generally, HSE employs different type of measurements which are RTUs and PMUs, and assumes that both are placed in a system. HSE is basically performed and considered for the maximum use of measurement devices in the system and reduction of meter placement cost. There have been several types of HSE methods: aggregation of conventional and synchronized measurements into the measurement vector [8], two stage HSE which performs PSE firstly with flat start and SCADA SE secondly with estimated states of the first stage and the available conventional measurements [9], two stage HSE which performs SCADA SE firstly and PSE secondly with estimated states of the first stage and additional synchronized measurements [10]. This research employs the method proposed by Jerin and Bindu [10], may be called SCADA SE-first PSE-second HSE. Since this two stage method begins from the SCADA SE, there are advantages. First, the method does not need

to begin with the flat start. Second, the method can ensure the observability at the first stage of HSE by conventional meters. This indicates the network observability redundancy can be supported by the redundant placements of the conventional measurements only. Thus, the total placement costs can relatively be reduced compared to the redundant placement of PMUs.

SCADA SE-first PSE-second HSE can be processed by overlapping the synchronized measurements on the complete estimated state by SCADA SE at the first stage. The modified observation equation is given by follows:

$$\mathbf{z}' = \mathbf{H}'\mathbf{x} + \boldsymbol{\varepsilon}' \tag{3.20}$$

$$\mathbf{z}' = \begin{bmatrix} \mathbf{V}_R^{SCADA} \\ \mathbf{V}_I^{SCADA} \\ \mathbf{V}_R^{PMU} \\ \mathbf{V}_I^{PMU} \end{bmatrix} = \begin{bmatrix} \mathbf{H}_{11} & \mathbf{H}_{12} \\ \mathbf{H}_{21} & \mathbf{H}_{22} \\ \mathbf{H}_{31} & \mathbf{H}_{32} \\ \mathbf{H}_{41} & \mathbf{H}_{42} \end{bmatrix} \begin{bmatrix} \mathbf{V}_R \\ \mathbf{V}_I \end{bmatrix} + \begin{bmatrix} \boldsymbol{\varepsilon}_R^{SCADA} \\ \boldsymbol{\varepsilon}_I^{SCADA} \\ \boldsymbol{\varepsilon}_R^{PMU} \\ \boldsymbol{\varepsilon}_I^{PMU} \end{bmatrix} \tag{3.21}$$

where superscripts *SCADA* and *PMU* mean the obtained measurement in SCADA SE and the inherent measurement by PMUs, respectively. Subscripts *R* and *I* indicate the real and imaginary parts of the complex quantities, respectively. Sets of measurement Jacobian from $\mathbf{H}_{11}$ to $\mathbf{H}_{42}$ are matrices which all the elements are 0 or 1. For simplification of HSE, the current measurements are used to compute pseudo voltage measurements, thus elements of $\mathbf{H}'$ are transformed into binary values [11]. Additionally, the set of measurement error vectors $\boldsymbol{\varepsilon}$ is originally calculated from the polar form quantities, so it is transformed into the rectangular form and divided into the real and imaginary parts. As well as PSE, since the observation equation (3.20) is linear, the state vector can be directly estimated as follows:

$$\hat{\mathbf{x}} = (\mathbf{H}'^{T}\mathbf{R}'^{-1}\mathbf{H}')^{-1}\mathbf{H}'^{T}\mathbf{R}'^{-1}\mathbf{z}' \,. \tag{3.22}$$

Then, $\mathbf{R}'$ is

$$\mathbf{R}' = \begin{bmatrix} (\sigma_1^{SCADA})^2 & 0 & \cdots & 0 \\ 0 & \ddots & & \\ & & (\sigma_{nx}^{SCADA})^2 & \vdots \\ \vdots & & (\sigma_1^{PMU})^2 & \\ & & & \ddots \quad 0 \\ 0 & \cdots & 0 & (\sigma_{nmPMU}^{PMU})^2 \end{bmatrix} = \begin{bmatrix} \mathbf{R}^{SCADA} & 0 \\ 0 & \mathbf{R}^{PMU} \end{bmatrix} \tag{3.23}$$

where *nx* is the number of states i.e. the length of the state vector, *nmPMU* is the number of PMU measurements. Diagonal covariance matrix of state vector estimated in SCADA SE $\mathbf{R}^{SCADA}$ is obtained as following procedure [12]. After

obtaining the estimated state $\hat{\mathbf{x}}$ by solving nonlinear SE WLS given by (3.1)-(3.11), the inverse of the gain matrix $\mathbf{G}=\mathbf{H}^T\mathbf{R}^{-1}\mathbf{H}$ arising in the last iteration (if WLS converged) provides the covariance matrix of the estimated state vector,

$$\mathrm{cov}\{\hat{\mathbf{x}}\} = \mathbf{G}^{-1} \tag{3.24}$$

where operator cov{·} is the covariance of ·. The estimated state vector $\hat{\mathbf{x}}$ is transformed to rectangular coordinates through a nonlinear function *f* given by:

$$\hat{\mathbf{x}}_r = f(\hat{\mathbf{x}}_p) \tag{3.25}$$

where subscripts *p* and *r* indicate the polar and rectangular form. The original form of the state vector is polar, $\hat{\mathbf{x}}_p = \hat{\mathbf{x}}$. The nonlinear functions $f(\cdot)$ represent the relationships,

$$\hat{V}_R = \hat{V}\cos(\hat{\theta}) \ , \tag{3.26}$$

$$\hat{V}_I = \hat{V}\sin(\hat{\theta}) \ . \tag{3.27}$$

To obtain the covariance of the estimated state in the rectangular form, the transformation is performed as follows:

$$\mathrm{cov}\{\hat{\mathbf{x}}_r\} = \mathbf{I}\cdot\mathrm{diag}\{F\cdot\mathrm{cov}\{\hat{\mathbf{x}}_r\}\cdot F^T\} \tag{3.28}$$

where *F* is the Jacobian of $f(\cdot)$ computed for $\hat{\mathbf{x}}_r$. Finally, $\mathbf{R}^{SCADA}$ is obtained as follows:

$$\mathbf{R}^{SCADA} = \mathrm{cov}^{-1}\{\hat{\mathbf{x}}_r\} \ . \tag{3.29}$$

$\mathbf{R}^{PMU}$ is obtained by the same manner as (3.2) and (3.3), however, the coordinate transformation is performed by (3.26) and (3.27) from the polar to the rectangular coordinate.

According the demonstration in the section 3.1.1.1 using WSCC 9-bus test system, SCADA SE-first PSE-second HSE is carried out with synchronized measurements added. Fig. 3.6 shows the meter placement on the test system diagram. Also, maximum measurement uncertainty is given in Table 3.2. After SCADA SE by (3.15), the final estimates are transformed from the polar to the rectangular coordinate and construct $\mathbf{V}^{SCADA}$. Since the system is observable by RTUs, the full state vector (all bus voltage phasors) are obtained. Regarding the covariance matrix $\mathbf{R}^{SCADA}$, the coordinate transformation is carried out based on the final value of **G**. Now, since a PMU is placed at bus 6 with current channel on line 6-4, voltage phasor measurements at buses 6 and 4 are obtained via direct and pseudo measurements, respectively. These measurement and error vectors are transformed into the rectangular coordinate, and construct $\mathbf{V}^{PMU}$ and $\mathbf{R}^{PMU}$. Finally, combining both quantities obtained by SCADA SE and synchronized measurements and building $\mathbf{H}'$, (3.21) is established. Fig. 3.7 shows the estimation error in both of SCADA SE and HSE. It is obviously found that the estimation

errors of state in buses that are estimated by PMU measurements are very accurate. Now, parts of the results of SCADA SE are altered by injecting a few PMU measurements.

3.1.2 Dynamic State Estimation

By virtue of PMU's accurate and high resolution of phasor measurement, the concept of dynamic state tracking [13] has been realized. It is assumed that the state of the system can be modeled as following mathematical model:

$$\mathbf{x}(t+\Delta t) = \mathbf{x}(t) + \mathbf{w}(t)$$
$$\mathbf{z}(t) = \mathbf{H}\mathbf{x}(t) + \boldsymbol{\varepsilon}(t) \tag{3.30}$$

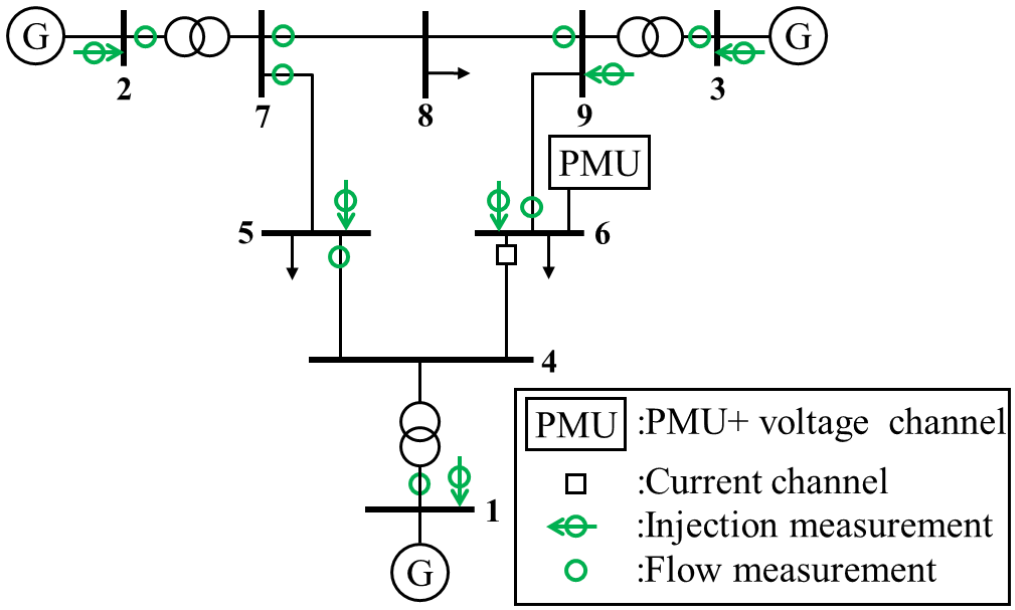

Fig. 3.6 WSCC 9-bus test system single line connection diagram with RTUs and PMUs.

Table 3.2 Measurement uncertainties for conventional and synchronized measurement quantities.

Classification	Quantity	Maximum Measurement Uncertainty
Conventional measurement	Voltage magnitude	0.2 %
	Power injection	2 %
	Power flow	2 %
Synchronized measurement	Voltage magnitude	0.02 %
	Current magnitude	0.03 %
	Phase angle	0.01 deg

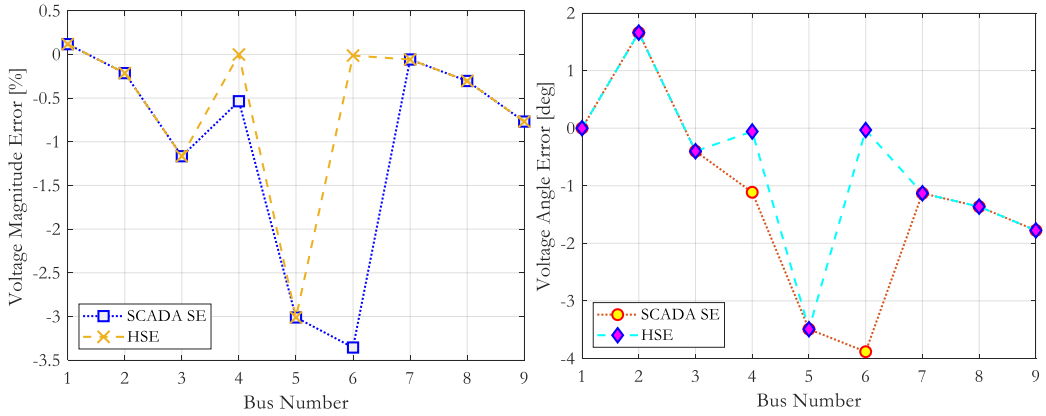

(a) Voltage magnitude (b) Voltage angle

Fig. 3.7 Estimation error of voltage magnitude and angle in SCADA SE and HSE.

where t is time , Δt is the time step, $\mathbf{w}(t)$ is a random change of the power system state. $\mathbf{w}(t)$ and $\boldsymbol{\varepsilon}(t)$ are modeled as zero mean, independent and Gaussian process, then the problem is essentially a Kalman filter problem. Hence, there has been many paper applied Kalman filter technique to this problem [14]. Nowadays, since Kalman filter technique is depending on the linearization resulting in a modeling error, data-driven dynamic SE based on machine learning such as ANN [15], and fuzzy logic based techniques [16] have been applied, with advancement of software computing technologies.

3.2 POWER SYSTEM OBSERVABILITY

3.2.1 Types of Observability

To carry out SE, the system needs to be observable by sufficient measurements well distributed throughout the system. If enough measurements are available to make the SE possible to be performed, the network is considered to be observable [17]. There are two major observability analyses: topological observability and numerical observability.

3.2.1.1 Topological Observability

Topological observability can be identified by graph theory approach, through the type and location of the measurements in the entire system [18]. In the observability analysis, the types of measurement (conventional or synchronized measurements) are separately considered. In topological observability, N-bus power system network can be reckoned as a non-oriented graph $G=(V,E)$ where V is a set of graph vertices (all system nodes) and E is a set of graph edges (all system branches). An N-bus system network is topological observable if at least one spanning measurement tree of full rank exists in the network [18]. In synchrophasor measurement based topological observability, a spanning measurement tree is a loop-free graph which connects all the nodes through branches with a metered or calculated current phasor assigned to each of them [19]. Search of the spanning measurement tree can be easily implemented by PMU direct/pseudo measurements explained in the later subsection. In recent consideration of topological

observability, in order to reduce the total placement cost including the infrastructure associated with SPCS by wired optic cables, Girish et al. applied Prim's algorithm to find the minimum spanning measurement tree for minimization of the distance between placed PMUs, treating a power system as an weighted non-oriented graph [20]. Fig. 3.8 depicts the concept of topological observability. Fig. 3.8 (a) shows the single line connection diagram of IEEE 14-bus test system and a PMU placement on it. The meaning of icons are reflected from Figures 3.5 and 3.6. Fig. 3.8 (b) is the non-oriented graph and the spanning measurement tree which is built by red line. The red line is drawn by connecting voltage phasor obtained by PMU direct/pseudo measurement.

3.2.1.2 Numerical Observability

While topological observability is based on the graph theory, numerical (algebraic) observability is achieved by checking the rank of Jacobian matrix **H** in the observation equation (3.6) [19]. This indicates that numerical observability is defined as the ability of the system model represented by the observation equation to be solved for SE. The system is numerically observable if Jacobian matrix **H** is full rank and well-conditioned [19]. Numerical observability implies topological observability, but the converse does not hold. Thus, in terms of practical utility, achieving numerical observability by a proper allocation of meters is of importance. This research considers to carry out the SE calculation, thus the meters are placed to satisfy the numerical observability. There have been several methodologies to check numerical observability in power systems. Gou and Abur proposed an algebraic method that uses the triangular factors of singular, symmetric gain matrix to determine the observable islands of a measured power system [21].

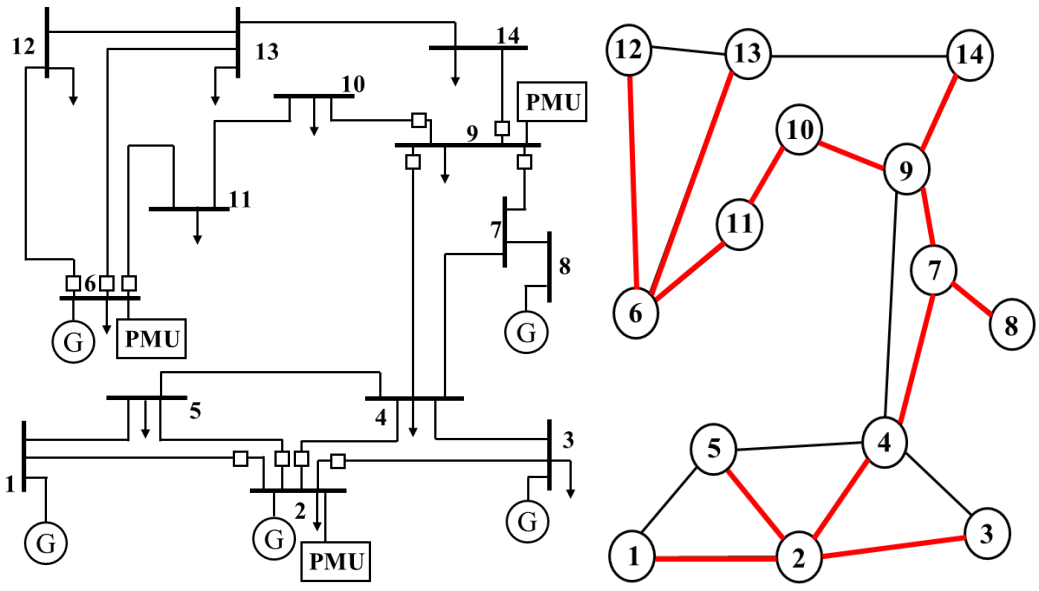

(a) System diagram and the PMU placement

(b) Equivalent non-oriented graph representation and the spanning measurement tree

Fig. 3.8 A topologically observable PMU placement in IEEE 14-bus system.

3.2.2 Types of PMU Measurement

In PSE or HSE, since these methods use the PMU measurements, the several types of measurements are to be introduced for the system topological/numerical observability.

3.2.2.1 Direct Measurement

As aforementioned in Chapter 2, a PMU has voltage and current measurement channels to measure their phasor quantities. Thus, a PMU can obtain the voltage phasor data at the bus (substation) where the PMU is placed and the current phasor data on the line incident to the bus with current measurement channel. Fig. 3.9 shows the example of the direct measurement and measured voltage/current phasors.

3.2.2.2 Pseudo Measurement

Pseudo measurement is a quantity which is obtained by calculation using other quantities such as direct/pseudo measurements. Direct measurement is directly measured value whereas pseudo measurement is indirectly obtained value. The factors determining the pseudo measurement are line admittance and/or voltage/current measurements, and it is generally obtained through electric circuit principles as Kirchhoff's laws and the Zero Injection Bus (ZIB) also known as the floating bus.

First, voltage pseudo measurement via voltage/current measurement is obtained based on calculated by π-model transmission line depicted in Fig. 3.10, as follows:

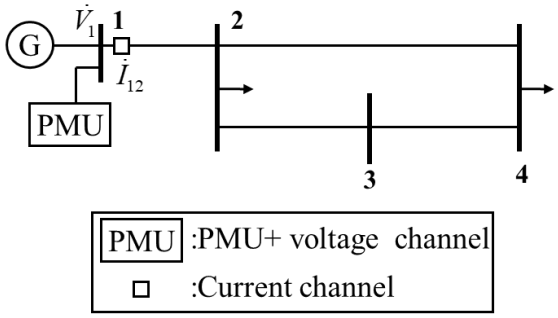

Fig. 3.9 An example of direct measurement on 4-bus test system.

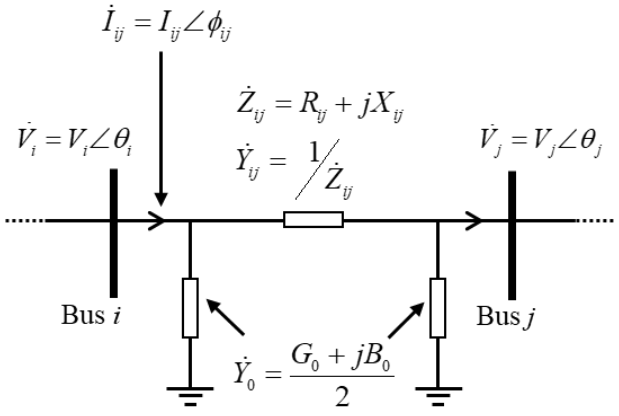

Fig. 3.10 π-model transmission line.

$$\dot{V}_j = \frac{\dot{V}_i(\dot{Y}_0 + \dot{Y}_{ij}) - \dot{I}_{ij}}{\dot{Y}_{ij}} \tag{3.31}$$

where $\dot{V}$, $\dot{I}$ and $\dot{Y}$ indicate the bus voltage phasor, line current phasor and admittance, respectively, subscripts *i* and *j* indicate the bus numbers, when those are seriated, that means the line between buses *i* and *j*. The subscript 0 means shunt component. As a pseudo measurement, (3.31) indicates that the voltage phasor at a bus and current phasor on the incident line are known by PMUs, the adjacent bus voltage connected by that line can be observed.

Second, current pseudo measurement on line is given by a variation of expression (3.31) as following equation:

$$\dot{I}_{ij} = \dot{V}_i\dot{Y}_0 + (\dot{V}_i - \dot{V}_j)\dot{Y}_{ij} \ . \tag{3.32}$$

If voltage phasors at both ends of a line are known, the current phasor on the line becomes observable.

Third, by using ZIB which is the no load and generation injection and Kirchhoff's Current Law (KCL), a pseudo measurement is applied in a situation like Fig.3.11. If one current phasor $\dot{I}_{ij}$ is unknown and all others from $\dot{I}_{1i}$ to $\dot{I}_{li}$ are known for incident lines to ZIB *i*, the unknown current phasor can be calculated by KCL, generally represented by follows:

$$\dot{I}_{ij} = \sum_{k=1}^{l} \dot{I}_{ki} \ . \tag{3.33}$$

If voltage phasors at both ends of a line are known, the current phasor on the line becomes observable.

Using above direct/pseudo measurements, the PMU observation network can be constructed. Note that PMU measurements are obtained and the measurement network is built in accordance with these three laws.

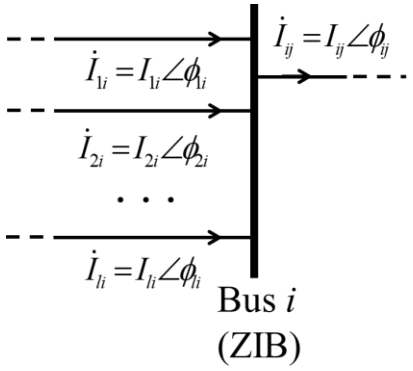

Fig. 3.11 π-model transmission line.

3.3 OPTIMAL PMU PLACEMENT PROBLEM

3.3.1 Single Objective Optimal PMU Placement Problem

OPP has begun with article by Baldwin et al. [19] who tried to minimize the number of placed PMUs in power system SE because of limited system planning budget. This subsection introduces a number of studies about OPP problem and its basic linear single objective formulation.

3.3.1.1 Literature Review

There have been several considerations and formulations in single objective OPP which minimizes the number of PMUs. In terms of mathematical optimization, OPP problem is Binary Integer Linear Programming (BILP), and most of OPP solved by BILP considers the topological observability as its constraint since the placement of PMU can be represented by a binary decision variable which only takes values 0 and 1. This BILP problem is solved using mathematical optimization toolbox or heuristic/metaheuristic methods since it is combinatorial optimization problem. The objective function is thoroughly the minimization of the number of PMUs.

In 1993, Baldwin et al. applied SA to OPP combined with BS and obtained a feasible solution in a large scale power system model [19]. Toward a satisfaction of the topological observability of entire system with a minimal number of PMUs, BS works to find the required number of PMUs and SA finds the suboptimal placement afterwards which is used as the upper bound of BS. In 2003, Marin et al. applied the simple GA to OPP with current channel capacity consideration in four of IEEE test systems [22]. However, compared to optimal solutions obtained in other articles [23][27], the simple GA-based solutions are still not the global optima because of GA's search ability in case of larger system. Xu and Abur obtained optimal solutions of OPP using TOMLAB Optimization Toolbox with or without the existence of conventional measurements (RTUs) in a power system in 2004 [23]. By this contribution, RTUs can make entire system observable easier. However, this research only focuses on the topological observability which ignores measurement error of meters because no actual SE is executed. In 2005, Nuqui and Phadke introduced the concept of "depth-of-observability" to extend the conventional OPP to solve pragmatically phased PMU installation. The authors applied SA to solve the proposed OPP with the optimal location for new communication facilities [24]. Peng et al. applied Tabu Search (TS) to OPP problem with a device that uses an augmented incidence matrix instead of the spanning measurement tree for judgement of topological observability, in order to accelerate the optimization in 2006 [25]. Jiang et al. firstly considered OPP problem to reduce the variance of SE error for distributed state estimator in 2007 [26]. In 2009, Chakrabarti and Kyriakides obtained the optimal solutions of OPP problem in IEEE 14, 30, 39-bus test systems by the exhaustive method [27]. Those solutions can be the benchmarks of the OPP problem. Sodhi et al. proposed a two-stage method to ensure the numerical observability along with the topological observability in 2010 [28]. After this era, the OPP trend tends to include other indices with multi objective optimization approach.

3.3.1.2 Basic Formulation

The main objective of the basic OPP problem is to determine the minimum number of PMUs and their appropriate placements to ensure full topological observability of a power system. The formulation is given as follows:

$$\min_{\mathbf{y}} \; w\mathbf{y}\mathbf{y}^T, \tag{3.34}$$

subject to constraints:

$$\mathbf{A}\mathbf{y}^T \geq \mathbf{b}, \tag{3.35}$$

$$\mathbf{b} = [1,...,1]^T, \tag{3.36}$$

where, vector **y** is PMU placement decision variable of size (1×*nb*), *nb* is the number of system buses:

$$\mathbf{y} = [y_1,...,y_{nb}], \tag{3.37}$$

$$y_i = \begin{cases} 1 & \text{if a PMU is placed at bus } i \\ 0 & \text{otherwise} \end{cases}, \tag{3.38}$$

matrix **A** is binary bus connectivity matrix of the system network of size (*nb*×*nb*):

$$\mathbf{A} = \begin{bmatrix} A_{11} & \cdots & A_{1nb} \\ \vdots & \ddots & \vdots \\ A_{nb1} & \cdots & A_{nbnb} \end{bmatrix}, \tag{3.39}$$

$$A_{ij} = \begin{cases} 1 & \text{if } i = j \text{ or if buses } i \text{ and } j \text{ are connected} \\ 0 & \text{otherwise} \end{cases}, \tag{3.40}$$

w is an weight coefficient scalar of PMU cost and **b** is an observation criterion vector which the all elements are 1, with size (1×*nb*).

3.3.2 Multi Objective Optimal PMU Placement Problem

As concerns of measurement redundancy to keep the power system observable against PMU losses or line contingencies, MOOPP problem has begun with an paper by Milosevic and Begovic [29]. Introduction of N−1 security for PMU and/or line outage for OPP problem has been originally conducted by Denegri et al. in 2002, its inclusion has been spread into OPP researchers [30].

3.3.2.1 Literature Review

In 2003, Milosevic and Begovic formulated MOOPP which simultaneously considers both of minimization of the number of PMUs and maximization of measurement redundancy [29]. The authors applied NSGA to the proposed MOOPP and obtained multiple Pareto solutions. Dua et al. proposed OPP problem via multistage optimization using master-slave model solved by BILP in 2008 [31].

The authors firstly minimized the number of PMUs as the master problem, and secondly maximizes the redundancy index SORI by changing the placement of PMUs as the slave problem subject to the minimum number of PMUs which is obtained at the master problem. In 2011, Ahmadi et al. applied BPSO to MOOPP which minimizes the number of placed PMUs and maximizes the measurement redundancy for PMU outages [32]. However, weighting both competing objectives into single function makes the goodness of a solution highly dependent on the determined weight coefficients which is normally difficult to set. Gomez et al. proposed a PMU measurement reliability index for single line contingencies based on a transmission line availability obtained by the historical log, in 2014 [33]. In 2016, Esmaili proposed an inclusive multi-objective PMU placement method for both minimization of placed PMUs and maximization of the measurement redundancy using fuzzy membership function in order to ensure the Pareto optimality of the solution [34]. In 2017, Tran et al. proposed a new line reliability index defined by line length, outage rate calculated from the historical data of a system and sum of power transferred on the path [35]. Also, the authors extended the non-oriented graph into the oriented graph weighted by the proposed reliability index, and obtained the minimum spanning measurement tree which indicates the most reliable path on the topologically observable network, using Prim's algorithm.

3.3.2.2 Multi Objective Optimization Approaches

In multi objective optimization, because the objectives are mutually competing, obtaining the desired solutions is more difficult compared to the single objective optimization. The main three approaches of multi objective optimization are introduced here.

The general constrained multi objective optimization (minimization) can be formulated as follows:

$$\min_{\mathbf{x}} \{ f_1(\mathbf{x}), f_2(\mathbf{x}), ..., f_K(\mathbf{x}), \} , \tag{3.41}$$

subject to constraints:

$$g_j(\mathbf{x}) \leq 0 \quad (j = 1, 2, ..., J) , \tag{3.42}$$

$$h_i(\mathbf{x}) = 0 \quad (i = 1, 2, ..., I) , \tag{3.43}$$

$$\mathbf{x} \in S , \tag{3.44}$$

where f is the K of objective functions, g is the J of inequality constraints, h is the I of equality constraints, $\mathbf{x}$ is the decision variable with n dimension. S is search space and the feasible region is $F \subseteq S$ [36]. Generally, when the number of objectives K>3, the problem is called many objective optimization problem.

Scalarization

Scalarization is performed by weighted sum of all objectives into a single objective function, and single optimal or sub-optimal solution is obtained by solving the singularized objective function [36]. Mathematically, by scalarizing (3.41) as:

$$\min_{\mathbf{x}} \sum_{i=1}^{K} w_i f_i(\mathbf{x}) , \tag{3.45}$$

where the weights of the objectives $w_i > 0$ are the parameters scalarization. In this case, the optimization engineer is required to determine those weights to obtain the solution desired by decision maker.

In other ways, to singularize the multi objective, $K-1$ of objectives can be transferred to inequality constraints when the decision maker knows and requires the acceptable maximums for objectives (ε_2, ε_3, …, ε_K) if the problem is minimization. This method is called ε-constraint method given as following objective function:

$$\min_{\mathbf{x}} f_1(\mathbf{x}) , \tag{3.46}$$

subject to constraints:

$$f_k(\mathbf{x}) \le \varepsilon_k \quad (k = 2,3,...,K) , \tag{3.47}$$

with original constraints (3.42), (3.43) and (3.44). The optimization target f_1 is preferably selected by the decision maker. In ε-constraint method, the non-dominated solutions are obtained by parametrically changing ε_i.

Priori Methods

Priori methods require that sufficient preference information is described before the optimization process. One of the several priori methods, the goal programming is introduced as an example. The goal programming is a method that targets a level of aspiration in each objective, and minimizes the difference of it [37]. The general explanation of objective function is given as follows:

$$\min_{\mathbf{x}} \left\| f(\mathbf{x}) - \hat{f} \right\| \tag{3.48}$$

where $\hat{f} = \left\{ \hat{f}_1, \hat{f}_2, ..., \hat{f}_K \right\}$ is the level of aspiration. In goal programming, the optimality of the problem highly depends on the level of aspiration set by the decision makers. Basically, goal programming requires the decision maker to know the level of aspiration before the optimization. Therefore, this method is based on decision making first, solution search second, i.e. the decision maker should have a certain insight on the problem space.

Posteriori Methods

Posteriori methods firstly find the solutions and make a decision afterwards whereas the priori methods are the converse. This methods aim at finding all the Pareto optimal solutions or a representative subset of the Pareto optimal solutions. Assuming that the all objectives are to be minimized, the general representation of Pareto optimal solution for $\mathbf{x}, \mathbf{y} \in F$ is given as follows:

$$\left[\forall i \in \{1,2,...,K\} : f_i(\mathbf{x}) \le f_i(\mathbf{y}) \right] \wedge \left[\exists j \in \{1,2,...,K\} : f_j(\mathbf{x}) < f_j(\mathbf{y}) \right]. \tag{3.49}$$

When (3.49) is satisfied, **x** dominates **y**: the solution **x** is superior to **y**. In this domination relationship, if there is no solution which is dominating **x**, **x** is called Pareto optimal solution. Therefore, Pareto optimal solution is a solution which at least one objective function value needs to be worsen in order to improve an objective function value. Also, a set of Pareto solutions is called Pareto front [38]. In multi objective optimization, there is no sole solution to dominate the everything else, obtaining the Pareto optimal front is the primary goal. Fig. 3.12 shows an example of Pareto optimality on K=2. In the figure, solutions **x** and **y** are not dominated by any other solutions according to (3.49), these are Pareto optimal solutions. A set of Pareto optimal solutions construct the Pareto front. A solution **w** is dominated by **x**, and a solution **z** is dominated by **x** and **y** in only focusing on **x**, **y**, **w** and **z**.

3.3.2.3 Basic Formulation

Inheriting equations from (3.34) to (3.40), objective function of MOOPP which minimizes the number of PMUs and maximizes SORI is given as follows:

$$\min_{\mathbf{y}} \left\{ w\mathbf{y}\mathbf{y}^T, -\sum_{i=1}^{n} \beta_i \right\}, \tag{3.50}$$

where, β_i is the number of observation at bus i by PMUs (the index BOI). Thus, its negative of the sum means maximization of SORI. There may be several form of MOOPP, to maximize the measurement redundancy for single contingencies, for both the PMU outages and single contingencies and so on. However, the minimization of the number of PMUs is consistently one of the objective. Note that MOOPP by (3.50) is out of the scope of this research, the different objective is set instead in the next chapter.

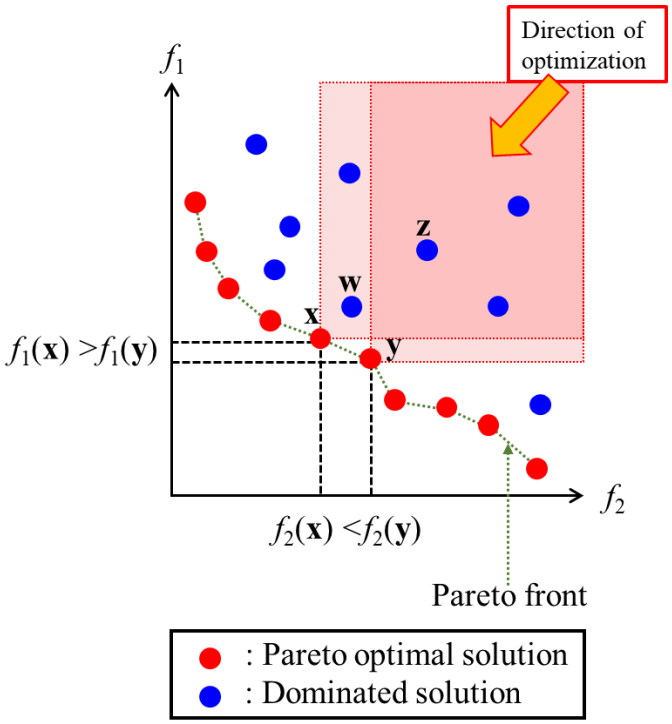

Fig. 3.12 Example of Pareto optimal solution.

3.4 SUMMARY

This chapter introduced the principles and demonstrations of SE, power systems observability, basic formulations and associated literature reviews of OPP and MOOPP.

3.5 REFERENCES

[1] A. Monticelli, *State Estimation in Electric Power Systems – A Generalized Approach*, 1st ed., Kluwer Academic Publishers, USA, Chapter 1, pp.1-13, 1999.

[2] F. Ahmed, A. Rasool, E. Ozsoy, S. Rajasekar, A. Sabanovic, and M. Elitas, Distribution system state estimation – A step towards smart grid, *Renewable and Sustainable Energy Reviews*, vol. 81, no. 1, pp. 2659-2671, 2018.

[3] R. Rubsa, I. Ivankovic, M. Rekic, and A. Jukic, Condition for establishing voltage var control function considering quality of input data, *2019 2nd International Colloquium on Smart Grid Metrology* (SMAGRIMET 2019), Split, Croatia, 2019.

[4] F. C. Schweppe, J. Wildes, and D. Rom, Power system static state estimation: Parts I, II, and III, *Power Industry Computer Applications Conference* (PICA), Denver, CO, USA, 1969.

[5] A. G. Phadke and J. S. Thorp, *Synchronized Phasor Measurements and Their Applications*, 1st ed., Supringer, USA, Chapter 7, pp. 135-170, 2008.

[6] S. Chakrabarti, E. Kyriakides, and M. Albu, Uncertainty in power system state variables obtained through synchronized measurements, *IEEE Transactions on Instrumentation and Measurement*, vol. 58, no. 8, pp. 2452-2458, 2009.

[7] S. Chakrabarti and E. Kyriakides PMU measurement uncertainty considerations in WLS state estimation, *IEEE Transactions on Instrumentation and Measurement*, vol. 24, no. 2, pp. 1062-1071, 2009.

[8] G. Valverde, S. Chakrabarti, E. Kyriakides, and V. Terzija, A constrained formulation for hybrid state estimation, *IEEE Transactions on Power Systems*, vol. 26, no. 3, pp. 1102-1109, 2011.

[9] N. M. Manousakis, G. N. Korres, J. N. Aliprantis, G. P. Vavourakis, and G. C. J. Makrinas, A two-stage state estimation for power systems with PMU and SCADA measurements, *IEEE PES PowerTech Conference*, Grenoble, France, 2013.

[10] J. Jerin and S. Bindu, Hybrid state estimation including PMU measurements, *2015 International Conference on Control, Communication and Computing* (ICCC 2015), Trivandrum, India, 2015.

[11] C. Rakpenthai and S. Uatrongjit, A new hybrid state estimation based on pseudo-voltage measurement, *IEEJ Transactions on Electrical and Electronic Engineering*, vol. 10, no. 1, pp. 19-27, 2015.

[12] A. Gomez-Exposito, A. de la Villa Jaen, A. Abur, P. Rousseaux, and C. Gomez-Quiles, On the use of PMUs in power system state estimation, 17*th Power Systems Computation Conference* (PSCC 2011), Stockholm, Sweden, 2011.

[13] A. S. Debs and R. E. Larson, A dynamic estimator for tracking the state of a power system, *IEEE Transactions on Power Apparatus and Systems*, vol. PAS-89, no. 7, pp.1670-1678, 1970.

[14] H. Tebianian and B. Jeyasurya, Dynamic state estimation in power systems using Kalman filters, *IEEE Electrical Power and Energy Conference*, Halifax, NS, Canada, 2013.

[15] S. Goleijani and M. T. Ameli, Neural network-based power system dynamic state estimation using hybrid data from SCADA and phasor measurement units, *International Transactions on Electrical Energy Systems*, vol. 28, no. 2, pp.e2481, 2017.

[16] J. R. Layne and K. M. Passino, A fuzzy dynamic model based state estimator, *Fuzzy Sets and Systems*, vol. 122, no. 1, pp. 45-72, 2001.

[17] A. Monticelli, *State Estimation in Electric Power Systems – A Generalized Approach*, 1st ed., Kluwer Academic Publishers, USA, Chapter 7, pp.161-198, 1999.

[18] M. Shahraeini and M. H. Javidi, A survey on topological observability of power systems, *2011 IEEE Power Engineering and Automation Conference* (PEAM 2011), Wuhan, China, 2011.

[19] T. L. Baldwin, J. S. Thorp, and K. J. Karimi, Power system observability with minimal phasor measurement placement, *IEEE Transactions on Power Systems*, vol. 8, no. 2, pp. 707-715, 1993.

[20] V. Girish, A. V. Anita, and T. Ananthapadmanabha, Heuristic based optimal PMU routing in KPTCL power grid, *International Journal of Electrical Engineering* & *Technology*, vol. 7, no. 1, pp. 1-16, 2016.

[21] B. Gou and A. Abur, A direct numerical method for observability analysis, *IEEE Transactions on Power Systems*, vol. 15, no. 2, 2000.

[22] F. J. Marin, F. Garcia-Lagos, G. Joya, and F. Sandoval, Genetic algorithms for optimal phasor measurement units in electrical networks, *IEEE Electronics Letters*, vol. 39, no. 19, pp. 1403-1405, 2003.

[23] B. Xu and A. Abur, Observability analysis and measurement placement for systems with PMUs, *Power Systems Conference and Exposition*, NY, USA, 2004.

[24] R. F. Nuqui and A. G. Phadke, Phasor measurement unit placement techniques for complete and incomplete observability, *IEEE Transactions on Power Delivery*, vol. 20, no. 4, pp. 2381-2388, 2005.

[25] J. Peng, Y. Sun, and H. F. Wang, Optimal PMU placement for full network observability using tabu search algorithm, *Electrical Power and Energy Systems*, vol. 28, pp. 223-231, 2006.

[26] W. Jiang, V. Vittal, and G. T. Heydt, A distributed state estimator utilizing synchronized phasor measurements, *IEEE Transactions on Power Systems*, vol. 22, no. 2, pp. 1-6, 2007.

[27] S. Chakrabarti and E. Kyriakides, Optimal placement of phasor measurements for power system observability, *IEEE Transactions on Power Delivery*, vol. 24, no. 1, pp. 12-19, 2009.

[28] R. Sodhi, S. C. Srivastava, and S. N. Singh, Optimal PMU placement method for complete topological and numerical observability of power system, *Electric Power Systems Research*, vol. 80, no. 9, pp. 1154-1159, 2010.

[29] B. Milosevic and M. Begovic, Nondominated sorting genetic algorithm for optimal phasor measurement placement, *IEEE Transactions on Power Systems*, vol. 18, no. 1, pp. 69-75, 2003.

[30] G. B. Denegri, M. Invernizzi, and F. Milano, A security oriented approach to PMU positioning for advanced monitoring of a transmission grid, *2002 IEEE International Conference on Power System Technology* (POWERCON 2002), Kunming, China, 2002.

[31] D. Dua, S. Dambhare, R. K. Gajbhiye, and S. A. Soman, Optimal multistage scheduling of PMU placement: An ILP approach, *IEEE Transactions on Power Delivery*, vol. 23, no. 4, pp. 1812-1820, 2008.

[32] A. Ahmadi, Y. Alinejad-Beromi, and M. Moradi, Optimal PMU placement for power system observability using binary particle swarm optimization and considering measurement redundancy, *Expert Systems with Applications*, vol. 38, pp. 7263-7269, 2011.

[33] O. Gomez, M. A. Rios, and G. Anders, Reliability-based phasor measurement unit placement in power systems considering transmission line outages and channel limits, *IET Generation, Transmission and Distribution*, vol. 8, no. 1, pp. 120-130, 2014.

[34] M. Esmaili, Inclusive multi objective PMU placement in power systems considering conventional measurements and contingencies, *International Transactions on Electrical Energy Systems*, vol. 26, pp. 609-626, 2016.

[35] V. -K. Tran, H. -S. Zhang, and V. -N. Nguyen, Optimal placement of phasor measurement unit for observation reliability enhancement, vol. 12, no. 3, pp. 996-1006, 2017.

[36] K. Deb and R. Agrawal, Multi-Objective Optimization using Evolutionary Algorithms, UK, Wiley, 2001.

[37] K. P. Benett and O. L. Mangasarian, Robust linear programming discrimination of two linearly inseparable sets, *Optimization Methods and Software*, vol. 1, pp. 23-24, 1992.

[38] H. Samonji and S. Watanabe, Escaping from local optimal and converge mechanisms based on search history in evolutionary multi-criterion optimization, *Transactions of the Japanese Society for Artificial Intelligence*, vol. 32, no. 3, pp. 1-12, 2017.

4 Multi Objective PMU Placement with Current Channel Selection

4.1 PMU CURRENT CHANNEL SELECTION

4.1.1 Costs of PMU Placement

As the PMU is expensive device, OPP and MOOPP for SE have been discussed by many researchers so far. For the PMU installation costs, the average overall costs per unit of typical PMU installed at transmission level substation range between USD 40,000 and USD 180,000 including the costs of procurement, installation, and commissioning reported by U. S. department of energy [1]. For only the device, it is reported that a PMU itself is about USD 20,000 and a current measurement channel cost is about USD 3,000 as of 2016, investigated by Ghamsari-Yazdel and Esmaili [2]. Normally, in order to collect the data obtained by placed PMUs, PDCs and super PDCs are also placed in some substations and communication infrastructure as SPCS is installed to transmit the data.

This thesis book focuses on the PMU device cost and reducing it whereas research about reduction of communication infrastructure cost in case of wired communication has been done by Almasabi and Mitra, defining the communication path routing problem solved by multisource Dijkstra method [3]. It is assumed that the costs except the device and the communication infrastructure are highly depending on the system operator's policy and cannot be handled by engineering. However, placement of PMUs and the channels depends on the power system structure, and is able to be generalized. In OPP and MOOPP so far, the cost of current channel has been considered as unit. However, along with the increase of the numbers of buses and lines of power system, the PMU device cost may increase with the current channel and become that existence of the current channel cost cannot be ignored depending on the system topology. Also, limiting the number of current channels does not solve the problem since it may not be a proper allocation of the current channel which minimizes the PMU device cost with keeping the HSE accuracy. Thus, this research proposes CCS-MOOPP for HSE for both of minimization of the PMU device cost and the maximization of the HSE accuracy.

4.1.2 Current Channel Selection Representation

To represent the current channel selection in MOOPP, the decision variable is augmented by hierarchical structure representation originally introduced by Hongesombut et al. for PSS parameter tuning problem [4]. To describe it, the decision variables in OPP is introduced again:

$$\mathbf{y} = [y_1, ..., y_{nb}], \tag{4.1}$$

$$y_i = \begin{cases} 1 & \text{if a PMU is placed at bus } i \\ 0 & \text{otherwise} \end{cases}, \tag{4.2}$$

where, vector **y** is PMU placement decision variable of size (1×*nb*), *nb* is the number of system buses. An element of vector **y** only takes values zeros and ones for placement of PMU device itself and the voltage measurement channel at substations. In addition, in CCS-MOOPP, the allocation of the current channel is modeled by the following decision matrix **C**:

$$\mathbf{C} = \begin{bmatrix} C_{11} & \cdots & C_{nb1} \\ \vdots & \ddots & \vdots \\ C_{1nb} & \cdots & C_{nbnb} \end{bmatrix}, \tag{4.3}$$

$$C_{ij} = \begin{cases} 1 & \text{if a PMU is placed at bus } i \text{ and the current channel is allocated on line } i\text{-}j \\ 0 & \text{otherwise} \end{cases}, \tag{4.4}$$

where, **C** is PMU current measurement channel placement decision matrix of size (*nb*×*nb*). An elements of **C** only takes values zeros and ones as well as **y**. Since there is no current channel is placed on the line from the PMU placed bus to the same bus, the diagonal element of **C** is always 0. There is only one constraint in **C**: dominance relationship between the voltage channel and current channel location. A current channel which obtains the current phasor on a line must be connected to a PMU, hence, the current channel cannot be placed by itself. This indicates the current channel cannot be placed on a line without a PMU placed bus. Hence, the elements of **y** is superior to the elements of **C**. This domination relationship is called the hierarchical structure representation and the conceptual figure is shown in Fig. 4.1 (a) with an example PMU placement on 5 bus test system shown in Fig. 4.1 (b). In the hierarchical structure representation, to vectorize the matrix **C**, only elements associated with actual lines are extracted and lined next to **y**, like Fig. 4.1 (a). In this augmented relationship, the part of augmented vector which determines the placement of PMU itself (voltage channel) is called primary locus, and the other part is called secondary locus which the elements are inactive if the corresponding

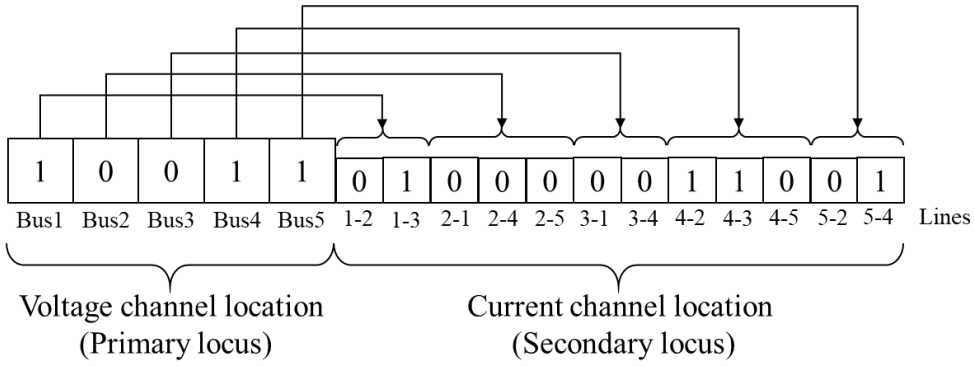

(a) Domination relationship

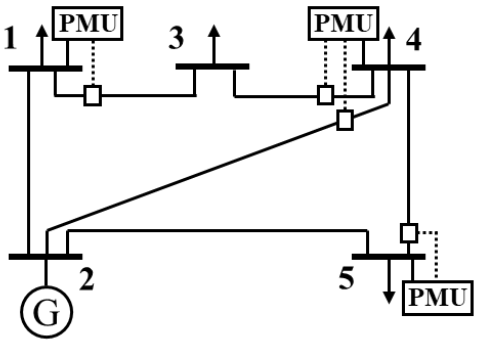

(b) The corresponding PMU placement

Fig. 4.1 The hierarchical structure representation and the demonstration.

primary locus is 0. The corresponding PMU placement of Fig. 4.1 (a) is shown in Fig. 4.1 (b).

By implementing this solution representation in optimization, it is expected that more cost effective PMU placements may be obtained with elimination of unnecessarily redundant PMU current channels which cannot be represented by the traditional solution representation. Note that the length of augmented decision variable is (nb + 2nl) where nl is the number of system lines, whereas the length of conventional decision variable is nb. This makes the problem search space bigger in the optimization, however, OPP and MOOPP are categorized as planning problem which the computation time is not an issue, thus this augmentation is acceptable.

4.2 CCS-MOOPP AND THE OPTIMIZATION

4.2.1 SE Accuracy Evaluation Index

In this chapter, the purposes of optimization are to minimize the PMU device cost including the current channel and to maximize the HSE accuracy by placing PMUs, and propose the multiple Pareto solutions by solving CCS-MOOPP which the current channel selection is realized by the hierarchical structure representation. To evaluate the HSE accuracy, Total Vector Error (TVE) is introduced [5]. There have been several ways to consider the SE accuracy, such as tracing the measurement error covariance matrix [6], taking absolute error of sum of voltage magnitude and phase angle at each bus [7], and so on. By tracing the diagonal measurement error covariance matrix, although the error of SE can be evaluated, the actual SE is not executed in the evaluation. The method takes the error of sum of voltage magnitude and phase angle does not consider the dimension of the quantities to be summed. On the other hand, TVE that this research employed is given as follows:

$$TVE = \frac{1}{nb}\sum_{i=1}^{nb}\sqrt{\left(V_R^i - \hat{V}_R^i\right)^2 + \left(V_I^i - \hat{V}_I^i\right)^2}\ , \tag{4.5}$$

where subscripts *R* and *I* of *V* indicate the real and imaginary parts of the complex voltage respectively, converted from the polar form by (3.23) and (3.24). The superscript *i* is the bus number, the hat mark (^) means the estimated value by HSE and the value without the mark is true value. Therefore, TVE evaluates the mean value of Euclidean distance between the true value and the HSE estimated value of the voltage vector for all system buses. Fig. 4.2 demonstrates the example of TVE in the complex space at *i* th bus section. This research assumes that the true value is obtained by Newton-Raphson power flow calculation. By minimizing (4.5), the proposal CCS-MOOPP attempts to minimize the HSE error.

4.2.2 Formulation

CCS-MOOPP is formulated by following equations:

$$\min_{\mathbf{y},\mathbf{D}} \ \{K_{VC}, TVE_{\max}\}, \tag{4.6}$$

subject to constraints:

$$\mathbf{y}\mathbf{y}^T > 0, \tag{4.7}$$

$$K_{VC} = w_V \mathbf{y}\mathbf{y}^T + w_C (\mathbf{C}^T\mathbf{b})^T \mathbf{b}, \tag{4.8}$$

$$\mathbf{b} = [1,...,1]^T, \tag{4.9}$$

$$TVE_{\max} = \max_{1\le j\le ns} \{TVE_j\}, \tag{4.10}$$

$$\left[\forall i \in \{1,2,...,nb\} \wedge \forall j \in \{1,2,...,ns\}\right] : \left(100 \frac{\left|V^i - \hat{V}^i\right|}{\left|V^i\right|}\right)_j < E_{\max}^{mag}, \tag{4.11}$$

$$\left[\forall i \in \{1,2,...,nb\} \wedge \forall j \in \{1,2,...,ns\}\right] : \left(\left|\theta^i - \hat{\theta}^i\right|\right)_j < E_{\max}^{ang}, \tag{4.12}$$

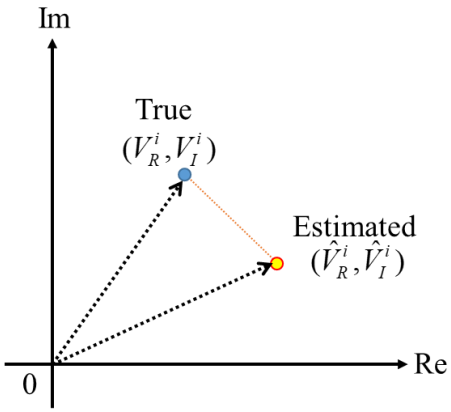

Fig. 4.2 Vector error on complex voltage.

where, w_V and w_C are device weight coefficients for PMU itself with a voltage channel and a current channel, respectively. ns is the number of scenarios, TVE_j is TVE at scenario j, V^i and θ^i are voltage magnitude and angle at bus i, respectively, $E_{\max}^{mag}$ and $E_{\max}^{ang}$ are the voltage magnitude and angle deviation upper bounds, respectively. The multi objective function (4.6) minimizes the total PMU device cost including the current channel and maximum deviation of TVE for a set of scenarios in accordance with (4.8) and (4.10). The inequality constraint (4.7) indicates that there is at least one PMU is placed on the system. The inequality constraints (4.11) and (4.12) bound the deviation of both voltage magnitude and angle in certain limits mentioned by the system operator. In optimization, RTUs are assumed to already be placed on a target system. Hence, PMUs with current channels are placed by optimization overlapped on the RTU observation network. Also, considering the uncertain and unpredictable change of system load and generation, MCS based HSE for many power system state scenarios is executed in the optimization.

4.2.3 Optimization by NSGA-II

CCS-MOOPP given by (4.6)-(4.12) is multi objective combinatorial optimization problem. Because this optimization problem is non-differentiable and the decision vector is discrete value, this category of problem is really hard to be solved. If exhaustive search is directly applied to be solved, it will be impossible to obtain the optimal solution in finite time when the power system scale larger. Hence, this research employed an evolutionally algorithm to obtain a set of approximate Pareto optimal solutions: NSGA-II [8].

NSGA-II was invented by Deb et al. as the improved version of NSGA in 2002, and has been used for many engineering problems. There are many multi objective optimization algorithms such as Multi Objective Evolutionary Algorithm on Decomposition (MOEA/D) [9], Multi Objective Particle Swarm Optimization (MOPSO) [10], Strength Pareto Evolutionary Algorithm (SPEA) [11] and so on. Among these methods, NSGA-II has good solution search ability to produce the Pareto suboptimal solutions in case of 2 or 3 objectives optimization problem. Fig. 4.2 shows the flowchart of NSGA-II. Besides the crossover, mutation and elitism in the normal genetic operator, the basic NSGA-II has two main features: non-dominated sorting and crowding distance calculation.

Non-dominated Sorting

In NSGA-II, the goodness of the solution is evaluated based on the “rank”. The rank is calculated based on how many times the individual is dominated by other individuals. The rank 1 solutions indicate the present Pareto front. NSGA-II proceeds solution search with holding the rank 1 individuals in an outer archive. After the convergence of optimization, the contents of the archive is obtained as the Pareto suboptimal solutions as the final Pareto front [8].

Crowding Distance

In multi objective optimization, obtaining widely distributed solutions is one of the important task. Crowding distance is used to maintain the diversity of the population. The mathematical formulation of crowding distance is given by follows:

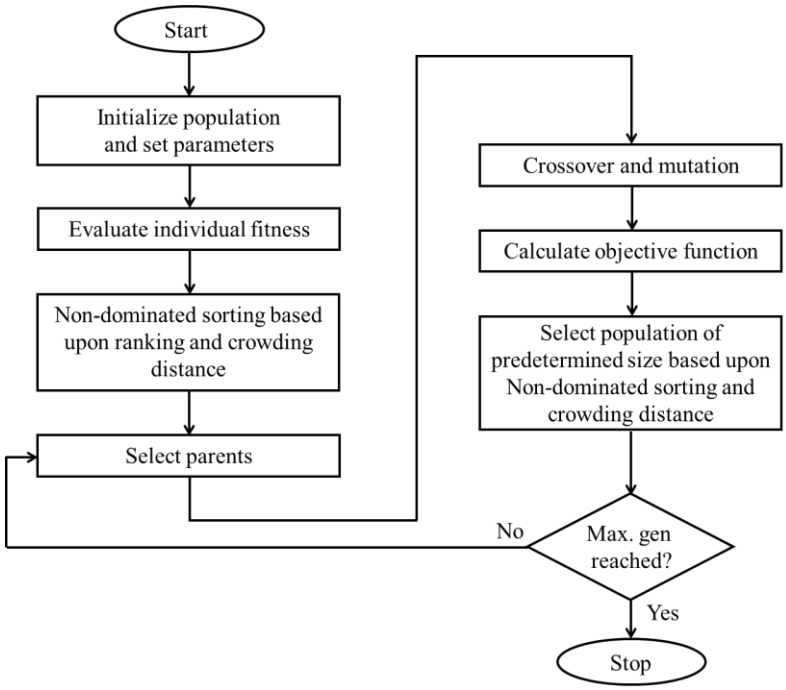

Fig. 4.3 NSGA-II flowchart.

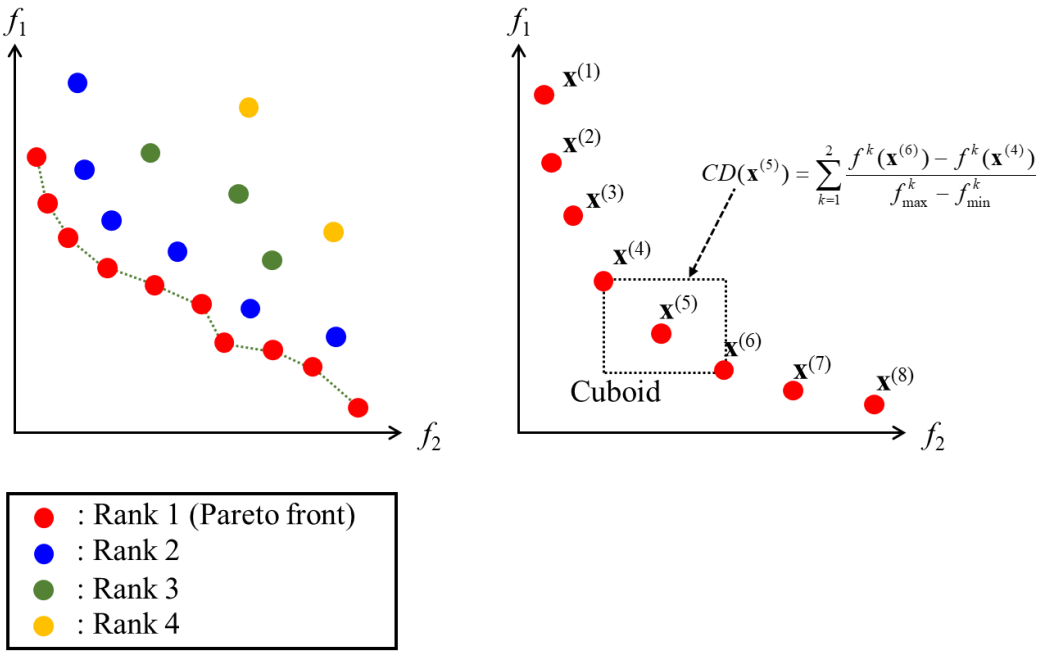

(a) Non-dominated sorting (b) Crowding distance

Fig. 4.4 NSGA-II features.

$$CD(\mathbf{x}^{(i)}) = \sum_{k=1}^{K} \frac{f_k(\mathbf{x}^{(i+1)}) - f_k(\mathbf{x}^{(i-1)})}{f_k^{\max} - f_k^{\min}}, \tag{4.13}$$

where $\mathbf{x}^{(i)}$ is the ith individual in the same rank, $f_k^{\max}$ and $f_k^{\min}$ are the maximum and minimum value of the objective function k. Crowding distance of $\mathbf{x}^{(i)}$ is defined

based on the nearest individuals $\mathbf{x}^{(i+1)}$ and $\mathbf{x}^{(i-1)}$. For the solutions of the front edges, infinite value for crowding distance is given [8]. Crowding distance is used for evaluation of individuals which possess a same rank in the selection stage. Fig. 4.4 shows the concept of non-dominated sorting and crowding distance.

4.3 NUMERICAL SIMULATION

4.3.1 Configuration

From this subsection, results of the numerical experiment are shown and discussed. To verify the effectiveness of the proposed CCS-MOOPP, numerical simulations on test systems as modified IEEE NE 39-bus and IEEE 57-bus are performed using NSGA-II with same parameters except the number of iterations and voltage magnitude/angle deviation upper bounds.

Table 4.1 Parameters for the numerical simulation.

Classification	Parameter	Value	
		Modified NE 39-bus	57-bus
NSGA-II	Population size	70	
	Crossover rate	0.95	
	Mutation rate	0.08	
	No. of generations	1000	2000
	Crossover method	Uniform Crossover	
Constraints in optimization	A PMU and a voltage channel device cost	1.0 p.u	
	A current channel device cost	0.15 p.u.	
	Voltage magnitude bound	5.5 %	18.5 %
	Voltage angle bound	2.0 deg	20.0 deg
	No. of scenarios	1000	
Maximum measurement uncertainty of meters	RTU voltage magnitude	0.2 %	
	RTU power injection	2 %	
	RTU power flow	2 %	
	PMU voltage magnitude	0.02 %	
	PMU current magnitude	0.03 %	
	PMU phase angle	0.01 deg	

The parameters of the test systems are listed in Appendix A. In the numerical simulation, finally obtained Pareto fronts are compared between both of CCS-MOOPP and the conventional MOOPP. Table 4.1 lists the parameters of NSGA-II, channel cost, HSE configuration and maximum measurement uncertainty of RTU/PMU measurements. The device costs are set considering that 20,000 USD = 1 p.u. referring to the article by Ghamsari-Yazdel and Esmaili [2]. Parameters for maximum measurement uncertainty of meters are configured referring to the article by Valverde et al. [12]. NSGA-II attempts 20 times in modified NE 39-bus, 10 times in 57-bus using different random initial points, and obtains the best Pareto front.

4.3.2 Comparison of Pareto Solutions

IEEE modified NE 39-bus

Fig. 4.5 shows the best Pareto fronts obtained by CCS-MOOPP and conventional MOOPP in modified NE 39-bus. Note that CCS-MOOPP allows the proposed current channel allocation based on the augmented decision variable represented by **y** and **C** in (4.1)-(4.4) whereas conventional MOOPP allocates the current channels on all lines incident to the PMU placed bus based on only **y** in (4.1) and (4.2). Comparing the Pareto frons obtained by CCS-MOOPP and MOOPP, the former is totally dominating the latter. This domination tends to occur in the high PMU device cost area. Figures 4.6 and 4.7 show the zoomed figure of Fig. 4.5 in high and low PMU device cost areas, respectively. This occurred because the number of PMU current channels increases alongside of increase of PMUs.

In order to quantitatively evaluate the Pareto front domination, Ratio of Non-dominated Individuals (RNI) is introduced. RNI is an index to evaluate the domination relationship numerically in between two methods. Let sets of Pareto solutions P' and P'' be obtained by different algorithms, then *RNI* of P' for P'' is given by follows:

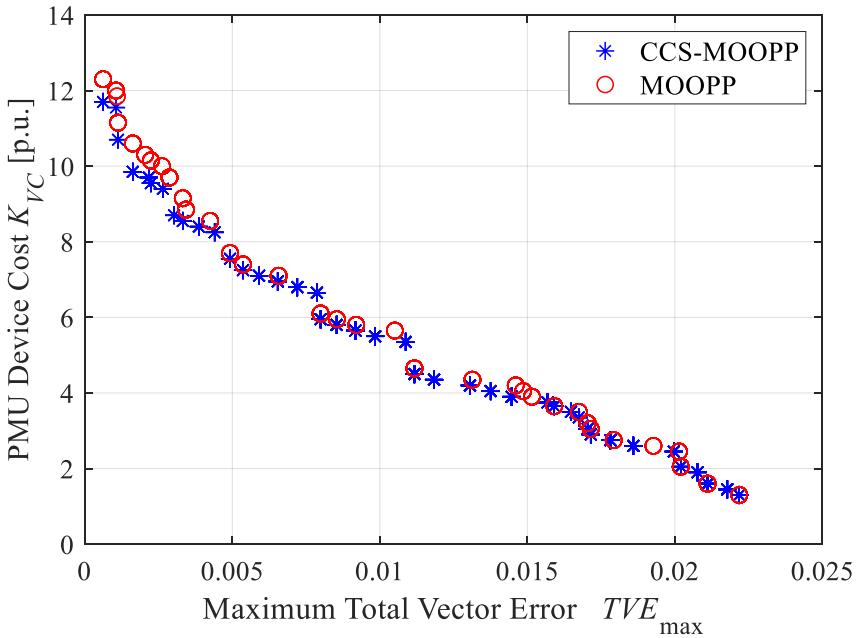

Fig. 4.5 Pareto front comparison in CCS-MOOPP and MOOPP in modified NE 39-bus.

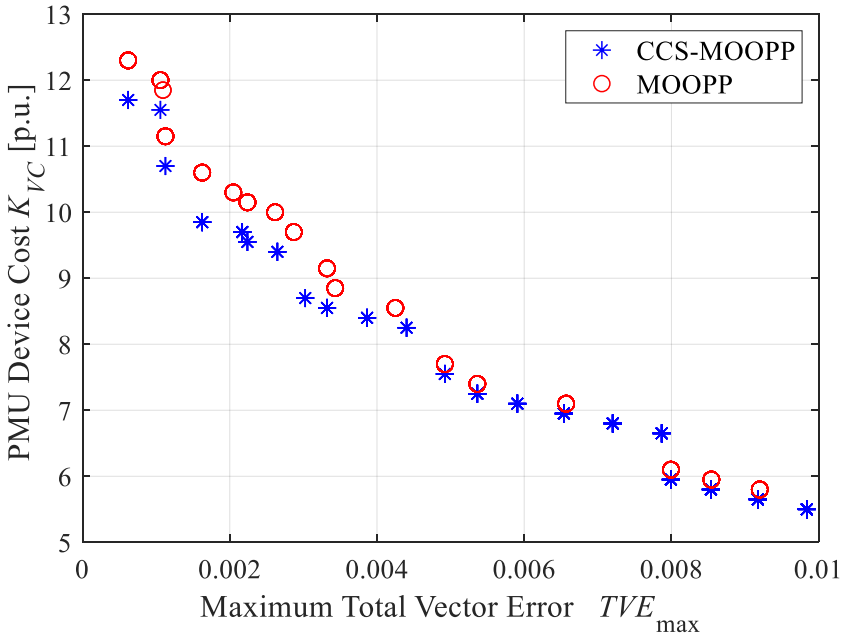

Fig. 4.6 Pareto front comparison in CCS-MOOPP and MOOPP in modified NE 39-bus zoomed at high PMU device cost.

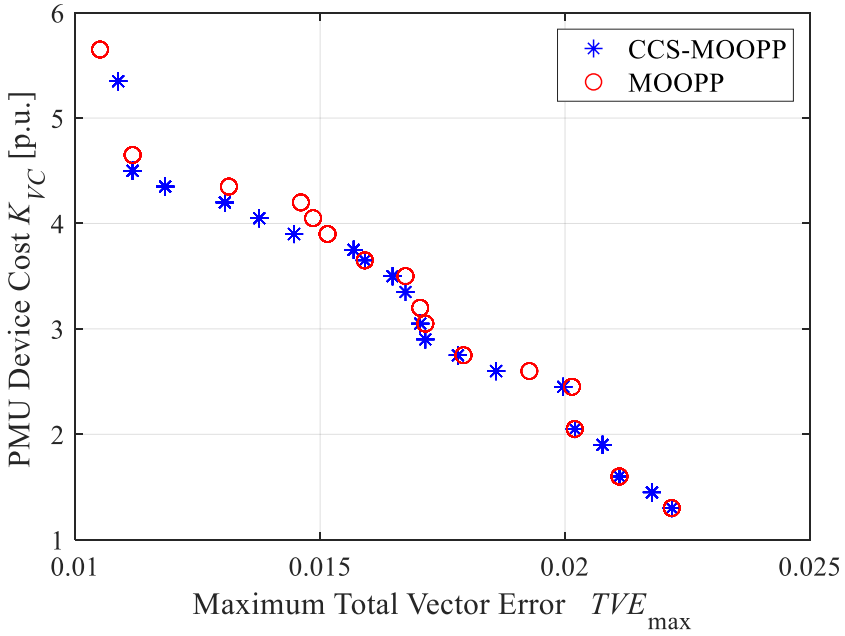

Fig. 4.7 Pareto front comparison in CCS-MOOPP and MOOPP in modified NE 39-bus zoomed at low PMU device cost.

$$RNI(P', P'') = |P'| / |P^D|, \tag{4.14}$$

where, P^D is non-dominated solutions of a sum set of P' and P'' which is $P^D \subseteq P = (P' \cup P'')$ [13]. If $RNI(P',P'') > 0.5$, then P' is dominating P'', which means more closer to the optimal Pareto front. Obviously, RNI ∈ [0,1]. Table 4.2 shows the RNI for both of CCS-MOOPP and the conventional MOOPP. As a result of calculation of RNI, proposed CCS-MOOPP is quantitatively much greater than MOOPP.

Table 4.2 Ratio of Non-dominated Individuals and Cover Rate in modified NE 39-bus.

Method	RNI	CR
CCS-MOOPP	0.9111	0.9250
MOOPP	0.0889	0.8750

Since above results are obtained by the stochastic optimization algorithm, there is no guarantee that those are the proper optimal Pareto front. However, in comparison of these methods, the proposed method is greater than the conventional method although its search space is larger by the augmented decision variable to select the PMU current channel allocation. Particularly in modified NE 39-bus, the search space of the problem of CCS-MOOPP is 2^{143} whereas MOOPP is 2^{39}. Nevertheless, CCS-MOOPP obtained better Pareto front by same optimization algorithm. This fact indicates that the CCS-MOOPP is worthwhile to be solved. The solution space of MOOPP is the subset of the solution space of CCS-MOOPP since CCS-MOOPP is also able to represent the full allocation of current channels to the all incident lines of the PMU placed buses. Thus, at least the Pareto front same as MOOPP can be found in CCS-MOOPP. Note that the improvement of problem difficulty and computation burden is not the purpose of this thesis.

In addition, as indices of multi objective optimization, Cover Rate (CR) which evaluates the width and the density of obtained Pareto front [15] is also calculated. Generally, CR is calculated based on how many individuals cover the objective function space. First, the objective function space is divided by a number *nd*, between the maximum and minim objective function values , $f_k^{\max}$ and $f_k^{\min}$ for each objective function. Then CR for an objective function *k* is given by follows:

$$CR_k = \frac{nc_k}{nd}, \tag{4.15}$$

where nc_k is the number of covered areas. Then, total CR is given by the average of all CR_k,

$$CR = \frac{1}{n_{obj}} \sum_{k=1}^{n_{obj}} CR_k . \tag{4.16}$$

The visual description of *CR* is shown in Fig. 4.8. In this demonstration, *nd*=5. For objective f_1, CR_1=2/5. For f_2, CR_2=3/5. By summing up them and dividing by n_{obj}=2, *CR*=0.25. If the divided areas are fully covered by individuals, *CR* is 1. If the coverage is sparse, *CR* gets close to 0. Table 4.2 in the third column also shows the CR in each method with *nd*=20. In this case with the number of division, *CR* in CCS-MOOPP is higher than MOOPP indicating the level of coverage for the objective function higher in CCS-MOOPP. It is caused by solution space expansion resulting in that the number of solution in CCS-MOOPP is bigger than MOOPP.

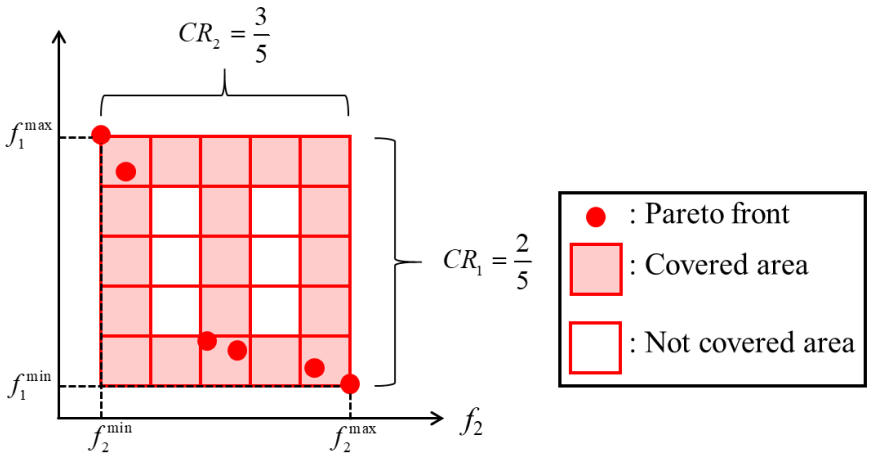

Fig. 4.8 Example of CR.

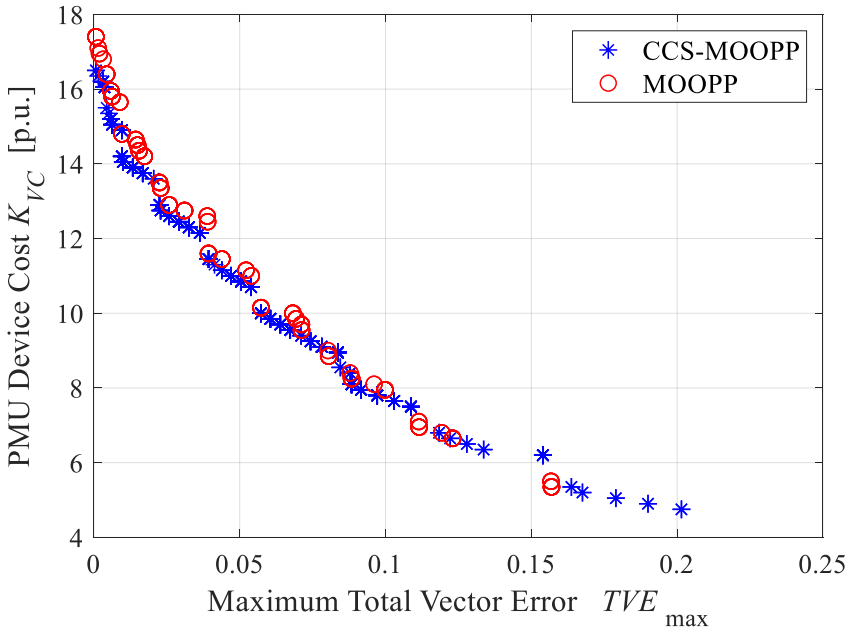

Fig. 4.9 Pareto front comparison in CCS-MOOPP and MOOPP in 57-bus.

IEEE 57-bus

Fig. 4.9 shows the Pareto fronts obtained by CCS-MOOPP and conventional MOOPP in IEEE 57-bus. In case of modified NE 39-bus, the proposed CCS-MOOPP is much dominating the conventional MOOPP, the same thing in modified NE 39-bus is true of 57-bus case which is bigger scale in terms of the numbers of buses and lines, qualitatively. Compared to modified NE 39-bus, in low PMU device cost area, the Pareto front of MOOPP is sparser. This may be occurred due to the system topology in 57-bus which has less loops. Since the search space of the problem of CCS-MOOPP is 2^{213} whereas MOOPP is 2^{57} in 57-bus system, CCS-MOOPP has many more number of solution possibilities compared to MOOPP by the current channel selection. Thus, system operator has more choices of solution selection. Figures 4.10 and 4.11 show zoomed figures of Fig. 4.9. As well as modified NE 39-bus, Pareto solutions in high PMU device cost seems more dominant. Also, Table 4.3 shows the RNI and CR with *nd*=30 of each Pareto front.

From the results of numerical evaluation, CCS-MOOPP is dominant to MOOPP and more covering the solution space than MOOPP, numerically. The level of dominance is little lower than case of modified NE 39-bus due to the problem search space (difficulty). Since its solution space is larger than modified 39-bus, NSGA-II as a stochastic optimization method could not find much more dominant solutions especially in the low PMU cost area in Fig. 4.11. However, Pareto front of CCS-MOOPP is still dominant to MOOPP found by NSGA-II with the same parameter.

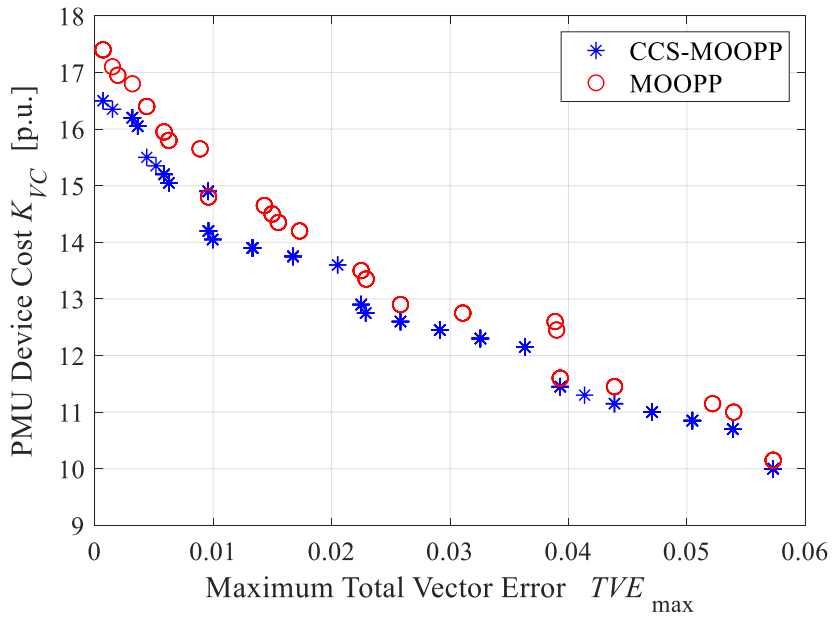

Fig. 4.10 Pareto front comparison in CCS-MOOPP and MOOPP in 57-bus zoomed at high PMU device cost.

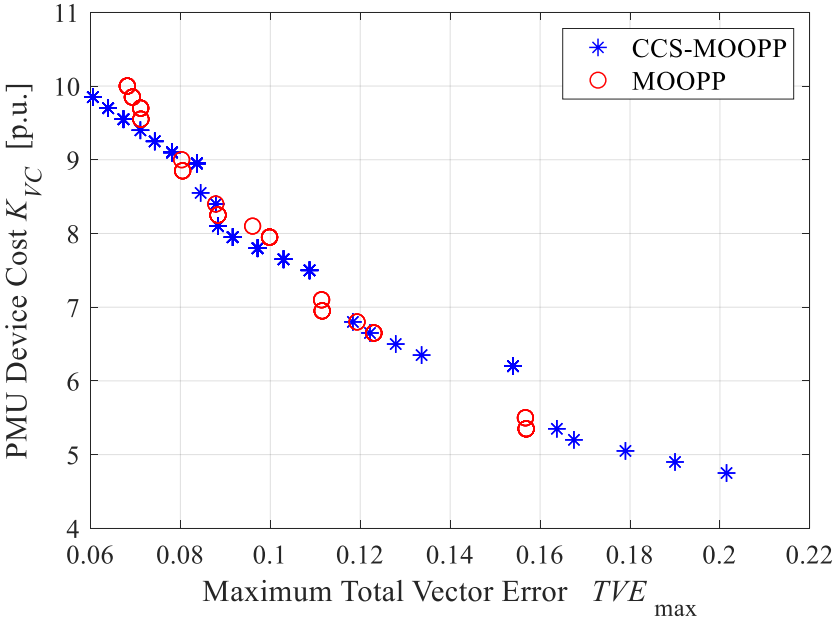

Fig. 4.11 Pareto front comparison in CCS-MOOPP and MOOPP in 57-bus zoomed at low PMU device cost.

Table 4.3 Ratio of Non-dominated Individuals and Cover Rate in 57-bus.

Method	RNI	CR
CCS-MOOPP	0.8727	0.8000
MOOPP	0.1273	0.6500

4.3.3 HSE Accuracy and PMU Placements

IEEE modified NE 39-bus

To confirm the HSE accuracy, single solution needs to be extracted from the set of Pareto solutions obtained in subsection 4.3.2. Also, it is important to select a solution which the system operator is satisfied comparing the system planning cost and SE accuracy, from the multiple solution. Hence, this research selected a solution from the Pareto front in order to set a criterion solution for the system operator. To select a criterion solution, this research employed the Best Compromised Solution (BCS) with fuzzy membership function [14].

The fuzzy membership function of objective *i* is given by follows:

$$h_i = \begin{cases} 1 & \text{if } f_i \le f_i^{\min} \\ \dfrac{f_i^{\max} - f_i}{f_i^{\max} - f_i^{\min}} & \text{if } f_i^{\min} \le f_i \le f_i^{\max} \\ 0 & \text{if } f_i \ge f_i^{\max} \end{cases}, \tag{4.17}$$

where, f_i is the objective function value of objective *i*. Then, weighted satisfaction degree *H* is obtained as follows:

$$H = \frac{1}{n_{obj}} \sum_{i=1}^{n_{obj}} w_{f_i} h_i \ , \tag{4.18}$$

where w_{fi} is the preference weight coefficient for objective function f_i, n_{obj} is the number of objectives and equal to 2. Figures 4.12 and 4.13 provide the results of calculation of satisfaction degree in CCS-MOOPP and MOOPP on each Pareto front by bar chart, respectively. Now assuming that the preference weight coefficients for both objectives are 1, the solution having the maximum value of *H* is selected, which is highlighted by an arrowed point on Figures 4.12 and 4.13. This solution is named "S1" (BCS). Obviously, the Pareto front obtained by MOOPP is almost totally dominated by the Pareto front by CCS-MOOPP, satisfaction degree in CCS-MOOPP is also totally higher. Now, information of the selected solutions is listed in Table 4.4. To compare the solutions in each method, target solutions are highlighted by also an arrowed point in Fig. 4.12 with same $TVE_{\max}$ as "S1". This solution named "S2" is also listed in Table 4.4. In addition, PMU placements have the minimum $TVE_{\max}$ are selected and named "S3" and "S4", respectively from the Pareto fronts of CCS-MOOPP and MOOPP. Fig. 4.14 shows the single line connection diagram of modified NE-39 bus test system. The bus number listed in Table 4.4 corresponds to the bus number in Fig. 4.14. The placement of RTU is also

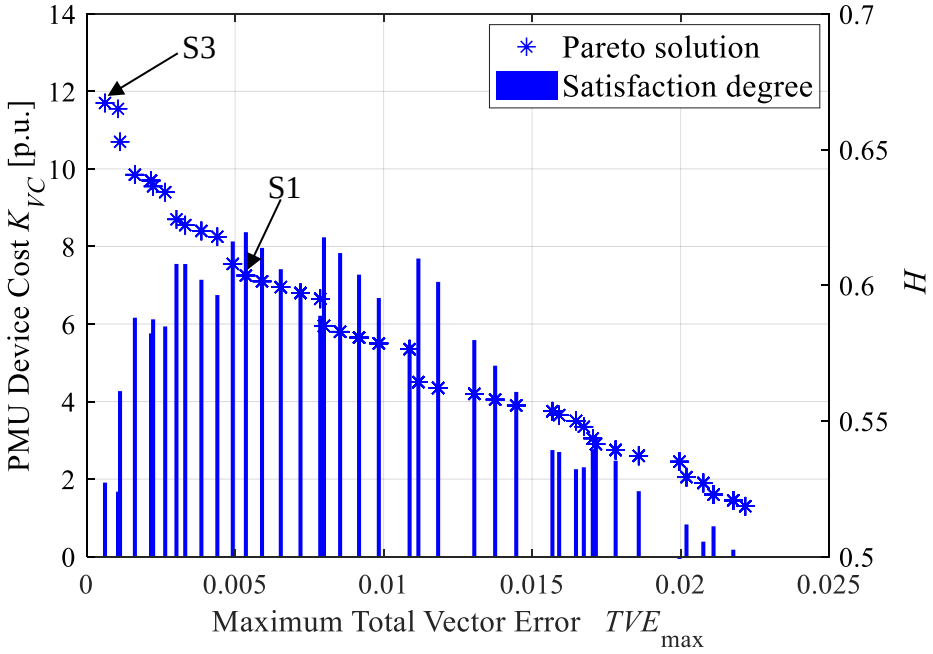

Fig. 4.12 Pareto front and satisfaction degree in CCS-MOOPP in modified NE 39-bus.

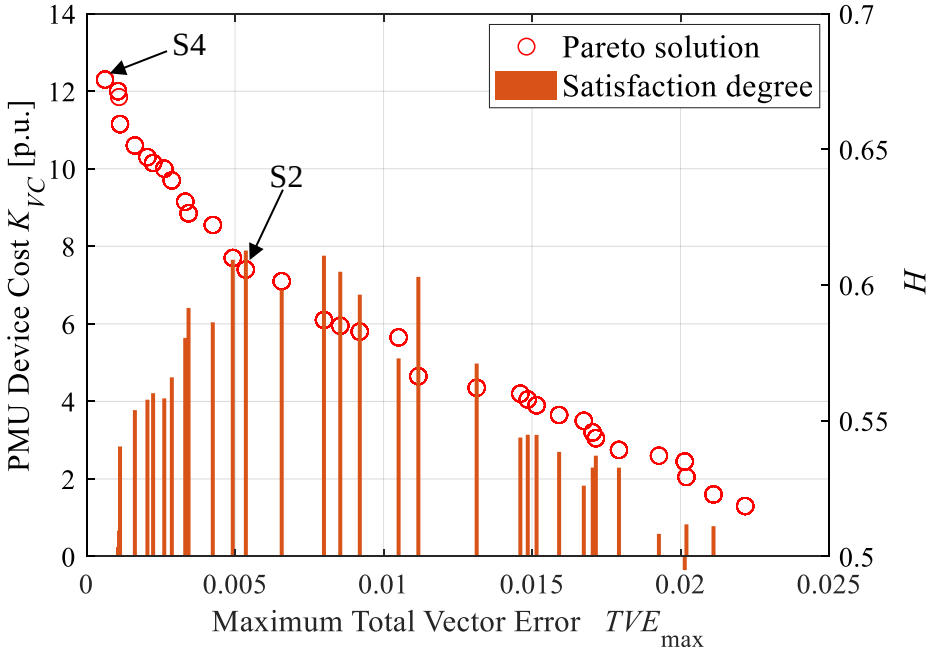

Fig. 4.13 Pareto front and satisfaction degree in MOOPP in modified NE 39-bus.

listed in Table 4.5. Comparing solutions S1 and S2, S1 realizes reducing the total PMU device cost by eliminating current channels on line 20-3 and 29-26 keeping same HSE accuracy in TVE_{max} as well as S2. For example, the current channel on line 20-3 is obtained by pseudo measurement by KCL. Since bus 20 is ZIB, the pseudo current phasor on line 20-3 is obtained by current phasors 20-21 and 20-23. Then, pseudo bus voltage phasor 21 is obtained by direct bus voltage phasor at bus 20 and pseudo current phasor on line 20-3. However, there is no current channel selectivity in MOOPP. By such difference, the redundant measurement channels

are eliminated by implementations of the hierarchical structure representation and the augmented decision variable. Many more of current channels is reduced in S3 compared to S4. Thus, the reduction of K_{VC} in both S3 and S4 is more significant comparing to S1 and S2 since the numbers of PMUs in S3 and S4 are bigger than S1 and S2: thus, a lot of redundant current channels are eliminated.

Figures from 4.15 to 4.18 show statistical boxplots of voltage magnitude and angle error from the true values by collecting all scenarios. Figures 4.15 and 4.16 show the values in SCADA SE. Figures 4.17 and 4.18 show the values in HSE with PMU placement of S1 (BCS). As aforementioned, two-stage HSE allows overlapping of PMUs on the RTU network to correct the error. By placing PMUs with direct and pseudo measurements, partial error which covered by PMUs becomes superiorly small, resulting the TVE smaller than SCADA SE.

Table 4.4 Selected solutions in modified NE 39-bus and PMU placements.

Solution	Placement: bus / line(bus No.-bus.No.)			K_{VC} [p.u.]	$TVE_{\max}$
	PMU + voltage channel	Current channel			
		Common parts	Difference		
S1	18, 20, 29, 33, 37	18-13, 18-15, 18-17, 18-19, 29-4, 29-24, 29-30, 29-31, 33-7, 33-32, 33-34, 37-27, 37-36	20-21, 20-23	7.25	5.36×10^{-3}
S2	18, 22, 29, 33, 37		22-21, 22-23, 29-26	7.40	5.36×10^{-3}
S3	5, 11, 18, 20, 27, 29, 33, 35, 39	18-13, 18-15, 18-17, 18-19, 29-4, 29-24, 29-30, 29-31, 33-7, 33-32, 33-34, 39-9, 39-38	20-3, 20-23, 27-37, 35-8, 35-36	11.70	6.20×10^{-4}
S4	5, 8, 10, 18, 22, 29, 33, 37, 39		5-30, 8-35, 10-12, 22-21, 22-23, 29-26, 37-27, 37-36, 39-36	12.30	6.20×10^{-4}

Table 4.5 RTU placement in modified NE 39-bus.

Power injection meter	Power flow meter
1, 2, 3, 4, 5, 6, 7, 8, 9, 10, 11, 12, 13, 14, 16 ,18, 20, 22, 23, 24, 25, 26, 29, 30, 31, 32, 33, 34, 35, 36, 37, 38, 39	2-11, 2-19, 12-13, 14-13, 28-13, 14-15, 16-15, 18-15, 18-17, 20-21, 14-24, 22-23, 23-24, 25-24, 26-25, 26-27, 26-31, 26-34, 39-36, 35-36, 38-36, 39-38

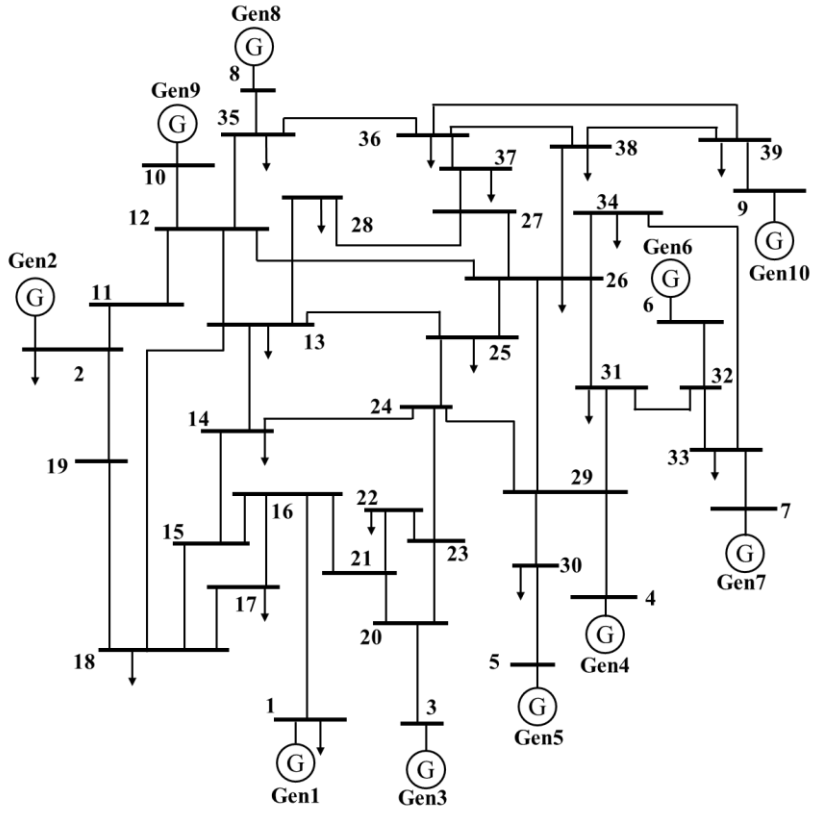

Fig. 4.14 IEEE modified NE 39-bus test system single line connection diagram.

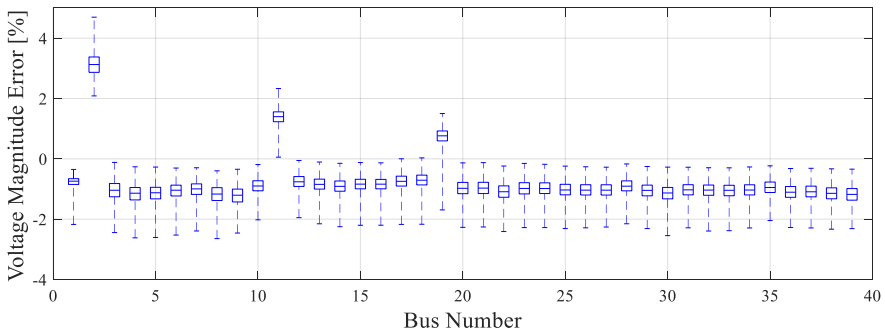

Fig. 4.15 Voltage magnitude error in SCADA SE in modified NE 39-bus.

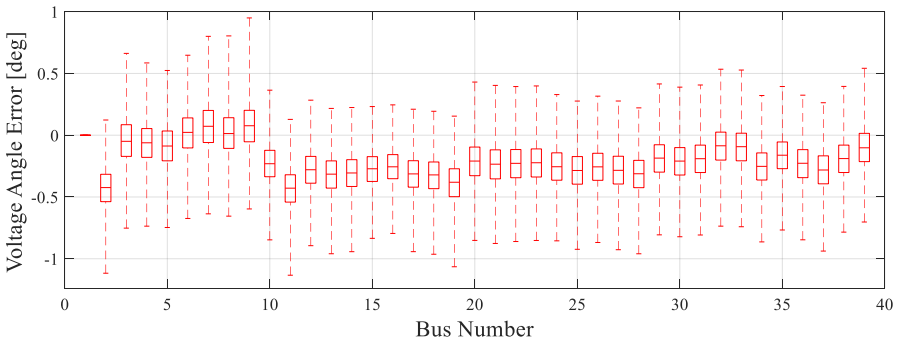

Fig. 4.16 Voltage angle error in SCADA SE in modified NE 39-bus.

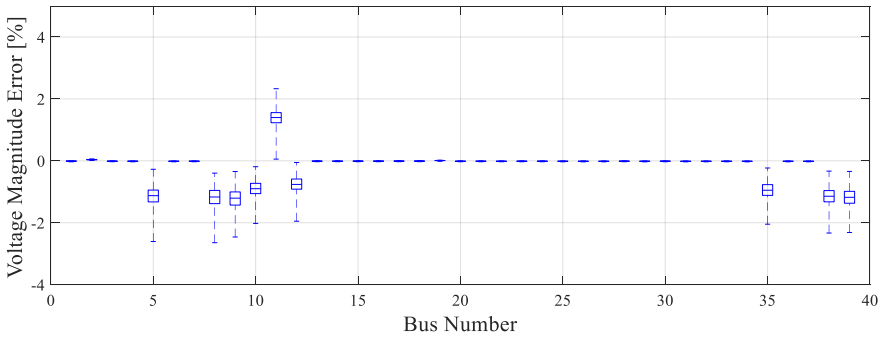

Fig. 4.17 Voltage magnitude error in HSE by PMU placement S1 in modified NE 39-bus.

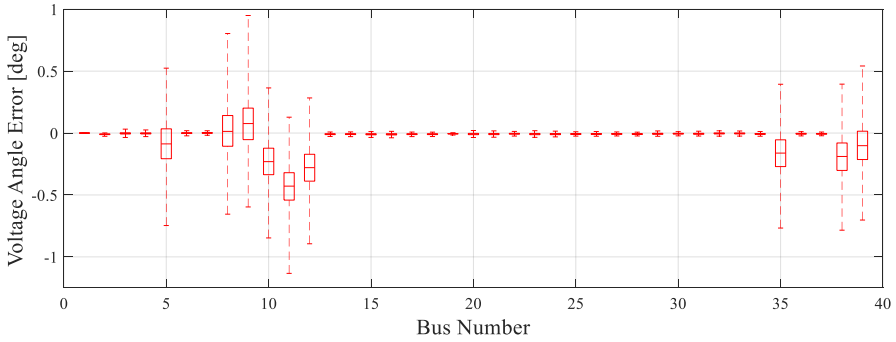

Fig. 4.18 Voltage angle error in HSE by PMU placement S1 in modified NE 39-bus.

IEEE 57-bus

Some analyses such as selection of the BCS and other solutions and checking the statistical SE accuracy are performed in 57-bus system case. Figures 4.19 and 4.20 show the Pareto front and a bar chart of satisfaction degree in each method. Solutions "S1" and "S2" are selected in the biggest value of *H*, "S3" and "S4" are selected as the highest PMU device cost on each method. Satisfaction degree in CCS-MOOPP is totally higher than MOOPP. Table 4.6 shows the placements of PMUs from S1 to S4, Table 4.7 lists the placement of RTUs. Both meter placements are corresponding to a single line diagram of 57-bus test system illustrated in Fig. 4.21. Comparing S1 and S2, S3 and S4, it is obvious that the CCS-MOOPP can produce the number of solutions that has lower PMU device cost by current channel selection. As well as case of modified NE 39-bus, the difference of PMU device cost becomes bigger when the many more PMUs are placed because of the same reason as modified NE 39-bus case. Figures 4.22 and 4.23 show the statistical boxplot for all MCS scenarios in SCADA SE, and Figures 4.24 and 4.25 show the statistical boxplot in HSE with PMUs of placement of S1.The dotted line is the bound for voltage magnitude/angle deviation in the optimization. From the results, the PMU reduces the error by its direct/pseudo measurement for those buses having big deviation. Comparing difference between S3 and S4 with the case of modified NE 39-bus in K_{VC}, the difference of K_{VC} between S3 and S4 in 57-bus is 0.90 p.u. whereas the difference of K_{VC} in modified NE 39-bus is 0.60 p.u. in Tables 4.4 and 4.6. By this numerical experiment, it is proven that CCS-MOOPP can also be applied in larger test system and the effect of current channel selectivity is bigger in the larger system.

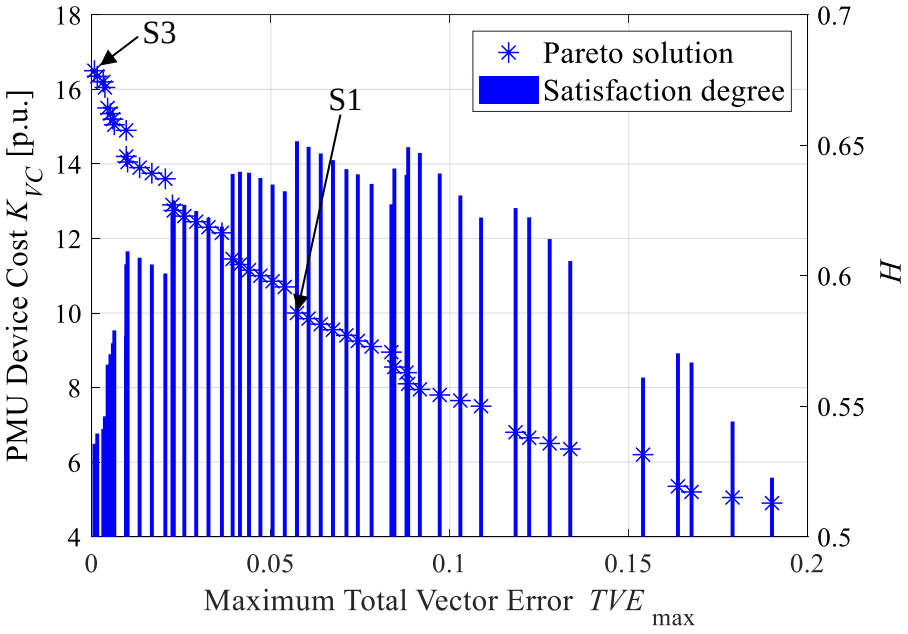

Fig. 4.19 Pareto front and satisfaction degree in CCS-MOOPP in 57-bus.

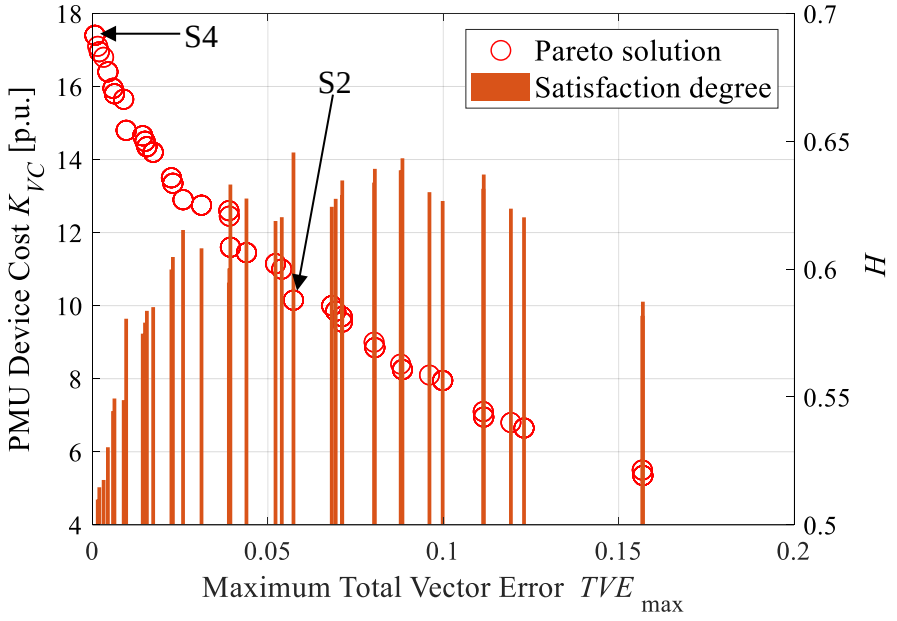

Fig. 4.20 Pareto front and satisfaction degree in MOOPP in 57-bus.

Table 4.6 Selected solutions in 57-bus and PMU placements.

Solu-tion	Placement: bus / line(bus No.-bus.No.)				K_{VC} [p.u.]	TVE_{max}
	PMU + voltage channel		Current channel			
	Common parts	Diff-erence	Common parts	Difference		
S1	6, 20, 25, 32, 47, 50, 56	N/A	6-5, 6-7, 6-11, 6-12 ,6-13, 6-55, 20-19, 20-21, 25-24, 25-30, 32-31, 32-33, 32-34, 47-46, 47-48, 50-49, 50-51, 56-40, 56-41, 56-42	N/A	10.00	5.73×10^{-2}
S2		N/A		56-57	10.15	5.73×10^{-2}
S3	1, 6, 20, 25, 32, 47, 53, 56	4, 15, 28, 50	1-2, 1-16, 1-17, 6-5, 6-7, 6-11, 6-12, 6-13, 6-55, 20-19, 20-21, 25-24, 25-30, 32-31, 32-34, 47-46, 47-48, 53-52, 53-54, 56-40, 56-41, 56-42	4-8, 4-9, 4-10, 15-3, 15-45, 50-49, 50-51	16.50	6.94×10^{-4}
S4		8, 29, 44, 51		1-15, 8-3, 8-4, 8-9, 8-18, 29-10, 29-28, 29-52, 32-33, 44-38, 44-45, 51-11, 51-50, 56-57	17.40	6.94×10^{-4}

Table 4.7 RTU placement in 57-bus.

Power injection meter	Power flow meter
1, 2, 3, 4, 5, 6, 7, 8, 9, 10, 11, 12, 13, 14, 16, 17, 18, 19, 20, 21, 22, 23, 24, 25, 26, 28, 30, 31, 32, 33, 34, 35, 36, 37, 38, 39, 40, 42, 43, 45, 46, 48, 49, 50, 51, 52, 53, 54, 56, 57	1-2, 3-8, 8-9, 13-14, 13-15, 10-5, 11-7, 12-13, 14-15, 18-19, 21-20, 22-23, 26-24, 26-27, 28-29, 10-29, 30-25, 25-30, 30-31, 31-30, 31-32, 35-36, 36-40, 41-42, 14-46, 47-48, 48-49, 50-51, 54-55, 54-53, 52-29, 52-53, 13-49 , 12-43, 44-45, 56-42, 57-56, 38-49, 38-48

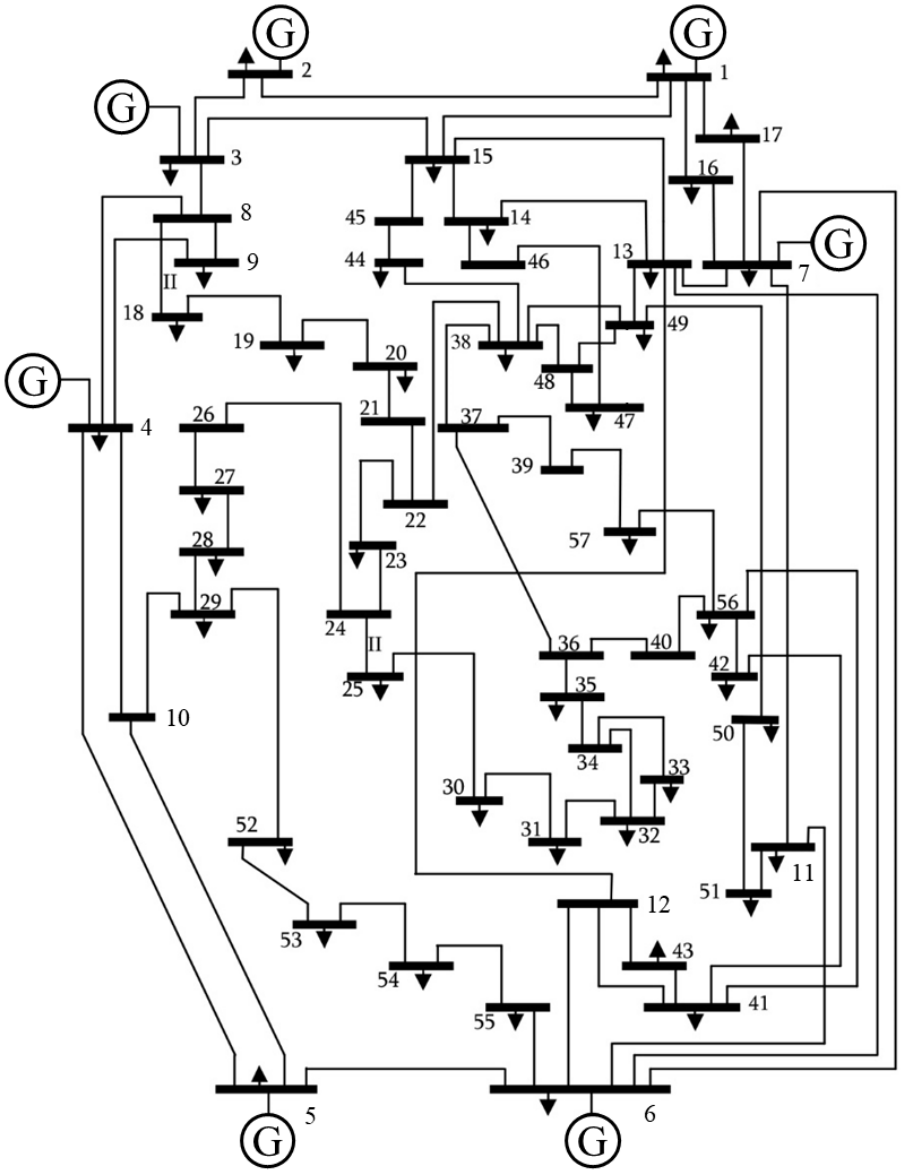

Fig. 4.21 IEEE 57-bus test system single line connection diagram.

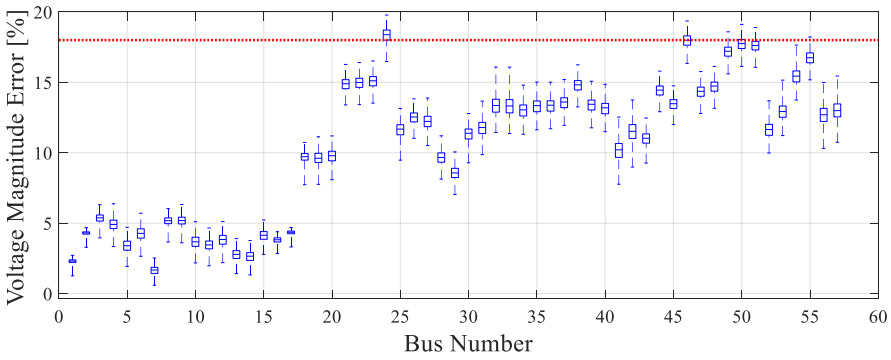

Fig. 4.22 Voltage magnitude error in SCADA SE in 57bus.

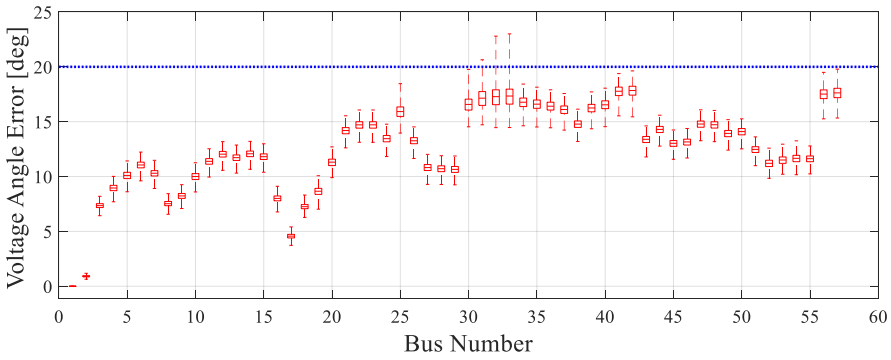

Fig. 4.23 Voltage angle error in SCADA SE in 57-bus.

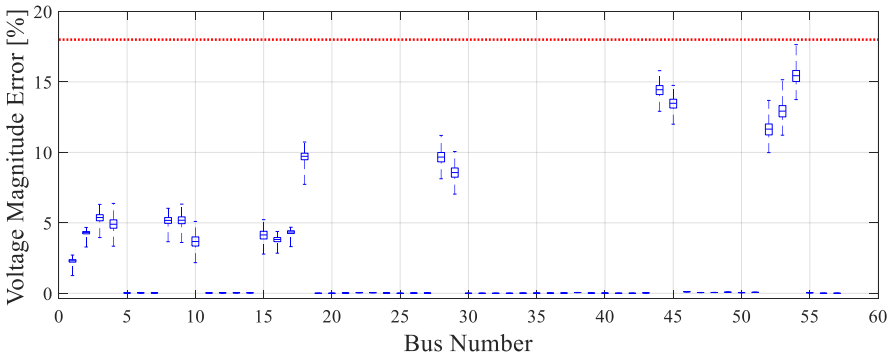

Fig. 4.24 Voltage magnitude error in HSE in 57bus.

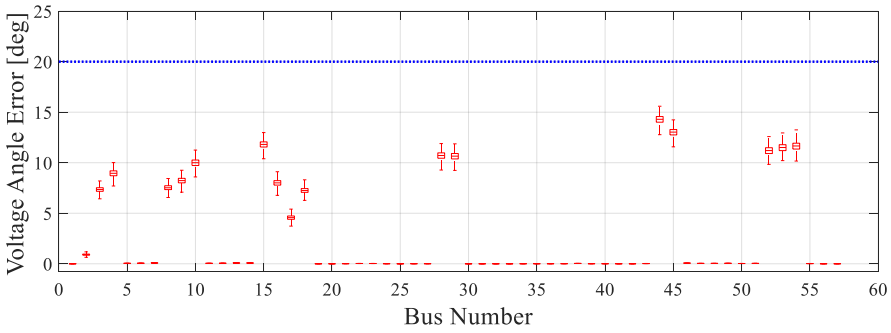

Fig. 4.25 Voltage angle error in HSE in 57-bus.

Table 4.8 Average cost contribution in each test system.

	Average PMU Device Cost [p.u.]	
	Modified NE 39-bus	57-bus
CCS-MOOPP	5.71	10.62
MOOPP	6.40	11.64
Difference	0.69	1.02

4.3.4 Contribution to Cost Reduction

Table 4.8 shows the average PMU device cost in both test power systems for CCS-MOOPP and MOOPP. The average PMU device costs are calculated for all solutions of the Pareto front in each optimization problem. Obviously the Average PMU device cost in CCS-MOOPP is lower than MOOPP in both test systems. Also, the difference of average cost between CCS-MOOPP and MOOPP in 57-bus is about 1.5 times bigger than modified NE 39-bus. This indicates that CCS-MOOPP can contribute to cost reduction and the effectiveness is significant when the system scale is larger. Note that this tendency depends on the system topology. If there is less loops in a power system, CCS-MOOPP may not work better than MOOPP. However, if the searching method is not stuck in a severe local optimum, it will not be worse because the solution space of MOOPP is included by CCS-MOOPP.

4.4 SUMMARY

This chapter formulated CCS-MOOPP through the PMU current channel selection by hierarchical structure representation. Also, HSE accuracy evaluation index in the optimization and detail of NSGA-II are introduced. As the results of numerical simulation in modified NE 39-bus and 57-bus test systems, the effectiveness of CCS-MOOPP to obtain better Pareto solution is proven. Also the effect of current channel reduction for redundant measurement is more significant when the system scale gets larger. As the results of the numerical simulation, this chapter contributes to spurring the installation of PMU which is capable to accurately estimate the system state vector into power systems by reducing the device cost by CCS-MOOPP while keeping the SE accuracy. Also, actual HSE is conducted in the optimization process evaluated by MCS which can consider the power flow variability by load uncertainty.

4.5 REFERENCES

[1] U. S. Department of Energy, *Factors Affecting PMU Installation Costs*, 2014.

[2] M. Ghamsari-Yazdel and M. Esmaili, Reliability-based probabilistic optimal joint placement of PMUs and flow measurements, *International Journal of Electric Power and Energy Systems*, vol. 78, pp. 857-863, 2016.

[3] S. Almasabi and J. Mitra, Multi-stage optimal PMU placement considering substation infrastructure, *2017 IEEE Industry Applications Society Annual Meeting*, Cincinnati, OH, USA, 2017.

[4] K. Hongesombut, Y. Mitani, and K. Tsuji, Simultaneous tuning of power system stabilizers based on a combined method of a Micre-GA, HGA and minimum phase control, *IEEJ Transactions on Power and Energy*, vol. 122, no.12, pp. 1270-1279, 2002.

[5] C. Rakpenthai and S. Uatrongjit, A new hybrid state estimation based on pseudo-voltage measurement, *IEEJ Transactions on Electrical and Electronic Engineering*, vol. 10, no. 1, pp. 19-27, 2015.

[6] S. Ogawa and H. Mori, Application of moment matching method to optimal allocation of PMUs in state estimation, *IEEJ Transactions on Power and Energy*, vol. 138, no. 2, pp. 121-130, 2018.

[7] M. S. Shahriar, I. O. Habiballah, and H. Hussein, Optimization of Phasor Measurement Unit (PMU) placement in Supervisory Control and Data Acquisition (SCADA)-based power system for better state-estimation performance, *Energies*, vol. 11, no. 3, pp.570-, 2018.

[8] K. Deb, S. Pratab, S. Agarwal, and T. Meyarivan, A fast and elitist multi-objective genetic algorithm: NSGA-II, *IEEE Transactions on Evolutionary Computation*, vol. 6, no. 2, pp. 182-197, 2002.

[9] Q. Zhang and H. Li, MOEA/D: A multi-objective evolutionary algorithm based on decomposition, *IEEE Transactions on Evolutionary Computation*, vol. 11, no. 6, pp. 712-713, 2007.

[10] C. A. Coello Coello and M. S. Lechuga, MOPSO: A proposal for multi objective particle swarm optimization, *2002 Congress on Evolutionary Computation* (CEC '02), Honolulu, HI, USA, 2002.

[11] E. Zitzlerm M. Laumanns, and L. Thiele, SPEA2: Improving the strength Pareto evolutionary algorithm, *TIK-Report*, no. 103, 2001.

[12] G. Valverde, S. Chakrabarti, E. Kyriakides, and V. Terzija, A constrained formulation for hybrid state estimation, *IEEE Transactions on Power Systems*, vol. 26, no. 3, pp. 1102-1109, 2011.

[13] S. Watanabe, T. Hiroyasu, and M. Miki, Parallel evolutionary multi-criterion optimization for mobile telecommunication networks optimization, *Evolutionary Methods for Design, Optimization and Control with Applications to Industrial Problems* (EUROGEN 2001), Athena, Greece, 2001.

[14] C. Peng, H. Sun, and J. Guo, Multi-objective optimal PMU placement using a non-dominated sorting genetic algorithm, *Electric Power and Energy*, vol. 32, no. 1, pp. 886-892, 2010.

[15] S. Watanabe, T. Hiroyasu, and M. Miki, Neighborhood cultivation genetic algorithm for multi-objective optimization algorithm, *IPSJ Transaction on Mathematical Modeling and its Applications*, vol. 43, no. SIG10, pp. 183-198, 2002.

5 Influence of Measurement Uncertainty Propagation in PMU Pseudo Measurement

5.1 MEASUREMENT UNCERTAINTY PROPAGATION

5.1.1 Measurement Uncertainty in Meters

SE basically assesses power systems static state considering meter errors which are never free from meters. In SE, correct assessment of measurement error is important to obtain the correct state vector. As previously introduced in the chapter 3, to proceed SE with calculation of elements **R** i.e. standard deviation of measurements is introduced. Given that the maximum measurement uncertainty is provided by the meter manufactures, the standard uncertainty in a measurement can be expressed in:

$$u(\mathbf{p}(k)) = \frac{\Delta\mathbf{p}(k)}{\sqrt{3}}, \tag{5.1}$$

where $\Delta\mathbf{p}(k)$ is a maximum uncertainty specified by the device manufacturer in the measurement $\mathbf{p}(k)$. Here, the probability distribution of measurement uncertainty is assumed as uniform distribution [1]. The standard uncertainty of measurement $\mathbf{p}(k)$ can be approximated by the standard deviation [2]:

$$u(\mathbf{p}(k)) = \sigma_{\mathbf{p}(k)}. \tag{5.2}$$

Then, **R** can be constructed by (3.3) based on (5.1) and (5.2).

5.1.2 Measurement Uncertainty Propagation by the Classical Theory of Uncertainty Propagation

When the measurement is calculated by the other measurements, the measurement uncertainty is propagated. It is known as the measurement uncertainty propagation. Since the PMU measurement rule employs pseudo measurement which is calculated by other direct/pseudo measurements, studies on measurement uncertainty propagation in the pseudo measurement have been investigated in power system SE. Mainly in the direct measurement, measurement uncertainty occurs in the PMU data acquisition process, such as in the instrument transformer, the A/D converter, and the cables connecting them [3]. Since the error of PMU direct measurement is pretty small, its SE performance is superior to RTUs as shown in the Chapter 4. However, due to multiple time of use of pseudo measurements (a pseudo measurement using pseudo measurements), the HSE

performance may be deteriorated. Thus, consideration of measurement uncertainty is necessary in SE.

There have been some studies about consideration of measurement uncertainty in pseudo measurement. Chakrabarti et al. applied random fuzzy variables to evaluate the measurement uncertainty associated with voltage magnitude and angle measurement uncertainty obtained by PMUs [3]. Asprou and Kyriakides included evaluation of measurement uncertainty propagation by the classical uncertainty propagation theory in HSE with PMU and RTU, referring to meter placements from another article [4]. Chakrabarti et al. also considered measurement uncertainty propagation in several SE algorithms such as polar or rectangular coordinates [5]. These papers have considered inclusion of uncertainty propagation of pseudo measurement in SE, however, there has been no consideration of measurement uncertainty propagation for optimally placing meters although it should be considered when the pseudo measurements are used. Thus, this chapter proposes CCS-MOOPP considering measurement uncertainty in PMU pseudo measurement, named CCS-MOOPP/U in order to obtain a Pareto front assuring the SE accuracy with measurement uncertainty propagation.

As the ways to obtain the pseudo measurement were introduced in the Chapter 3, this section builds how measurement uncertainty propagation occurs in those pseudo measurement patterns via the classical uncertainty propagation theory. By the classical uncertainty propagation theory, the standard uncertainty of measurement n obtained via measurements $\mathbf{p}$ is generally given by [1]:

$$u(n) = \sqrt{\sum_{k=1}^{m} \left[\frac{\partial n}{\partial \mathbf{p}(k)} u(\mathbf{p}(k)) \right]^2} , \tag{5.3}$$

where $\mathbf{p}$ is a measurement vector used to compute the pseudo measurements, $u(n)$ is the standard uncertainty of measurement n, m is the length of vector $\mathbf{p}$.

Firstly, the case of obtaining the voltage phasor at the adjacent bus of the PMU placement bus using direct voltage/current phasor is given as follows by rewriting (3.28):

$$\dot{V}_j = \frac{\dot{V}_i(\dot{Y}_0 + \dot{Y}_{ij}) - \dot{I}_{ij}}{\dot{Y}_{ij}} , \tag{5.4}$$

where $\dot{V}$, $\dot{I}$ and $\dot{Y}$ indicate the bus voltage phasor, line current phasor and admittance, respectively, subscripts i and j indicate the bus numbers, when those are seriated, that means the line between buses i and j. The subscript 0 means shunt component. Now, pseudo measurements are V_j and θ_j. Hence, standard uncertainties $u(V_j)$ and $u(\theta_j)$ are calculated based on partial derivatives by each element of $\mathbf{p}$=[V_i, θ_i, I_{ij}, φ_{ij}]. (5.4) can be written as:

$$\dot{V}_j = \dot{V}_i + \dot{V}_i \frac{\dot{Y}_0}{\dot{Y}_{ij}} - \frac{\dot{I}_{ij}}{\dot{Y}_{ij}} . \tag{5.5}$$

Then, by writing the complex voltage $\dot{V}_j = A + jB$, A and B are:

$$A = V_i \cos(\theta_i) + V_i \frac{Y_0}{Y_{ij}} \cos(\theta_i + \psi_0 - \psi_{ij}) - \frac{I_{ij}}{Y_{ij}} \cos(\varphi_{ij} + \psi_{ij}) , \tag{5.6}$$

$$B = V_i \sin(\theta_i) + V_i \frac{Y_0}{Y_{ij}} \sin(\theta_i + \psi_0 - \psi_{ij}) - \frac{I_{ij}}{Y_{ij}} \sin(\varphi_{ij} + \psi_{ij}) , \tag{5.7}$$

where, θ_i is voltage angle at bus i, φ_{ij} is current angle at line i-j, ψ_0 is angle of shunt admittance ψ_{ij} is angle of series admittance of line i-j. By A and B, voltage phasor at bus j in polar form is represented as follows:

$$V_j = \sqrt{A^2 + B^2} , \tag{5.8}$$

$$\theta_j = \tan^{-1}\left(\frac{B}{A}\right). \tag{5.9}$$

For V_j and θ_j, partial derivatives by measurements $\mathbf{p}$=[V_i, θ_i, I_{ij}, φ_{ij}] are derived as:

$$\frac{\partial V_j}{\partial V_i} = \begin{pmatrix} B\left(\sin(\theta_i) + Y_0 / Y_{ij} \sin(\theta_i + \psi_0 - \psi_{ij})\right) \\ +A\left(\cos(\theta_i) + Y_0 / Y_{ij} \cos(\theta_i + \psi_0 - \psi_{ij})\right) \end{pmatrix} \Big/ \sqrt{A^2 + B^2} , \tag{5.10}$$

$$\frac{\partial V_j}{\partial \theta_i} = \begin{pmatrix} A\left(-V_i \sin(\theta_i) + V_i Y_0 / Y_{ij} \sin(\theta_i + \psi_0 - \psi_{ij})\right) \\ +B\left(V_i \cos(\theta_i) + V_i Y_0 / Y_{ij} \cos(\theta_i + \psi_0 - \psi_{ij})\right) \end{pmatrix} \Big/ \sqrt{A^2 + B^2} , \tag{5.11}$$

$$\frac{\partial V_j}{\partial I_{ij}} = \frac{B\left(-1/Y_{ij} \sin(\varphi_{ij} - \psi_{ij})\right) - A\left(1/Y_{ij} \cos(\varphi_{ij} - \psi_{ij})\right)}{\sqrt{A^2 + B^2}} , \tag{5.12}$$

$$\frac{\partial V_j}{\partial \varphi_{ij}} = \frac{A\left(I_{ij}/Y_{ij} \sin(\varphi_{ij} - \psi_{ij})\right) - B\left(I_{ij}/Y_{ij} \cos(\varphi_{ij} - \psi_{ij})\right)}{\sqrt{A^2 + B^2}} , \tag{5.13}$$

$$\begin{aligned} C = {} & V_i^2 Y_{ij}^2 + 2V_i^2 Y_{ij} Y_0 \cos(\psi_0 - \psi_{ij}) + V_i^2 Y_0^2 - 2V_i Y_{ij} I_{ij} \cos(\theta_i - \varphi_{ij} - \psi_{ij}) \\ & - 2V_i Y_0 I_{ij} \cos(\psi_0 + \theta_i - \varphi_{ij}) + I_{ij}^2 \end{aligned} , \tag{5.14}$$

$$\frac{\partial \theta_j}{\partial V_i} = -\frac{I_{ij}\left(Y_{ij} \sin(\theta_i - \varphi_{ij} + \psi_{ij}) + Y_0 \sin(\psi_0 + \theta_i - \varphi_{ij})\right)}{C} , \tag{5.15}$$

$$\frac{\partial \theta_j}{\partial \theta_i} = -V_i \begin{pmatrix} V_i Y_{ij}^2 + 2V_i Y_{ij}^2 Y_0 \cos\left(\psi_0 - \psi_{ij}\right) + V_i Y_0^2 \\ -I_{ij} Y_{ij} \cos\left(\theta_i - \varphi_{ij} + \psi_{ij}\right) - Y_0 I_{ij} \cos\left(\psi_0 + \theta_i - \varphi_{ij}\right) \end{pmatrix} \Big/ C \,, \tag{5.16}$$

$$\frac{\partial \theta_j}{\partial I_{ij}} = \frac{V_i \left(Y_{ij} \sin(\theta_i - \varphi_{ij} + \psi_{ij}) + Y_0 \sin(\psi_0 + \theta_i - \varphi_{ij})\right)}{C} \,, \tag{5.17}$$

$$\frac{\partial \theta_j}{\partial \varphi_{ij}} = \frac{I_{ij} \left(-V_i Y_{ij} \cos(\theta_i - \varphi_{ij} + \psi_{ij}) - V_i Y_0 \cos(\psi_0 + \theta_i - \varphi_{ij}) + I_{ij}\right)}{C} \,. \tag{5.18}$$

After obtaining $u(V_j)$ and $u(\theta_j)$ based on (5.3) and corresponding partial derivatives, these are converted from polar to rectangular coordinate since the HSE in this research allows to use the rectangular coordinate in the measurement vector shown in (3.18). Thus, measurement uncertainty propagation also occurs in this transformation. The polar coordinate quantities are converted to the rectangular coordinate by (3.23) and (3.24), standard uncertainties of real and imaginary voltage $u(V_{j,\mathrm{R}})$ and $u(V_{j,\mathrm{I}})$ are given by follows:

$$\begin{aligned} u(V_{j,R}) &= \sqrt{\left[\left(\frac{\partial V_{j,R}}{\partial V_j}\right) u(V_j)\right]^2 + \left[\left(\frac{\partial V_{j,R}}{\partial \theta_j}\right) u(\theta_j)\right]^2} \\ &= \sqrt{\left[\cos(\theta_j) \cdot u(V_j)\right]^2 + \left[V_j \sin(\theta_j) \cdot u(\theta_j)\right]^2} \end{aligned} \,, \tag{5.19}$$

$$\begin{aligned} u(V_{j,I}) &= \sqrt{\left[\left(\frac{\partial V_{j,I}}{\partial V_j}\right) u(V_j)\right]^2 + \left[\left(\frac{\partial V_{j,I}}{\partial \theta_j}\right) u(\theta_j)\right]^2} \\ &= \sqrt{\left[\sin(\theta_j) \cdot u(V_j)\right]^2 + \left[V_j \cos(\theta_j) \cdot u(\theta_j)\right]^2} \end{aligned} \,. \tag{5.20}$$

Second, the case of obtaining current pseudo measurement on line between buses which both of the voltage phasors are known is given by arranging (5.4) as following equation:

$$\dot{I}_{ij} = \dot{V}_i \dot{Y}_0 + (\dot{V}_i - \dot{V}_j) \dot{Y}_{ij} \,. \tag{5.21}$$

Then, by writing the complex current $\dot{I}_{ij} = D + jE$, D and E are:

$$D = V_i Y_0 \cos(\theta_i + \psi_0) + V_i Y_{ij} \cos(\theta_i + \psi_{ij}) - V_j Y_{ij} \cos(\theta_j + \psi_{ij}) \,, \tag{5.22}$$

$$E = V_i Y_0 \sin(\theta_i + \psi_0) + V_i Y_{ij} \sin(\theta_i + \psi_{ij}) - V_j Y_{ij} \sin(\theta_j + \psi_{ij}) \,. \tag{5.23}$$

By the same procedure of previous case, for I_{ij} and φ_{ij}, partial derivatives by measurements $\mathbf{p}$=[V_i, θ_i, V_j, θ_j] are derived as:

$$\frac{\partial I_{ij}}{\partial V_i}=\begin{pmatrix}E\left(Y_{ij}\sin(\theta_i+\psi_{ij})+Y_0\sin(\theta_i+\psi_0)\right)\\+D\left(Y_{ij}\cos(\theta_i+\psi_{ij})+Y_0\cos(\theta_i+\psi_0)\right)\end{pmatrix}\Big/\sqrt{D^2+E^2}\ , \tag{5.24}$$

$$\frac{\partial I_{ij}}{\partial \theta_i}=\begin{pmatrix}D\left(-V_iY_{ij}\sin(\theta_i+\psi_{ij})-V_iY_0\sin(\theta_i+\psi_0)\right)\\+E\left(V_iY_{ij}\cos(\theta_i+\psi_{ij})+V_iY_0\cos(\theta_i+\psi_0)\right)\end{pmatrix}\Big/\sqrt{D^2+E^2}\ , \tag{5.25}$$

$$\frac{\partial I_{ij}}{\partial V_j}=\frac{E\left(-Y_{ij}\sin(\theta_j+\psi_{ij})\right)+D\left(-Y_{ij}\cos(\theta_j+\psi_{ij})\right)}{\sqrt{D^2+E^2}}\ , \tag{5.26}$$

$$\frac{\partial I_{ij}}{\partial \theta_j}=\frac{D\left(V_jY_{ij}\sin(\theta_j+\psi_{ij})\right)+E\left(-V_jY_{ij}\cos(\theta_i+\psi_{ij})\right)}{\sqrt{D^2+E^2}}\ , \tag{5.27}$$

$$\begin{aligned}F=&V_i^2Y_{ij}^2+2V_i^2Y_{ij}Y_0\cos(\psi_0-\psi_{ij})+V_i^2Y_0^2-2V_iV_jY_{ij}^2\cos(\theta_i-\theta_j)\\&-2V_iV_jY_{ij}Y_0\cos(\psi_0+\theta_i-\theta_j-\varphi_{ij})+V_j^2Y_{ij}^2\end{aligned}\ , \tag{5.28}$$

$$\frac{\partial \varphi_{ij}}{\partial V_i}=\frac{-V_jY_{ij}\left(Y_{ij}\sin(\theta_i-\theta_j)+Y_0\sin(\psi_0+\theta_i-\theta_j-\psi_{ij})\right)}{F}\ , \tag{5.29}$$

$$\frac{\partial \varphi_{ij}}{\partial \theta_i}=V_i\begin{pmatrix}V_iY_{ij}^2+2V_iY_{ij}Y_0\cos(\theta_0-\psi_{ij})+V_iY_0^2\\-V_jY_{ij}^2\cos(\theta_i-\theta_j)-V_jY_{ij}Y_0\cos(\psi_0+\theta_i-\theta_j-\psi_{ij})\end{pmatrix}\Big/F\ , \tag{5.30}$$

$$\frac{\partial \varphi_{ij}}{\partial V_j}=\frac{V_jY_{ij}\left(Y_{ij}\sin(\theta_i-\theta_j)+Y_0\sin(\psi_0+\theta_i-\theta_j-\psi_{ij})\right)}{F}\ , \tag{5.31}$$

$$\frac{\partial \varphi_{ij}}{\partial \theta_j}=\frac{V_jY_{ij}\left(-V_iY_{ij}\cos(\theta_i-\theta_j)-V_iY_0\cos(\psi_0+\theta_i-\theta_j-\psi_{ij})+V_jY_{ij}\right)}{F}\ . \tag{5.32}$$

After obtaining $u(I_{ij})$ and $u(\varphi_{ij})$ based on (5.3) and corresponding partial derivatives, these are converted from polar to rectangular coordinate by the same procedure in case of V_i and θ_i by (5.19) and (5.20). Then, standard uncertainties $u(I_{ij,\mathrm{R}})$ and $u(I_{ij,\mathrm{I}})$ are obtained.

Third, current pseudo measurement on a line connected to a ZIB *i* when the other current phasors incident to the ZIB *i* is known is given by:

$$\dot{I}_{ij}=\sum_{k=1}^{l}\dot{I}_{ki}\ . \tag{5.33}$$

where the line *i*-*j* is connected to ZIB *i* and the adjacent bus *j*. Then, by writing the complex current $\dot{I}_{ij}=G+jH$, G and H are:

$$G = \sum_{i=1}^{l} I_{ki} \cos(\varphi_{ki}) \,, \tag{5.34}$$

$$H = \sum_{i=1}^{l} I_{ki} \sin(\varphi_{ki}) \,. \tag{5.35}$$

By the same procedure of previous case, for I_{ij} and φ_{ij}, partial derivatives by measurements $\mathbf{p}=[I_{1i}, \varphi_{1i}, \ldots I_{li}, \varphi_{li}]$ (l >1) are derived. Here, for example, the case of l=2 is derived:

$$\frac{\partial I_{ij}}{\partial I_{1i}} = \frac{H \sin(\varphi_{1i}) + G \sin(\varphi_{1i})}{\sqrt{G^2 + H^2}} \,, \tag{5.36}$$

$$\frac{\partial I_{ij}}{\partial \varphi_{1i}} = \frac{H I_{1i} \cos(\varphi_{1i}) - G I_{1i} \sin(\varphi_{1i})}{\sqrt{G^2 + H^2}} \,, \tag{5.37}$$

$$\frac{\partial I_{ij}}{\partial I_{2i}} = \frac{H \sin(\varphi_{2i}) + G \sin(\varphi_{2i})}{\sqrt{G^2 + H^2}} \,, \tag{5.38}$$

$$\frac{\partial I_{ij}}{\partial \varphi_{2i}} = \frac{H I_{2i} \cos(\varphi_{2i}) - G I_{2i} \sin(\varphi_{2i})}{\sqrt{G^2 + H^2}} \,, \tag{5.39}$$

$$J = I_{1i}^2 + 2 I_{1i} I_{2i} \cos(\varphi_{1i} - \varphi_{2i}) + I_{2i}^2 \,, \tag{5.40}$$

$$\frac{\partial \varphi_{ij}}{\partial I_{1i}} = \frac{I_{2i} \sin(\varphi_{1i} - \varphi_{2i})}{J} \,, \tag{5.41}$$

$$\frac{\partial \varphi_{ij}}{\partial \varphi_{1i}} = \frac{I_{1i} \left(I_{1i} + I_{2i} \cos(\varphi_{1i} - \varphi_{2i}) \right)}{J} \,, \tag{5.42}$$

$$\frac{\partial \varphi_{ij}}{\partial I_{2i}} = \frac{-I_{1i} \sin(\varphi_{1i} - \varphi_{2i})}{J} \,, \tag{5.43}$$

$$\frac{\partial \varphi_{ij}}{\partial \varphi_{2i}} = \frac{I_{2i} \left(I_{2i} + I_{1i} \cos(\varphi_{1i} - \varphi_{2i}) \right)}{J} \,, \tag{5.44}$$

After obtaining $u(I_{ij})$ and $u(\varphi_{ij})$ based on (5.3) and corresponding partial derivatives, these are converted from polar to rectangular coordinate by the same procedure in case of V_i and θ_i by (5.19) and (5.20). Then, $u(I_{ij,\mathrm{R}})$ and $u(I_{ij,\mathrm{I}})$ are obtained.

By those above equations, measurement uncertainty propagation occurs in PMU pseudo measurement. CCS-MOOPP/U includes calculation of all of those in every MCS scenario. Therefore, it is expected that the computation burden

increases compared to CCS-MOOPP which totally ignores measurement uncertainty propagation.

5.2 NUMERICAL SIMULATION

5.2.1 Configuration

In order to verify the betterness of consideration of measurement uncertainty propagation by CCS-MOOPP/U, numerical experiment in modified NE 39-bus is conducted. The single line connection diagram of modified NE 39-bus is reshown in Fig. 5.1. Using the same parameters as Table 4.1 and RTU placement as Table 4.7, NSGA-II is applied and obtained Pareto fronts in both methods: CCS-MOOPP and CCS-MOOPP/U. Pareto fronts are compared between the one by CCS-MOOPP/U and the other one by CCS-MOOPP with applying measurement uncertainty propagation.

5.2.2 Comparison of Pareto Solutions

Fig. 5.2 shows Pareto fronts obtained by two methods: CCS-MOOPP/U and CCS-MOOPP. The black square dot is the Pareto solutions which the blue asterisk dot is moved by applying measurement uncertainty propagation. It indicates that the SE accuracy is worsened from the original solution in CCS-MOOPP because of multiple time of use of PMU pseudo measurement. It especially happens when PMU device cost K_{VC} is high: the many PMUs are placed, the many pseudo measurements are used and the level of pseudo measurements is deeper. For the

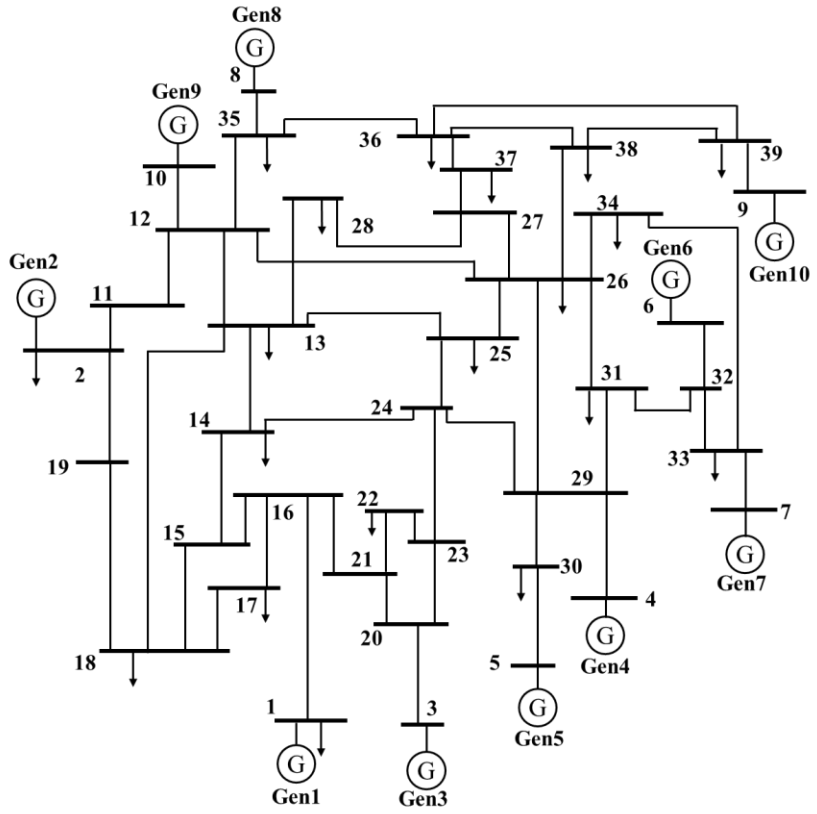

Fig. 5.1 IEEE modified NE 39-bus test system single line connection diagram.

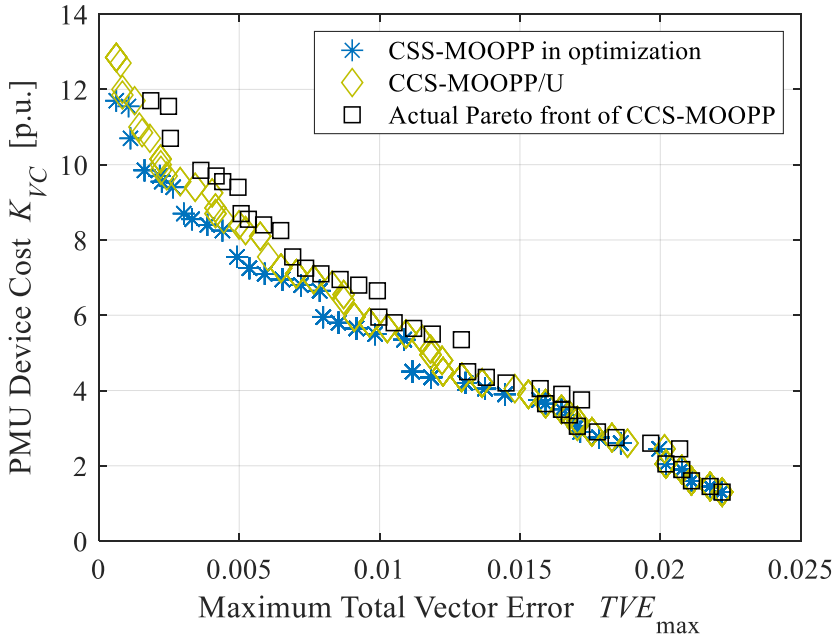

Fig. 5.2 Pareto front comparison in CCS-MOOPP/U and CCS-MOOPP in modified NE 39-bus.

Table 5.1 Ratio of Non-dominated Individuals in modified NE 39-bus.

Method	RNI	CR
CCS-MOOPP/U	0.8727	0.9500
CCS-MOOPP (actual Pareto front)	0.1273	0.8500

quantitative evaluation, Table 5.1 shows RNI and CR for each method. From the table, the Pareto front of CCS-MOOPP/U is numerically dominating the one obtained by CCS-MOOPP with evaluation including measurement uncertainty propagation. CR is computed by *nd*=20. Looking at CR, CCS-MOOPP/U is bigger than CCS-MOOPP because the solution space is bigger. This is caused by introduction of measurement uncertainty propagation. In CCS-MOOPP, there are different PMU placements having same cost and same TVE (in the optimization). However, it can be different TVE depending on how to obtain pseudo measurements and how many times pseudo measurement is used multiply.

5.2.3 Verification of Measurement Uncertainty Propagation

To check how measurement uncertainty propagation influences the HSE error, a solution is selected from Pareto front of CCS-MOOPP/U and CCS-MOOPP having same PMU device cost. Fig. 5.3 shows the zoomed figure of Fig. 5.1, S1 and S2 are selected from Pareto front obtained by CCS-MOOPP/U and CCS-MOOPP, respectively. The details of these solutions are listed in Table 5.2. Also, types of measurement: direct and pseudo measurements are listed in Table 5.3 by bus number in detail. For the pseudo measurement, how many times it is used is discussed. In the third column of Table 5.3, it is represented as a set as $\{\ \}_n$. The

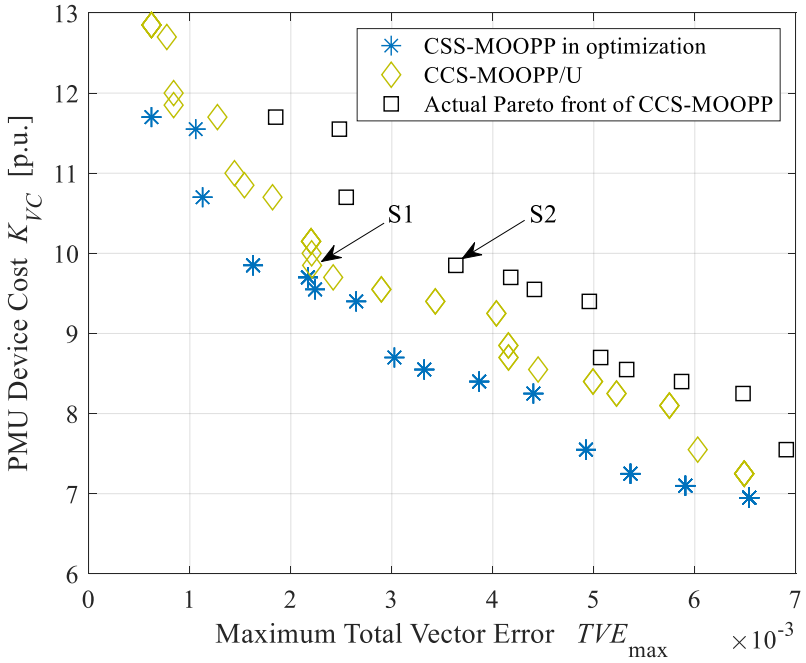

Fig. 5.3 Pareto front comparison in CCS-MOOPP/U and CCS-MOOPP in modified NE 39-bus.

Table 5.2 Selected solutions in modified NE 39-bus and PMU placements.

Solu-tion	Placement: bus / line(bus No.-bus.No.)				K_{VC} [p.u.]	TVE_{max}
	PMU + voltage channel		Current channel			
	Common parts	Diff-erence	Common parts	Difference		
S1	12, 33	16, 23, 26, 30, 36	12-10, 12-11, 12-13, 33-7, 33-32	16-1, 16-15, 16-21, 23-22, 23-24, 26-25, 26-27, 26-31, 26-34, 30-5, 30-29, 36-37, 36-38, 36-39	10.00	5.73×10^{-2}
S2		18, 22, 28, 29, 39		18-15, 18-17, 18-19, 22-21, 22-23, 28-27, 29-24, 29-26, 29-30, 29-31, 33-34, 39-9, 39-36, 39-38	10.15	5.73×10^{-2}

elements of a set includes bus number, the subscript *n* indicates a pseudo measurement level. Here, the pseudo measurement level is defined as how many times direct/pseudo voltage phasor measurement at bus is used through until the pseudo measurement is obtained. The many more the pseudo measurement is used, the bigger *n* is. The fourth column of Table 5.3 is buses which have no PMU measurements. However, estimated state by SCADA SE is already obtained beforehand of the linear SE part in HSE, observability of the system is ensured.

Table 5.3 Measurement type classification in each solution.

Solu -tion	PMU measurement bus		No PMU measurement bus
	Direct measurement	Pseudo measurement	
S1	12, 16, 23, 26, 30, 33, 36	{1, 5, 7, 10, 11, 13, 15, 21, 22, 24, 25, 27, 29, 31, 32, 34, 37, 38, 39}$_1$, {2, 4, 6, 14, 17, 20, 28, 35}$_2$, {3, 18}$_3$	8, 9, 19
S2	12, 18, 22, 28, 29, 33, 39	{7, 9, 10, 11, 13, 15, 17, 19, 21, 23, 24, 26, 27, 30, 31, 32, 34, 36, 38}$_1$, {2, 4, 6, 20, 35, 37}$_2$, {3, 16}$_3$, {1, 14}$_4$, {25}$_5$,	5, 8

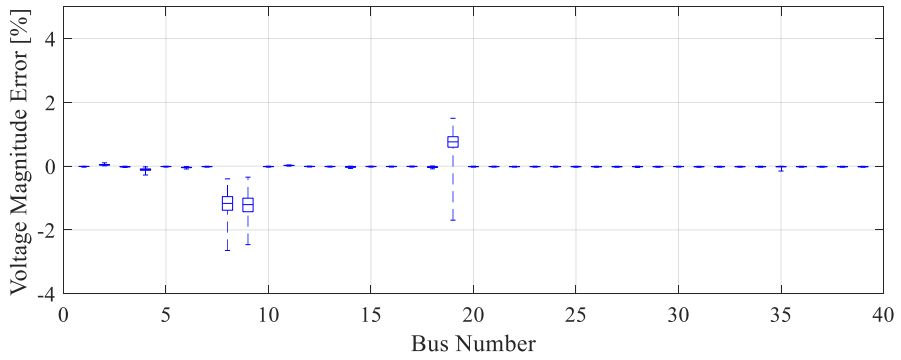

Fig. 5.4 Voltage magnitude error of PMU placement S1.

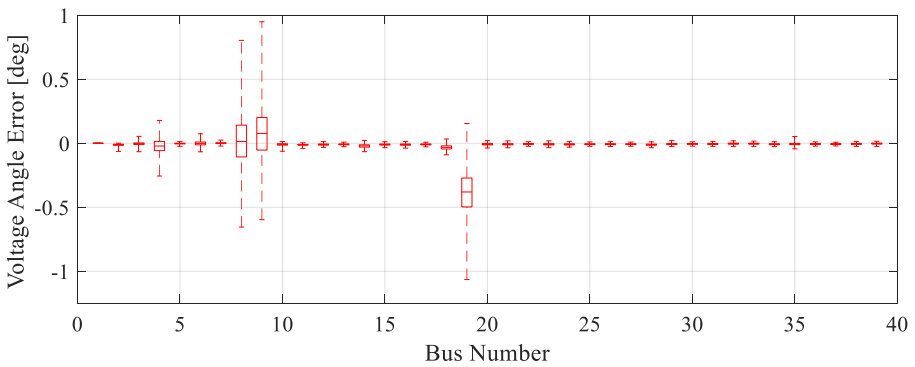

Fig. 5.5 Voltage angle error of PMU placement S1.

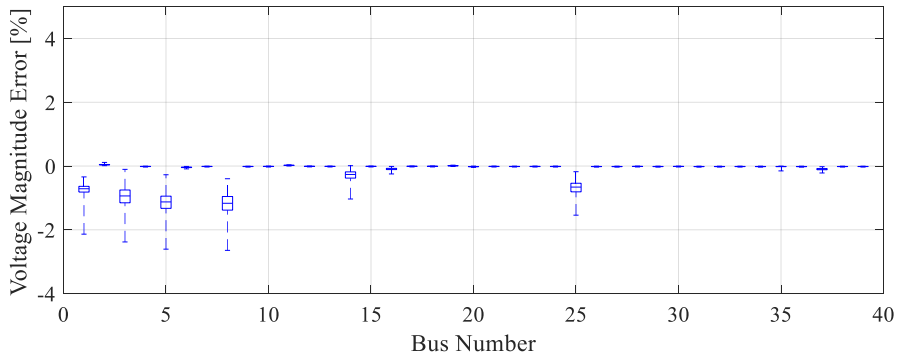

Fig. 5.6 Voltage magnitude error of PMU placement S2.

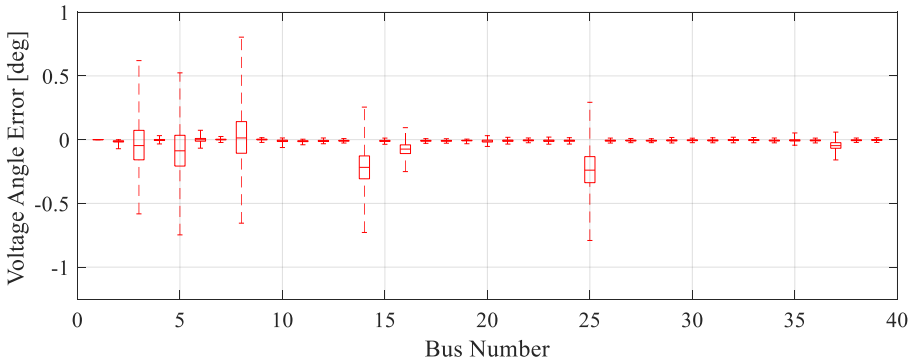

Fig. 5.7 Voltage angle error of PMU placement S2.

From Table 5.3, there are pseudo measurements with at most pseudo measurement level 3 in S1 from CCS-MOOPP/U whereas S2 from CCS-MOOPP uses the pseudo measurements with pseudo measurement levels 3, 4, 5. This indicates that S2 uses more multiple time of use of the pseudo measurements which may increase standard uncertainty of the PMU measurements. Figures 5.4 and 5.5 show boxplots of the HSE estimation errors in S1 for voltage magnitude and angle, respectively. Figures 5.6 and 5.7 show boxplots of the HSE estimation errors in S2 for voltage magnitude and angle, respectively. Comparing these pairs of figures, the error increases by measurement uncertainty propagation in pseudo measurement in S1 is well controlled by considering uncertainty propagation in the optimization process. However, estimation errors in S2 get increased especially in buses 3, 14, 25 due to ignoring the uncertainty propagation in the optimization process. This eventually causes making $TVE_{\max}$ bigger. Thus, there are some gaps between Pareto front of CCS-MOOPP/U and the actual Pareto front of CCS- MOOPP in terms of $TVE_{\max}$.

5.3 SUMMARY

This chapter investigated the influence of measurement uncertainty propagation in use of pseudo measurement of PMU in MOOPP problem. Because it has not been considered in the past OPP problem even though it has been included in research of SE, this chapter included occurrence of measurement uncertainty

propagation by PMU pseudo measurements by three ways, based on the classical uncertainty propagation theory. As the results of numerical simulation in modified NE 39-bus, influence of measurement uncertainty propagation is significant when pseudo measurements are multiply used to obtain a pseudo measurement. By considering uncertainty propagation in the optimization, the proper SE error evaluation can be conducted. This chapter contributes to a PMU placement assessment with a proper SE error evaluation and spurring the installation of PMU that enables more accurate system security assessment to prevent future blackouts.

5.4 REFERENCES

[1] ISO-IEC-OMIL-BIPM, Guide to the Expression of Uncertainty in Measurement, JCGM, Sèvres, France, 1992.

[2] S. Chakrabarti, and E. Kyriakides, PMU measurement uncertainty consideration in WLS state estimation, *IEEE Transactions on Power Systems*, vol. 24, no. 2, pp. 1062-1071, 2009.

[3] S. Chakrabarti, E. Kyriakides, and M. Albu, Uncertainty in power system state variables obtained through synchronized measurements, *IEEE Transactions on Instrumentation and Measurement*, vol. 58, no. 8, pp. 2452-2458, 2009.

[4] M. Asprou and E. Kyriakides, Enhancement of hybrid state estimation using pseudo flow measurements, *2011 IEEE PES General Meeting*, Detroit, MI, USA, 2011.

[5] S. Chakrabarti, E. Kyriakides, G. Ledwich, and A. Ghosh, Inclusion of PMU current phasor measurements in a power system state estimator, *IET Generation, Transmission and Distribution*, vol. 4, no. 10, pp.1104-1115, 2010.

6 Phasor-Assisted Voltage Stability Assessment Based on Optimally Placed PMUs

6.1 VOLTAGE STABILITY ASSESSMENT IN POWER SYSTEMS

6.1.1 Voltage Stability

Voltage stability in a power system is the ability to maintain the system bus voltage by a certain level when load increase or generator/line outage occurs. Bus voltage gradually decreases in accordance with a lack of reactive power supply. If bus voltage is not maintained, the decrease of voltage eventually results in voltage collapse in the whole power system. The bus voltage profile is somewhat complicated in recent power systems by operation closer to stability limits due to increasing demand and deregulation in the electricity market in recent years.

The voltage stability problem in power systems has been an issue since 1965 with the voltage collapse of the French power system [1]. Also, there have been several voltage instability instances in some other countries. Some of them are cited for this introduction: in the interconnected power system of the western part of US, a system separation into five islands by a single phase-to-ground fault caused voltage collapse in 1996 [2]. The Chilean power system experienced the blackout in May 1997, triggered by a reverse action of On Load Tap Changers (OLTC) which resulted in the voltage collapse with an increase of reactive power consumption [3]. The Athenian power system experienced a whole blackout by voltage collapse due to staged load shedding as a result of heavy loading in the summer of 2004 [4]. There had been plans to upgrade the voltage stability in preparation for the Olympic Games in Athens. Unfortunately, the system experienced a blackout before the upgrading. The severe blackout by voltage collapse in India in July 2012 is still fresh in our memory [5]. The direct cause of the blackout was overloading under the circumstance of planned outage on several transmission lines. Since voltage collapse resulting in blackout impacts the economics, the voltage security level must be maintained by power system preventive security controls. To understand how far the power system is away from the voltage collapse point, VSI is calculated.

6.1.2 Voltage Stability Index

VSI is calculated and used for understanding the voltage stability level using several quantities to avoid the voltage collapse. In research of VSI, there have been some different voltage stability indices, summarized in a review paper [6].

Bus VSI

Bus VSI is an index based on evaluation in an aggregated system by the Thevenin's equivalent circuit. For the typical bus VSI, there are Voltage Stability Load Index (VLSI) [7], L-Index [8], Voltage Collapse Proximity Index (VCPI) [9], and so on. By the Thevenin's equivalent circuit, the system is represented as a studied system and an external system. After that, VSI is calculated based on the equivalent circuit. Bus VSI determines the voltage stability of system buses and does not provide any information about the weak facilities with potential voltage problems.

Line VSI

Line VSI is an index based on two bus representation of a system, and calculated for each component. Line VSI is directly calculated for a line connecting two buses whereas bus VSI is calculated based on the equivalent circuit. For the typical line VSI, there are Fast Voltage Stability Index (FVSI) [10], L_{mn} [11], Line Collapse Proximity Index (LCPI) [12], Critical Boundary Index (CBI) [13] and so on. Line VSI does not have a process of system reduction and can be computed quickly, it is able to be used for online voltage stability assessment. For this reason, this research employed line VSI.

Jacobian Matrix Based Sensitivity Analysis

Jacobian matrix based VSI can calculate the voltage collapse point and determine the voltage stability margin. In this analysis, Jacobian matrix which represents the relationship between active, reactive power and voltage magnitude, angle in power flow equation, is built. After focusing on the reactive power change, V-Q sensitivity on given operation point determines the stability by its plus or minus sign [6]. However, the computation time is high and any topological change leads to change the Jacobian matrix: hence, this type of analysis is not suitable for online voltage stability assessment.

6.1.3 SE based Voltage Stability Assessment

VSI is calculated using several quantities in a power system. SE gives the state vector assessed by known measurements with errors (uncertainty). Because these two fields are deeply connected, researchers have studied use of estimated state by PMU measurement data for VSI calculation by SE. Tnag et al. proposed an adaptive load shedding method based on both frequency and voltage stability assessment using PMUs [14]. Although the authors established a novel load shedding method based on voltage stability assessment by modal analysis, the basic assumption is that a number of PMUs are sufficient. This assumption indicates the unrealistic situation because placing PMUs at all buses will result in an explosive growth of the system planning cost. Makasa and Venayagamoorthy considered voltage stability assessment based on an optimal PMU placement [7]. However, the authors did not consider the SE error of pseudo measurement which may result in bigger SE errors, via measurement uncertainty propagation shown in the Chapter 5. The ignorance of SE error by not performing actual SE may result in a huge error in the next security assessment. Kesherwani calculated L-index [8] based on optimally placed PMUs by full topological observability of a system [15]. However, incorrect assessment of SE without measurement uncertainty propagation in case of multiple use of ZIB may make the calculation error of L-index bigger. Having

reviewed articles associated with VSI, SE and PMU, to the best of our knowledge, the VSI estimation and the power system SE by optimal PMU placement have not yet been bridged. Therefore, SE based VSI estimation should be considered in detail.

6.2 CRITICAL BOUNDARY INDEX CALCULATION

6.2.1 Critical Boundary Index

From the many VSIs, this research employs CBI proposed by Furukakoi at al. in 2018 [13]. CBI is the most recent line VSI, it numerically shows how far an operation point represented by active and reactive power is away from the critical boundary. On a line between two buses *k* and *l*, receiving complex power is represented as follows:

$$P_l + jQ_l = V_l \angle \theta_l \left(\frac{V_k \angle \theta_k - V_l \angle \theta_l}{R_{kl} + jX_{kl}} \right), \tag{6.1}$$

where, *P*, *Q*, *V*, θ, *R* and *X* are active, reactive power, voltage magnitude, angle, line resistance and reactance, respectively. By separating the real and imaginary parts of (6.1), the following equation can be derived:

$$\begin{aligned} &\left(P_l R_{kl} + Q_l X_{kl}\right) + j\left(P_l X_{kl} - Q_l R_{kl}\right) \\ &= V_k V_l \cos\left(\theta_k - \theta_l\right) - jV_k V_l \sin\left(\theta_k - \theta_l\right) - V_l^2 \cdot \end{aligned} \tag{6.2}$$

By summing the real and imaginary parts of (6.2) using $\sin^2\theta + \cos^2\theta = 1$:

$$\left(P_l R_{kl} + Q_l X_{kl} + V_l^2\right)^2 + \left(P_l X_{kl} - Q_l R_{kl}\right)^2 = V_k^2 V_l^2 , \tag{6.3}$$

$$\left(V_l^2\right)^2 + 2\left(P_l R_{kl} + Q_l X_{kl} + \frac{V_k^2}{2}\right) V_l^2 + \left(R_{kl}^2 + X_{kl}^2\right)\left(P_{kl}^2 + Q_{kl}^2\right) = 0 . \tag{6.4}$$

Hereby, (6.4) is a biquadratic equation, V_l^2 can be derived as follows:

$$\begin{aligned} V_l^2 = &-\left(P_l R_{kl} + Q_l X_{kl} + \frac{V_k^2}{2}\right) \\ &\pm \sqrt{\left(P_l R_{kl} + Q_l X_{kl} + \frac{V_k^2}{2}\right)^2 - \left(R_{kl}^2 + X_{kl}^2\right)\left(P_{kl}^2 + Q_{kl}^2\right)} . \end{aligned} \tag{6.5}$$

Based on (6.5), the voltage stability limit is valid when the part of square root is 0. In order to verify the distance between the current operation point and the critical boundary point, Lagrange multiplier is applied. From (6.5), the critical boundary point *C*(*X*, *Y*) can be represented as follows:

$$C(X,Y) = \left(P_l R_{kl} + Q_l X_{kl} + \frac{V_k^2}{2}\right)^2 - \left(R_{kl}^2 + X_{kl}^2\right)\left(P_{kl}^2 + Q_{kl}^2\right) = 0 . \tag{6.6}$$

The distance between the current stable operation point $K(P_0, Q_0)$and the nearest point of the voltage collapse $C(X, Y)$ is given by function of $f(X, Y)$. The minimum distance between them is as:

$$f^2 = (X - P_0)^2 + (Y - Q_0)^2 . \tag{6.7}$$

The graphical explanation is shown in Fig. 6.1. The following equation is obtained by using Lagrange multipliers:

$$F(X, Y, \lambda) = f^2(X, Y) - \lambda C(X, Y), \tag{6.8}$$

$$F(X, Y, \lambda) = (X - P_0)^2 + (Y - Q_0)^2 - \lambda \left[\left(P_l R_{kl} + Q_l X_{kl} + \frac{V_k^2}{2} \right)^2 - \left(R_{kl}^2 + X_{kl}^2 \right)\left(P_{kl}^2 + Q_{kl}^2 \right) \right] . \tag{6.9}$$

By applying the partial derivative for X, Y and λ in the above equation, the following equation can be obtained:

$$2X - 2P_0 - \lambda \left[2\left(XR_{kl} + YX_{kl} + \frac{V_k^2}{2} \right)^2 R_{kl}^2 - \left(R_{kl}^2 + X_{kl}^2 \right) X \right] = 0 . \tag{6.10}$$

$$2Y - 2Q_0 - \lambda \left[2\left(XR_{kl} + YX_{kl} + \frac{V_k^2}{2} \right)^2 X_{kl} - 2\left(R_{kl}^2 + X_{kl}^2 \right) Y \right] = 0 . \tag{6.11}$$

$$-\left(XR_{kl} + YX_{kl} + \frac{V_k^2}{2} \right)^2 + \left(R_{kl}^2 + X_{kl}^2 \right)\left(X^2 + Y^2 \right) = 0 . \tag{6.12}$$

Solving simultaneous nonlinear equation (6.10), (6.11) and (6.12), the value of X, Y and λ are simultaneously obtained. After the nearest stable point is determined by X and Y, the shortest distance between the current operation point and the critical boundary is expressed as follows:

$$\Delta P_{kl} = X - P_0 , \tag{6.13}$$

$$\Delta Q_{kl} = Y - Q_0 , \tag{6.14}$$

$$CBI_{kl} = \sqrt{\Delta P_{kl}^2 + \Delta Q_{kl}^2} . \tag{6.15}$$

The obtained CBI_{kl} is the critical boundary index on the line k-l. CBI approaches from a certain value to 0, which means the voltage stability limit.

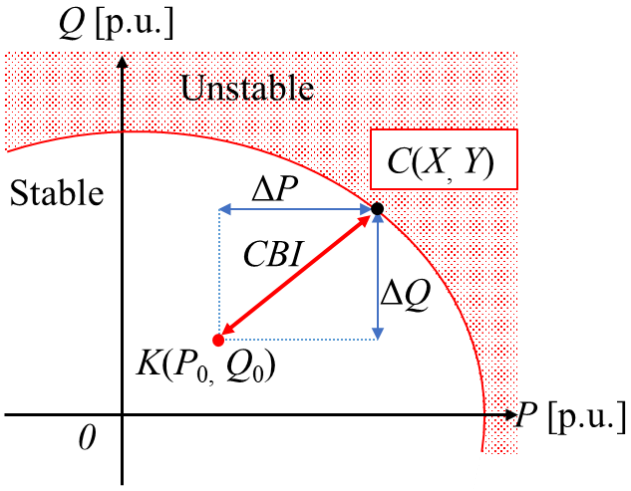

Fig. 6.1 Graphical explanation of CBI.

6.2.2 Procedure of CBI Calculation using Estimated State Vector

In order to calculate CBI on a line connecting buses, the active and reactive power flow of the stable operation point need to be known. In two-stage HSE, the system is assumed to be observable by installed RTUs only which indicates the state vector i.e. voltage phasors at all buses are known, and PMUs are overlapped on the RTU meter network to upgrade the SE accuracy. The receiving-end active and reactive power on a line connecting buses *k*-*l* are calculated as follows:

$$P_l = V_l^2\left(G_{sh} + G_{kl}\right) + V_k V_l\left(G_{kl}\cos\left(\theta_{kl}\right) + B_{kl}\sin\left(\theta_{kl}\right)\right). \tag{6.16}$$

$$Q_l = -V_l^2\left(B_{sh} + B_{kl}\right) + V_k V_l\left(G_{kl}\sin\left(\theta_{kl}\right) + B_{kl}\cos\left(\theta_{kl}\right)\right). \tag{6.17}$$

where, *G* and *B* indicate conductance and susceptance, respectively. The subscripts *sh* and *kl* are the shunt and the line components, respectively. θ_{kl} is the voltage phase angle difference between buses *k* and *l*. The procedure of CBI calculation and following voltage stability assessment and prediction based on HSE is illustrated in Fig. 6.2. As previously described in HSE (Two-stage HSE) two different meters having different order of standard uncertainty simultaneously exist. Based on this procedure, it is assumed that different order of standard uncertainty may cause a big error in CBI estimation since the voltage phase angle difference θ_{kl} is subtraction of those values. To investigate it, a numerical simulation is conducted from the next section.

6.3 Numerical Simulation

6.3.1 Configuration

To perform the CBI calculation using result of HSE, numerical simulation in IEEE modified NE 39-bus reshown in Fig. 6.3 is employed as a target system. Firstly, optimal PMU placement is obtained as a Pareto front by NSGA-II with parameters in Table 4.1. The optimization problem is CCS-MOOPP/U. RTU

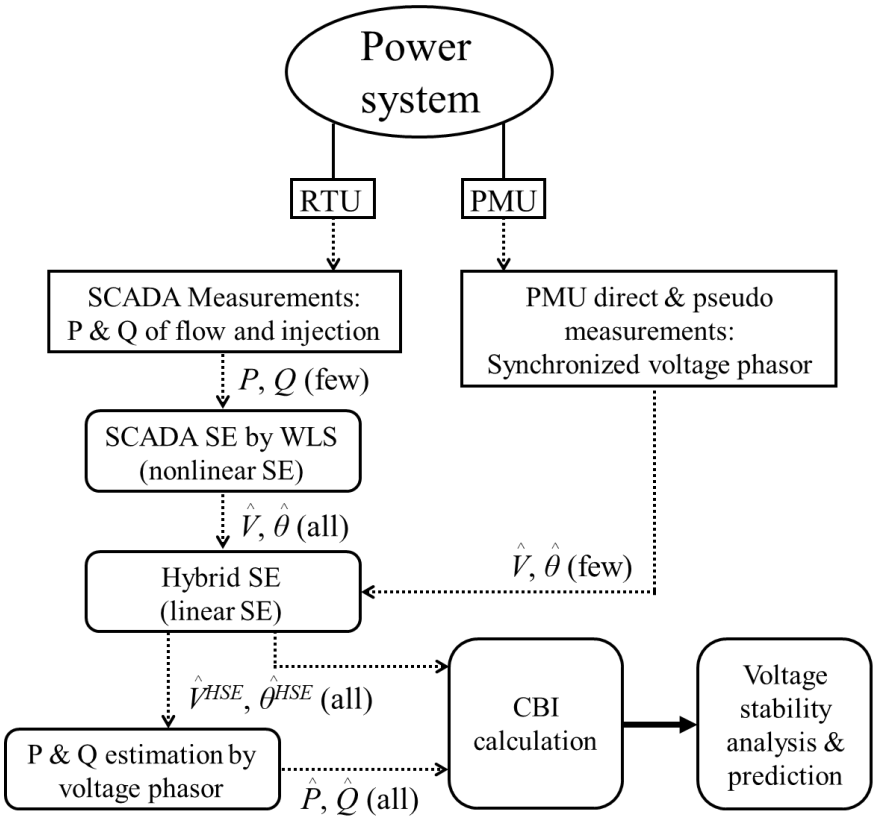

Fig. 6.2 Procedure of CBI and voltage stability assessment by HSE.

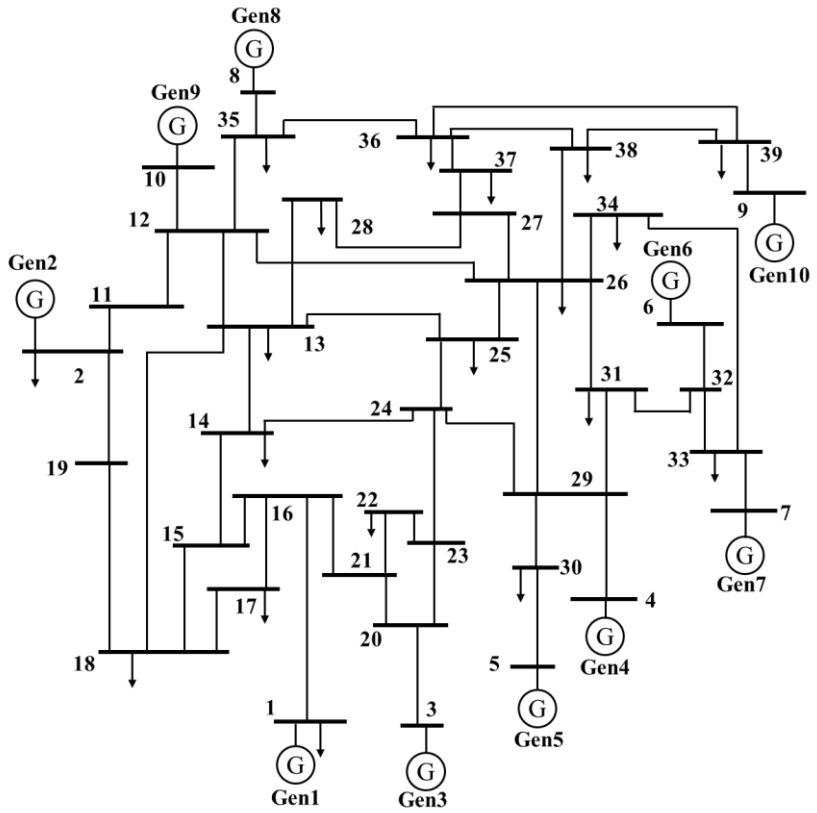

Fig. 6.3 IEEE modified NE 39-bus test system single line connection diagram.

Table 6.1 RTU placement in modified NE 39-bus.

Power injection meter	Power flow meter
1, 4, 5, 6, 7, 8, 9, 10, 11, 12, 13, 14, 15, 16, 17, 18, 19, 20, 21, 22, 23, 24, 25, 26, 27, 28, 29, 30, 31, 32, 33, 34, 35, 36, 37, 38, 39	13-12, 13-14, 13-18, 13-25, 13-28, 14-13, 14-15, 14-24, 17-16, 17-18, 18-13, 18-15, 18-17, 18-19, 22-21, 25-13, 25-24, 25-26, 28-13, 28-27, 30-5, 30-29, 30-29, 31-26, 31-29, 31-32, 33-7, 33-32, 33-34, 34-26, 34-33, 35-8, 35-12, 35-36, 36-35, 36-37, 36-38, 36-39, 37-27, 37-36, 38-26, 38-36, 38-39, 39-9, 39-36, 39-38

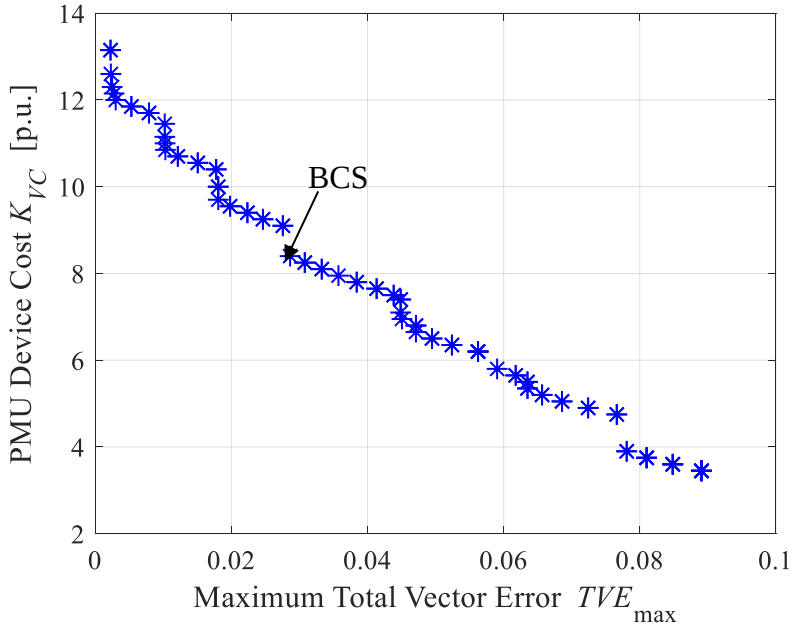

Fig. 6.4 Pareto front obtained by CCS-MOOPP/U using NSGA-II.

Table 6.2 Selected solutions in modified NE 39-bus and PMU placements.

Solu-tion	Placement: bus / line(bus No.-bus.No.)		K_{VC} [p.u.]	TVE_{max}
	PMU + voltage channel	Current channel		
BCS	2, 5, 16, 23, 26, 39	2-11, 2-19, 5-30, 16-1, 16-15, 16-21, 23-22, 23-24, 26-25, 26-27, 26-29, 26-31, 26-34, 39-9, 39-36, 39-38	8.40	2.86×10^{-2}

placement is listed in Table 6.1. The obtained Pareto front is shown in Fig. 6.4. The BCS is selected from the Pareto front by (4.17) and (4.18) (highlighted by the arrowed line on Fig. 6.4), CBI calculation is discussed based on this PMU placement. The PMU placement information is listed in Table 6.2, and the statistical

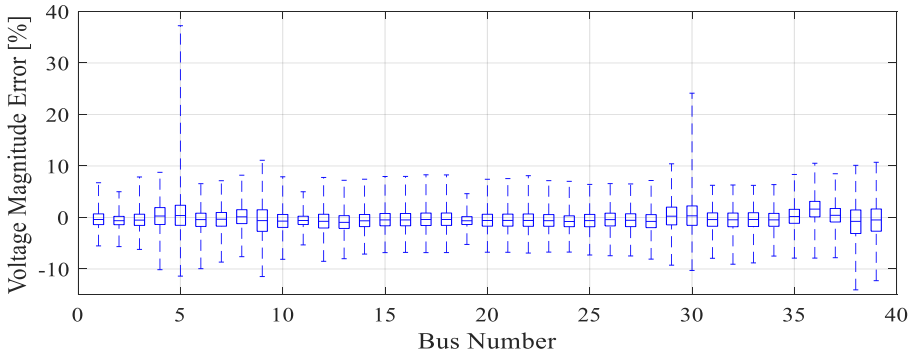

Fig. 6.5 Voltage magnitude error in SCADA SE in modified NE 39-bus.

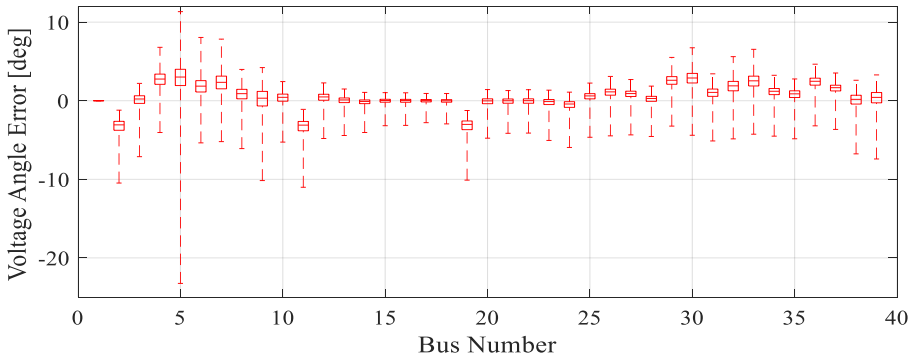

Fig. 6.6 Voltage angle error in SCADA SE in modified NE 39-bus.

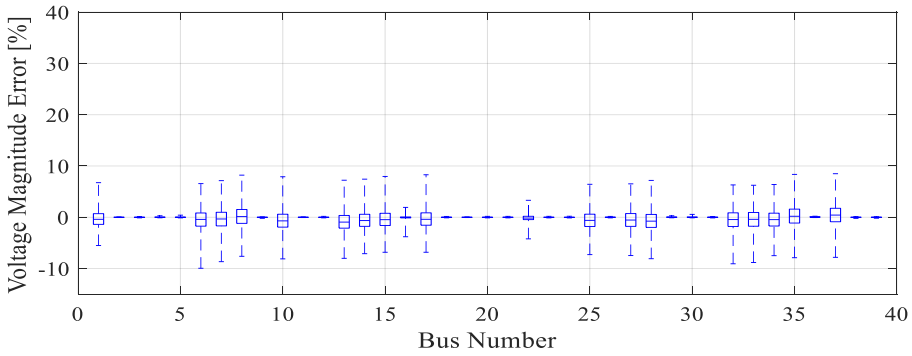

Fig. 6.7 Voltage magnitude error in HSE by S1 in modified NE 39-bus.

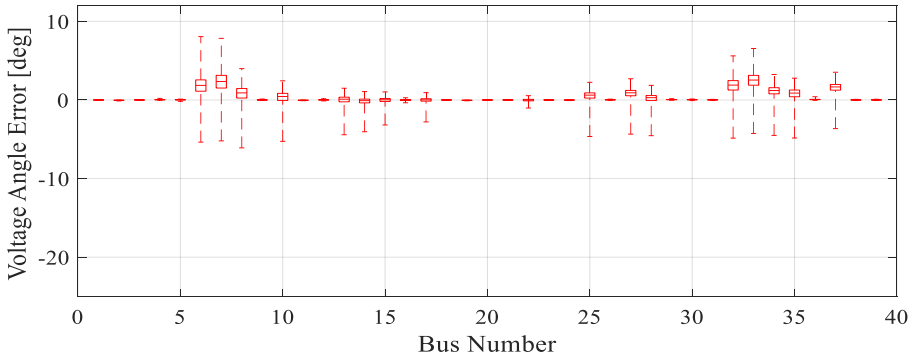

Fig. 6.8 Voltage angle error in HSE by S1 in modified NE 39-bus.

boxplots for all MCS scenarios are shown in Figures 6.5-6.8. Figures 6.5 and 6.6 are SE error by SCADA SE, figures 6.7 and 6.8 are SE error by HSE with PMU placement listed in Table 6.1. PMU's direct/pseudo measurements reduce the SE error at some buses.

6.3.2 CBI Calculation Based on State Vector

By calculating CBI based on the obtained state vector via HSE with optimally placed PMUs, assessing the voltage security level correctly is the target of this chapter. In this process, a concern about CBI calculation error by using voltage phasors at buses which are estimated via different estimator (SCADA and PMU) is assumed. To investigate this, the single load increment test is performed on three cases below for CBI calculation on line *k*-*l*.

Case 1: voltage phasors at buses *k* and *l* are estimated via SCADA SE.

Case 2: voltage phasors at buses *k* and *l* are estimated via PSE.

Case 3: voltage phasors at buses *k* and *l* are estimated via HSE, the one at bus *k* is by PSE, the other one is by SCADA SE.

A CBI calculation line on 38-39 is picked up for example. Active and reactive load increment with an interval of 0.05 p.u. is tested in the load at bus 38. Then, CBI on line 38-39 as $CBI_{38\text{-}39}$ is calculated based on the estimated voltage phasor in three cases above. Fig. 6.9 shows CBI calculation and the transition according to single load increment of bus 38. True value is calculated based on Newton-Raphson power

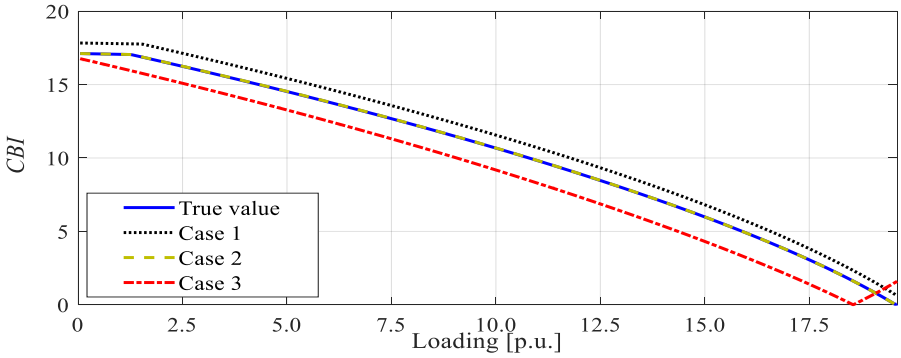

Fig. 6.9 CBI on line 38-39.

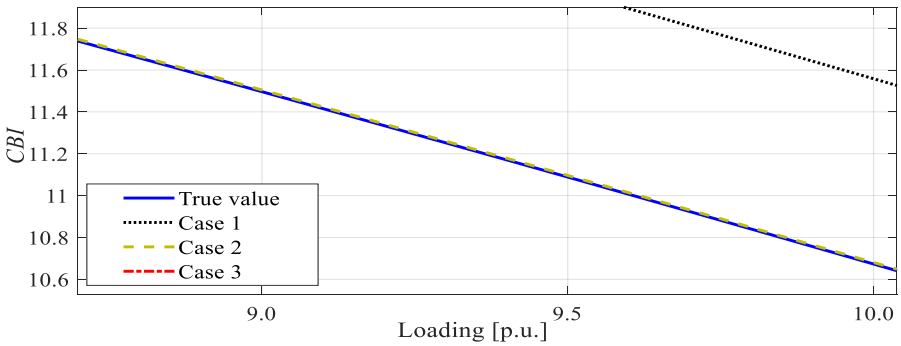

Fig. 6.10 CBI on line 38-39 (zoomed).

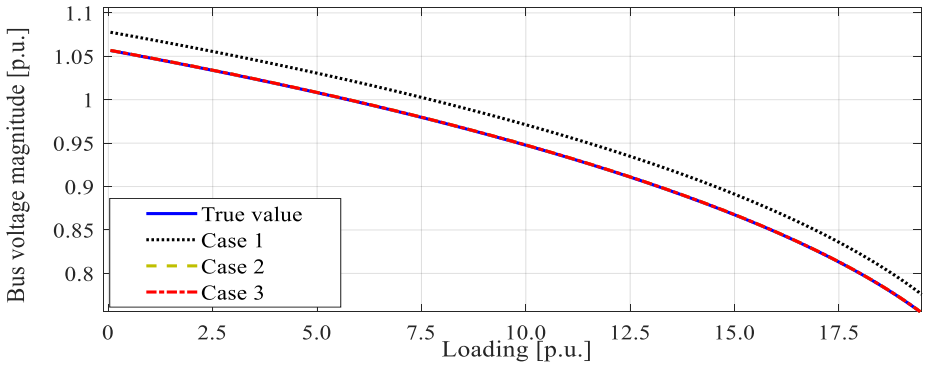

Fig. 6.11 Voltage magnitude at bus 38.

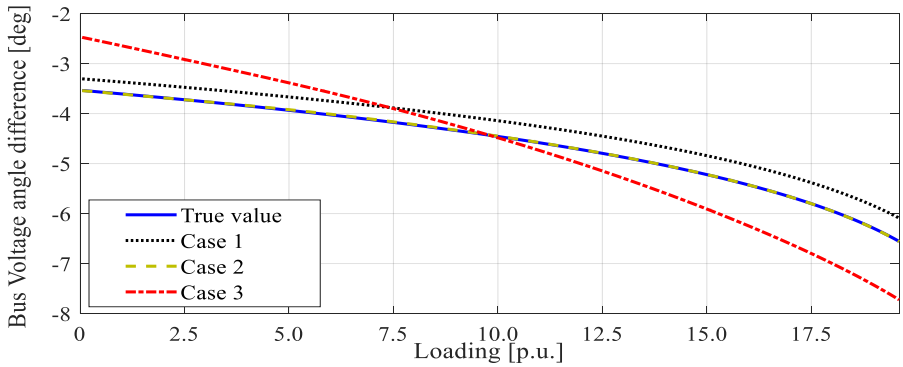

Fig. 6.12 Voltage angle difference between buses 38 and 39.

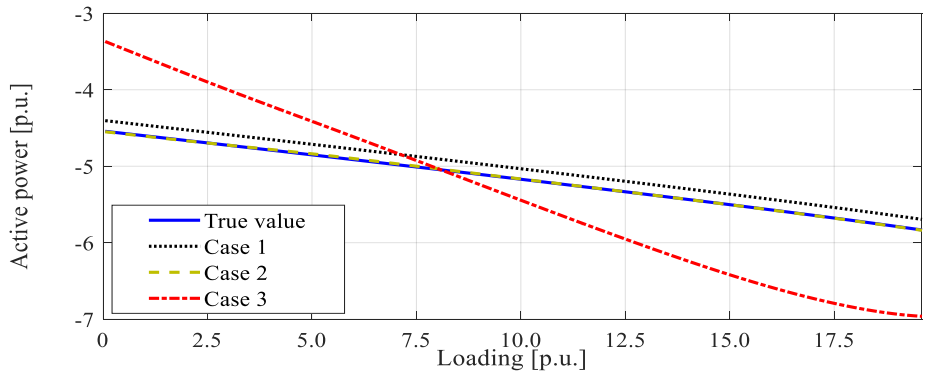

Fig. 6.13 Active power at receiving end on line 38-39.

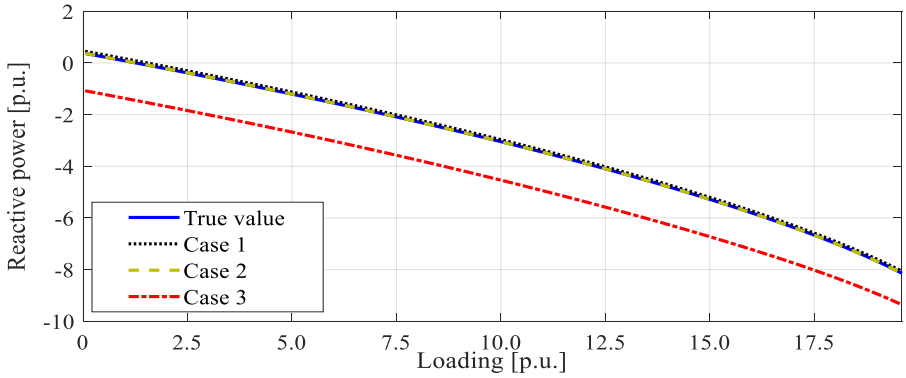

Fig. 6.14 Reactive power at receiving end on line 38-39.

flow calculation method. According to load increment, CBI gradually decreases and finally reaches almost 0. This indicates that the stable operation point transitions to an unstable region by voltage reduction of the system, and it finally reaches the critical boundary. Fig. 6.10 shows zoomed figure of Fig. 6.9. CBI in case 2 is estimated very accurately owing to PMU's direct voltage phasor measurement. In case 1, calculated CBI follows the true value with a certain deviation. However, in case 3, CBI has bigger deviation from the true value than case 1 even though case 3 uses voltage phasor estimated by PMU measurement. Figures 6.11-6.14 are necessary quantities to calculate $CBI_{38\text{-}39}$. Fig. 6.11 shows voltage magnitude at bus 38. Cases 1 and 2 well follow the true values transition. However, when the voltage angle difference between both ends of the line, its transition becomes huge error from the true value shown in Fig. 6.12. Also the transition tendency is different from cases 1 and 2. This is caused by taking subtraction of estimates which are obtained through different estimators. Voltage phasor at bus 38 is obtained via PSE using PMU measurement in the second step of HSE whereas voltage phasor at bus 39 is obtained via SCADA SE using RTU measurement in the first step of HSE. The meter's maximum measurement uncertainties are set as Table 4.1, and the statistical SE error difference between SCADA SE and PSE can be confirmed in figures 6.5-6.8. By the error of voltage phase angle difference, following active and reactive power calculation are affected shown in figures 6.13 and 6.14. Finally, CBI calculation error is influenced by those active and reactive power calculation using voltage phasor at both ends of the line. Therefore, the bigger CBI calculation error is caused by calculation of voltage angle difference between estimates which are obtained through different estimators. In the mixed measurement condition such as two-stage HSE, there is a possibility that bigger VSI calculation error is caused although PMUs are installed. This indicates that the merit of PMU installation is degraded.

For correct understanding of voltage security by CBI using estimated state vector, some voltage phasors at buses may be suggested not to be used. Thus, the following countermeasure is considered: if voltage phasor at a bus is estimated via PSE using PMU measurement and the adjacent bus voltage phasor is not, the former one is discarded and state vector estimated by SCADA SE is used instead only for the calculation of CBI on this line. This is possible since all of voltage phasors are already obtained by SCADA SE in the first step of HSE. Note that this strategy does not discard all voltage phasors, does discard the estimate by PSE in case of mixed measurement condition like case 3 in the previous analysis. In order to validate the proposed strategy mitigates the degradation of CBI calculation error caused by the mixed measurement situation, Mean Absolute Percentage Error (MAPE) is introduced and calculated for all Pareto solutions with all MCS scenarios. MAPE is given as follows:

$$MAPE = \frac{1}{nl}\sum_{l=1}^{nl}\left(\frac{100}{ns}\sum_{k=1}^{ns}\left|\frac{\hat{CBI}_{l,k} - CBI_{l,k}}{CBI_{l,k}}\right|\right). \tag{6.17}$$

where, nl is the number of lines and ns is the number of scenarios. The hat mark upon CBI is estimated value by obtained state vector by HSE, CBI without the hat mark is calculated by the true value. $CBI_{l,k}$ is CBI value on line l in scenario k. Here, two strategies are compared by MAPE: discarding estimates via HSE using PMUs

in case of the mixed measurement situation, and without discarding any estimates. MAPE calculation for CBI is performed for all Pareto solutions in Fig 6.4. Figures 6.15 and 6.16 show the decreasing ratio of MAPE from SCADA SE in the discarding some estimates strategy and not discarding strategy, respectively. Comparing figures, at the high PMU device cost which means many PMUs are placed and comparatively many voltage phasors are estimated via PSE. There is almost no change in between both strategies. However, as the PMU device cost decreases, the decrease ratio of MAPE from SCADA SE is deteriorated in the not discarding strategy. Sometimes it is even worse than SCADA SE by reaching the negative value of decrease ratio of MAPE. This is considered to be caused by use of estimates in the case of mixed measurements at both ends of a line. This may be easier to happen when the number of placed PMUs is small because a few of placed

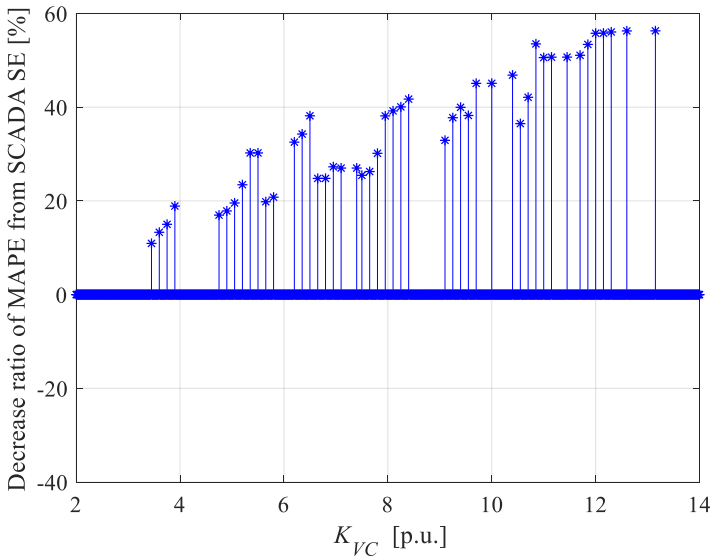

Fig. 6.15 Decrease ratio of MAPE from SCADA SE for all Pareto solutions in the discarding strategy.

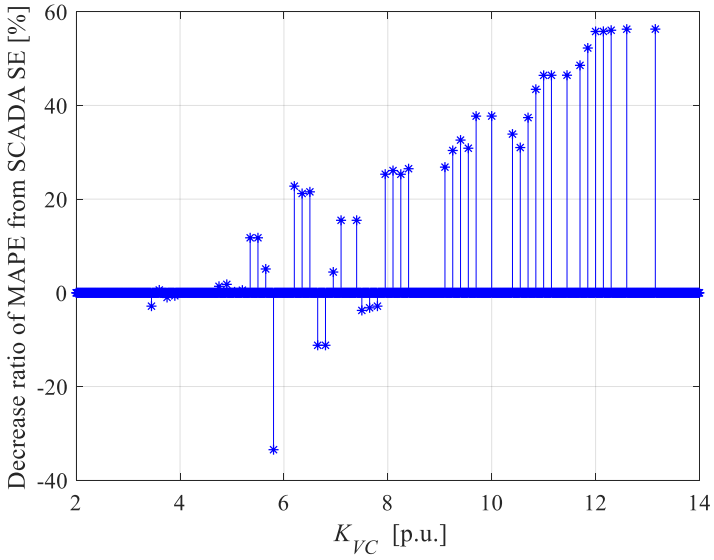

Fig. 6.16 Decrease ratio of MAPE from SCADA SE for all Pareto solutions in the not discarding strategy.

PMUs make many more mixed measurement situations than a lot of placed PMUs. Therefore, the discarding strategy is effective in the HSE mixed measurement situation to improve the accuracy of CBI calculation using estimated state vector. By this strategy, it is possible to maximize the effectiveness of PMU to improve the accuracy of power system voltage security assessment. In this numerical experiment, voltage stability assessment in a power system evaluated by CBI using estimated state vector by HSE based on an optimally placed PMUs is performed. The proposed CBI calculation procedure and the strategy can contribute to accurate voltage stability assessment in order to prevent voltage instability of power systems.

6.4 SUMMARY

In this chapter, voltage stability in power systems using estimated state vector by HSE based on an optimally placed PMUs is investigated because it has not been deeply considered. Among many voltage stability indices, CBI as a line VSI is employed for its understandability and precision. After obtaining a PMU placement by CCS-MOOPP/U and choosing the BCS, CBI calculation is conducted using estimated state vector based on the PMU placement of the BCS. By the numerical simulation by single load increment on bus 38 of modified 39-bus test system, CBI calculation accuracy is deteriorated in the case that voltage phasors at both ends of the line are obtained via different estimator: SCADA SE and PSE, compared to the case that both voltage phasors are obtained by same estimators. To avoid it, the strategy to discard estimates in such situation is proposed and showed better CBI estimation performance compared to using all estimates for CBI calculation. The results of the numerical experiment signify system operators the importance of evaluation of PMU placement by SE for voltage stability assessment using estimated state vector. Additionally, obtained state vector should be treaded carefully in HSE mixed measurement situation not to deteriorate the accuracy of CBI calculation which eventually results in cancelling the merit PMU placement.

6.5 REFERENCE

[1] V. Ajjarapu, Chapter 1 *Introduction*, Chapter 4 *Sensitivity Analysis for Voltage Stability*. In C*omputational Technique for Voltage Stability Assessment and Control*, M. A. Pai, A. Stankovic, (eds), 1st ed., Springer: New York, NY, USA, 2006.

[2] NERC, *1996 System Disturbances: Review of Selected Electric System Distributions in North America*, 1996.

[3] L. S. Vergas, V. H. Quintana, and D. R. Miranda, Voltage collapse scenario in the Chilean interconnected system, *IEEE Transactions on Power Systems*, vol. 14, no. 4, pp. 1415-1421, 1999.

[4] C. Vournas, *Technical Summary of the Athens and Southern Greece Blackout of July 12, 2004*, National Technical University of Athens, Greece, 2004.

[5] S. Liu, H. Deng, and S. Guo, Analyses and discussions of the blackout in Indian power grid, *Energy Science and Technology*, vol. 6, no. 1, pp.61-66, 2013.

[6] J. Modarresi, E. Gholipour, and A. Khodabakhshian, A comprehensive review on the voltage stability indices, *Renewable and Sustainable Energy Reviews*, vol. 63, no. 1, pp. 1-12, 2016.

[7] K. J. Makasa and G. K. Venayagammorthy, On-line voltage stability index estimation based on PMU measurements, *2011 IEEE PES General Meeting*, Detroit, MI, USA, 2011.

[8] P. Kessel and H. Gilavitsch, Estimating the voltage stability of a power system, *IEEE Transactions on Power Delivery*, vol. 1, no. 3, pp. 346-354, 1986.

[9] F. Gubina and B. Strmcnik, Voltage collapse proximity index determination using voltage phasors approach, *IEEE Transactions on Power Systems*, vol. 10, no. 2, pp. 788-794, 1995.

[10] I. Musirin and T. K. Abdul Rahman, On-line voltage stability based contingency ranking using fast voltage stability index (FVSI), *IEEE PES Transmission and Distribution Conference and Exhibition: Asia and Pacific*, Yokohama, Japan, 2002.

[11] M. Moghavvemi, F. M. Omar, Technique for contingency monitoring and voltage collapse prediction, *IEE Proceedings: Generation, Transmission and Distribution*, vol. 145, no. 6, pp. 634-640, 1998.

[12] R. Tiwari, K. R. Niazi, and V. Gupta, Line collapse proximity index for prediction of voltage collapse in power systems, *International Journal of Electrical Power and Energy Systems*, vol. 41, no. 1, pp. 105-111, 2012.

[13] M. Furukakoi, O. B. Adewuyi, M. S. S. Danish, A. M. Howlader, T. Senju, and T. Funabashi, Critical Boundary Index (CBI) based on active and reactive power deviations, *International Journal of Electrical Power and Energy Systems*, vol. 100, no. 1, pp. 50-57, 2018.

[14] J. Tang, J. Liu, F. Ponci, and A. Monti, Adaptive load shedding based on combined frequency and voltage stability assessment using synchrophasor measurements, *IEEE Transactions on Power Systems*, vol. 28, vol. 2, pp. 2035-2047, 2013.

[15] S. Kesherwani, S. P. Singh, and S. P .Singh, Voltage stability assessment using phasor measurement units in power network with full system observability, *2012 2nd International Conference on Power, Control and Embedded Systems* (ICPCES 2012), Allahabad, India, 2012.

7 PMU Placement for Dynamic Vulnerability Assessment

7.1 Dynamic Vulnerability Assessment Based on Fast Coherent Area

7.1.1 Dynamic Vulnerability Assessment

Until the Chapter 6, the main topic is static SE and the subsequent static security assessment for the preventive control. This chapter focuses on the Dynamic Vulnerability Assessment (DVA) for the power system corrective security control. DVA is an assessment process of the symptom of post-contingency system instability, and its indicator evaluates the dynamic system security level which is used as the input of the corrective control. The initiation of DVA was developed by Kamwa et al. in 2006 [1]. The authors assessed the dynamic vulnerability of the power system modeling a real power system in Hydro-Québec, using an index called Wide Area Severity Index (WASI). Since the dynamic responses of the post-contingency in the power system is quite short term phenomena, use of PMU allows the real time assessment of the power system dynamic vulnerability [2], and the study of PMU application to DVA has been developed lead by Cepeda et al. [3][4][5]. The key of DVA is how to capture the symptom of the system vulnerability accurately and give information to the operator quickly, PMU's synchronized voltage/current phasor measurement with high sampling resolution is superior in DVA.

7.1.2 Power System Coherency

DVA and the subsequent corrective control are performed by the coherent area basis. Hence, partitioning the power system to coherent areas is the first step of vulnerability assessment. There are two types of power system coherent area: fast coherency and slow coherency. The fast coherent area is partitioned based on an analysis through measured transients after a perturbation, whereas the slow coherent area is partitioned based on an analysis through model-based eigenvalue analysis. Generally, the fast coherent area is used to predict and assess the post-contingency system security level, the slow coherent area is used for system dimension reduction via aggregation of generators [3]. This chapter targets the fast coherence since DVA is performed based on the fast coherent areas, and it shall be treated by online/real-time data obtained by PMUs with high sampling rate.

7.1.3 Center-of-Inertia Based Area Frequency

In DVA, a symptom of the system vulnerability is detected by capturing signals of some quantities of the power system. Normally, as the PMU signals, voltage magnitude, voltage angle and frequency are used for DVA [3]. In this research, frequency is employed. Frequency is the major indicator of monitoring

imbalance between generation and load in a power system, and its deviation from the nominal value can evaluate how vulnerable the system is. For the power system security, the area-based instability in which some generators in the same area go out of step after a fault, which will result in cascading blackout must be avoided, thus, COI based index is calculated [5]. In the multi generator system, the swing equation is represented as:

$$\frac{2H_i}{f_0}\frac{df_i}{dt} = \Delta p_i \,, \tag{7.1}$$

where, i is the generator number, H_i is unit inertia constant in second, f_i is generator frequency, f_0 is nominal frequency, Δp_i is power mismatch of a generator. In a power system with ng generators, the disturbance power in the system in per unit can be expressed as [6]:

$$\begin{aligned}\Delta P &= \sum_{i=1}^{ng} \Delta p_i \\ &= \frac{2\sum_{i=1}^{ng} H_i}{f_0}\frac{df_{COI}}{dt} \,,\end{aligned} \tag{7.2}$$

where, f_{COI} is frequency at equivalent inertial center and given by follows:

$$f_{COI} = \frac{\sum_{i=1}^{ng} H_i f_i}{\sum_{i=1}^{ng} H_i} \,. \tag{7.3}$$

f_{COI} is calculated based on identified each fast coherent area for given power flow and fault point. In security control actions, typical under/over frequency threshold values for generator protection are set to be 2.5 % to 5.0 % [4]. In an article by Seethalekshmi et al., the under frequency threshold value settings are 57-58.5 Hz for a 60 Hz system and 48-48.5 Hz for a 50 Hz system: the frequency deviation threshold $\Delta f_{\max}$ is ranging from 2.5 % to 5.0 % [6]. Similarly, over frequency protection of generators has a threshold value of 61.7 Hz ($\Delta f_{\max}$ is around 2.8 % for a 60 Hz system) specified in IEEE C37.106 [7].

7.2 FAST COHERENT AREA IDENTIFICATION BY CLUSTERING

7.2.1 Disturbance Based Dissimilarity Matrix

The fast coherent area differs according to the system power flow condition and the disturbance location. Therefore, statistical analysis based on MCS is carried out to consider all possible operating scenarios, and different fast coherent areas are grouped by clustering in each scenario. In order to partition a power system into coherent areas, cluster analysis is typically used in several studies, such as use of HC [8], NHC [9][10] and support vector clustering [11]. To give an input to a clustering algorithm, the data should form the dissimilarity matrix which builds the

distance among the data point (bus). This research employs the recursive method proposed by Kamwa et al. [9].

An element of the dissimilarity matrix **D** is computed as follows:

$$d_{ij} = \sqrt{\frac{1}{T}\left(\int_{tc}^{T} \left[\Delta f_i(t) - \Delta f_j(t) \right]^2 dt \right)}, \tag{7.4}$$

where, i and j are arbitrary bus number ($i \neq j$), $\Delta f_i(t)$ is frequency deviation from the nominal frequency at bus i, tc is fault clearing time and T is observation time window. Then, dissimilarity matrix **D** forms as follows:

$$\mathbf{D} = \begin{bmatrix} d_{11} & \cdots & d_{1nb} \\ \vdots & \ddots & \vdots \\ d_{nb1} & \cdots & d_{nbnb} \end{bmatrix}. \tag{7.5}$$

Obviously, **D** is the symmetric matrix. Generally writing the recursive method, a quantity of a system $X_i(t)$ at bus i on time t after a disturbance is as follows:

$$X_i(t) = x_i(t) - x_{i0} - \bar{X}, \tag{7.6}$$

where, $x_i(t)$ is a value of the quantity at bus i on time t, which may be voltage magnitude or angle or frequency assuming the PMU's synchronized measurement. x_0 is the initial value of the quantity before the disturbance. $\bar{X}$ is the average value for all buses. To build **D**, the difference of quantities between two buses i and j are:

$$X_{ij}(t) = \left[x_i(t) - x_{i0} \right] - \left[x_j(t) - x_{j0} \right]. \tag{7.7}$$

Then, let Y be the time integral of squared X:

$$Y_{ij}(t) = \int_{tc}^{T} X_{ij}^2(t) dt. \tag{7.8}$$

(7.8) can be approximately solved by trapezoidal integration:

$$Y_{ij}(T) = \sum_{k=tc}^{T} \frac{X_{ij}^2(t_k) + X_{ij}^2(t_{k-1})}{2} \Delta t, \tag{7.9}$$

where $\Delta t = t_k - t_{k-1}$. Finally, the element of **D** is calculated by:

$$d_{ij} = \frac{\sqrt{Y_{ij}(T)}}{T}. \tag{7.10}$$

The built dissimilarity matrix **D** has dimension of ($nd \times nd$), high dimension sometimes causes misclassification by error of distance computation called the curse of dimensionality in the clustering algorithm. Thus, the matrix dimension should be reduced while keeping information as intact as possible, using Classical Multi-Dimensional Scaling (CMDS) [12]. CMDS is the well-known data

dimension reduction method as well as Principal Component Analysis (PCA). The main difference is how to construct matrix. PCA computes the matrix based on the variance-covariance matrix whereas CMDS builds the distance matrix from the dissimilarity matrix. From the dissimilarity matrix, the corresponding similitude matrix can be obtained as follows [3]:

$$\mathbf{Q} = -\frac{1}{2}\left[\mathbf{I} - \frac{1}{nb}\mathbf{b}\mathbf{b}^T\right]\mathbf{D}\left[\mathbf{I} - \frac{1}{nb}\mathbf{b}\mathbf{b}^T\right], \tag{7.11}$$

where **I** is the identity matrix and **b**=[1, …, 1]. The similitude matrix **Q** represents the variability between elements, similar to the variance-covariance matrix in PCA. By eigenanalysis, eigenvalues **Λ** and eigenvectors **V** of the matrix **Q** can be obtained. Then, It is possible to calculate a corresponding principal coordinate **Z**:

$$\mathbf{Z} = \mathbf{V}\mathbf{\Lambda}^{1/2}. \tag{7.12}$$

The newly obtained **Z** is an orthogonal matrix which retains information of **D** with a certain level. Dimension reduction is performed until the cumulative contribution ratio of the eigenvalue is above 95 %.

7.2.2 A Novel Clustering Method: HC-max

Since the number of fast coherent areas is different in MCS scenarios, the cluster number has to be automatically determined according to a criterion. In studies of DVA, clustering accuracy has not been considered in past articles [1][3][5][9]. Due to the variability of fast coherent area depending on power flows and fault locations, ignorance of accuracy on area partition may lead an incorrect control action. Thus, this research invents a novel clustering method called "HC-max" which delivers the optimal clustering in terms of a point-biserial correlation coefficient between clustering input and output.

Fig. 7.1 shows the algorithm flowchart of HC-max. Before the loop, HC-max needs to set two things: the maximum cluster number $n_{area\text{-}max}$ and cluster linkage methods defined. HC-max tests the clustering with a number of clusters and a linkage method by iteratively changing them, and obtains the clustering result with the maximum value of the point-biserial correlation coefficient explained later. Thus, user of HC-max needs to set a finite number of maximum area partitions and linkage methods. The distance metric between data is fixed to be the Euclidean distance. For the clustering accuracy evaluation, the point-biserial correlation coefficient is defined as follows [13]:

$$R_{PB}(A,B) = \frac{\mu_{A1} - \mu_{A0}}{\sigma_n}\sqrt{\frac{n_{A1}n_{A0}}{N^2}}, \tag{7.13}$$

where, A is clustering input: the reduced dissimilarity matrix. B is clustering output: binary matrix which the element is 1 if the two data points lie in the same cluster and 0 otherwise. The value of A are dispatched into two groups A_0 and A_1 depending on the corresponding value in B. μ is the mean value, σ is the standard deviation, n denotes the number of elements in each group, N is the size of A. Therefore, R_{PB}

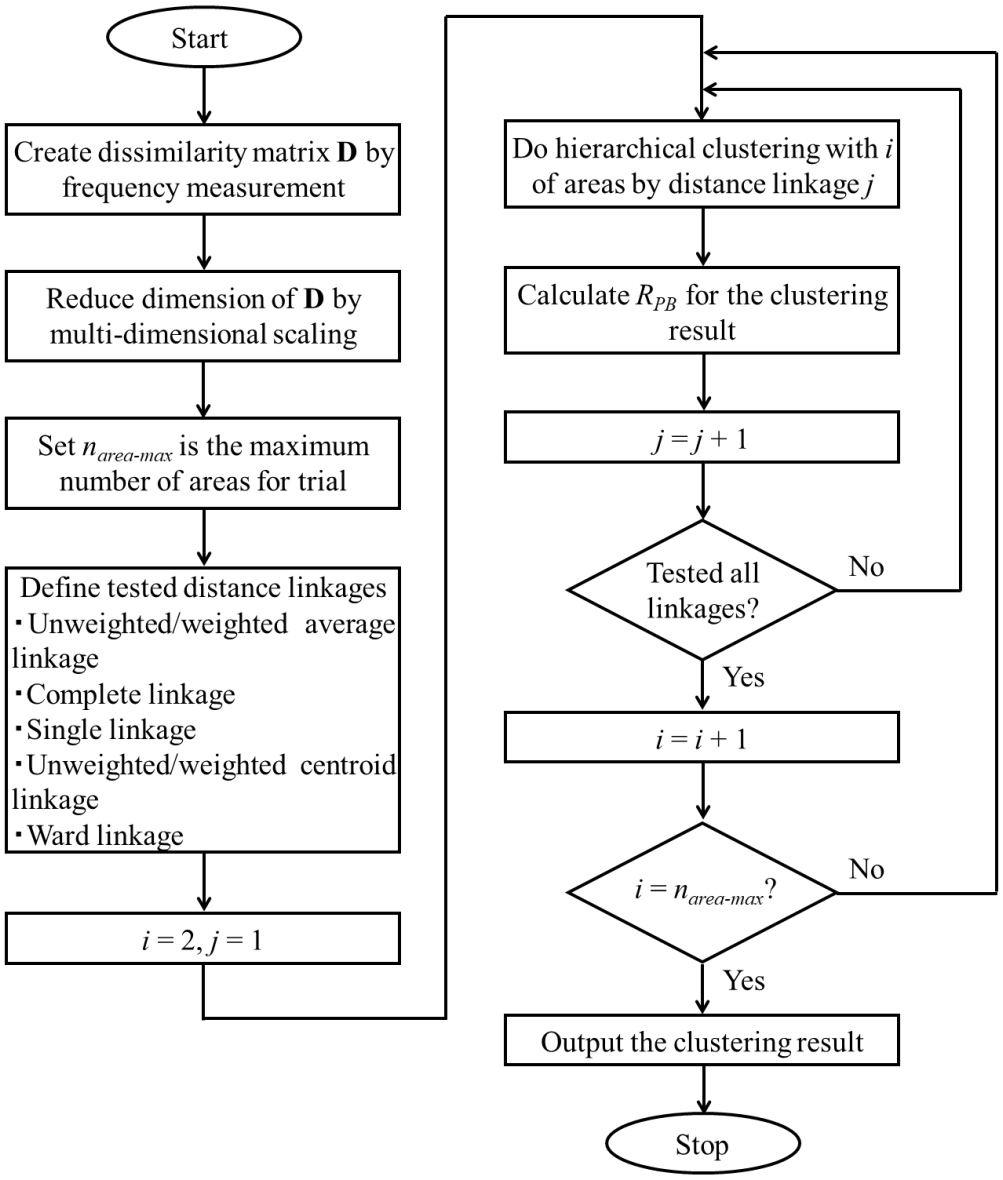

Fig. 7.1 HC-max algorithm flow chart.

approaches to 1 if the dissimilarity matrix has positive relation with the clustering result, 0 if there is no relation in them and −1 if they are negatively related.

7.3 Optimal PMU Placement for DVA

In order to estimate COI based frequency f_{COI} in fast coherent areas identified by clustering analysis, the PMU observing the bus frequency signal has to be optimally placed. Hence, the optimal PMU placement formulation for DVA is designed to cover the variable areas and trace the COI based frequency by signal of placed PMUs. The optimization function is formulated as follows:

$$\min_{\mathbf{y}} \; z = \frac{1}{n_s} \sum_{i=1}^{n_s} \Omega_i \;, \tag{7.14}$$

$$\Omega_i = \frac{1}{n_{area,i}} \sum_{j=1}^{n_{area,i}} \gamma_{i,j} \ , \tag{7.15}$$

$$\gamma_{i,j} = \begin{cases} \min\left\{m_{i,j,k}\right\} \ \forall k \in A_j & \text{if a PMU at bus } k \text{ is in area } j \\ 100 & \text{otherwise} \end{cases} , \tag{7.16}$$

$$m_{i,j,k} = \frac{100}{n} \sum_{t=t_c}^{n} \left| \frac{f_{COI,j}^t - f_{k,j}^t}{f_{COI,j}^t} \right| , \tag{7.17}$$

subject to constraints:

$$\mathbf{y}\mathbf{y}^T = n_{PMU} \ , \tag{7.18}$$

where, subscripts i, j and k indicate the scenario, area and bus numbers. n_s is the number of total scenarios, $n_{area,i}$ is the number of areas at scenario i. A_j is a set of buses in area j, n is the number of samples at the time domain simulation, superscript t indicates the time point. n_{PMU} is the number of PMUs placed, $\mathbf{y}$ is the decision variable to determines the PMU placement, used in the Chapter 4 and 5. Thus, (7.17) evaluates the estimation accuracy of COI-based frequency of a coherent area j by bus frequency signal obtained by PMU placed at bus k. Here, it is assumed that the bus frequency signal is obtained by differentiating voltage phase angle. (7.16) takes the minimum value of m in buses belonging to A_j. If there is no PMU placed at buses belonging to A_j, γ of scenario i in area j gets penalty by 100. After that, (7.15) calculates the average of γ by the number of areas in scenario i ($n_{area,i}$ differs depending on the power flow and the fault location). Finally, (7.14) minimizes average of Ω by the total number of scenarios. The optimization problem formulated by (7.14)-(7.18) is named as OPP-DVA.

7.4 NUMERICAL SIMULATION

7.4.1 Configuration

From this subsection, results of the numerical experiment are shown and discussed. The numerical simulation is separated into 2 steps. In the first step, the power system fast coherent area partition is performed for all operation and fault scenarios using HC-max. The accuracy of HC-max is compared with other NHC methods evaluated by the point-biserial correlation coefficient. After clustering of power system fast coherent area, in the second step, OPP-DVA is solved according to the determined area partition by clustering. The target power system is IEEE NE 39-bus specified in Appendix A. 10000 possible scenarios are produced in MCS with different power flow conditions and fault locations. To construct the dissimilarity matrix, the bus frequency signals are sampled in a window ranging from t_c=0.08s, to T=2s. Every fault is assumed to be 3-phase short circuit occurred at 0s and cleared at 0.08s by CB. Also, this research assumes that the under\over frequency deviation thresholds are set to 2.5% from the nominal value considering the corrective security control actions [6][7]. Hence, the frequency signal sample is cut out when any bus frequency signals reached the threshold values in cases that

the system goes unstable. Data processing, clustering analysis, obtaining optimal PMU placement are conducted in Matlab R2019a, Modeling of NE 39-bus and dynamic simulation are conducted in DigSILENT PowerFactory 2018.

7.4.2 Clustering Accuracy for Fast Coherent Area Partition

Clustering accuracy is compared with three methods: a method combining Subtractive Clustering (SC) [14] and FCM [15] called SC+FCM, Adaptive Affinity Propagation (AAP) [16] and HC-max. First two of them are NHC class method. Because of variability of fast coherent area, the clustering algorithm must be able to determine the number of clusters automatically and fairly. FCM itself cannot determine the number of clusters automatically, but SC supports its decision. Thus, in SC+FCM, SC determines the number of clusters and gives it to FCM, thereafter, FCM can perform clustering according to the number of clusters given by SC. FCM is one of the most famous fuzzy clustering method, performing clustering by fuzzification of data membership to clusters. AAP performs adaptive scanning of preferences to each space of the number of clusters to find the optimal clustering solution, including automatic determination of the number of clusters. Both of them are the NHC method which minimizes the evaluation function to judge the goodness of clustering. NHC may highly depend on the randomly generated initial points of the search. The parameters of each method are listed in Table 7.1.

The goodness of clustering for 10000 MCS scenarios is evaluated by point-biserial correlation coefficient R_{PB} in (7.13) Fig. 7.2 shows boxplots of point-biserial correlation coefficient for three methods. The red cross dot is outlier. The best value is almost same in three methods. However, In terms of median and the worst value, HC-max is the best clustering method among these. HC-max keeps the worst value R_{PB} = 0.530, which indicates weak positive correlation between the clustering input and output. In addition to that, 25 and 75 percentiles are ranging

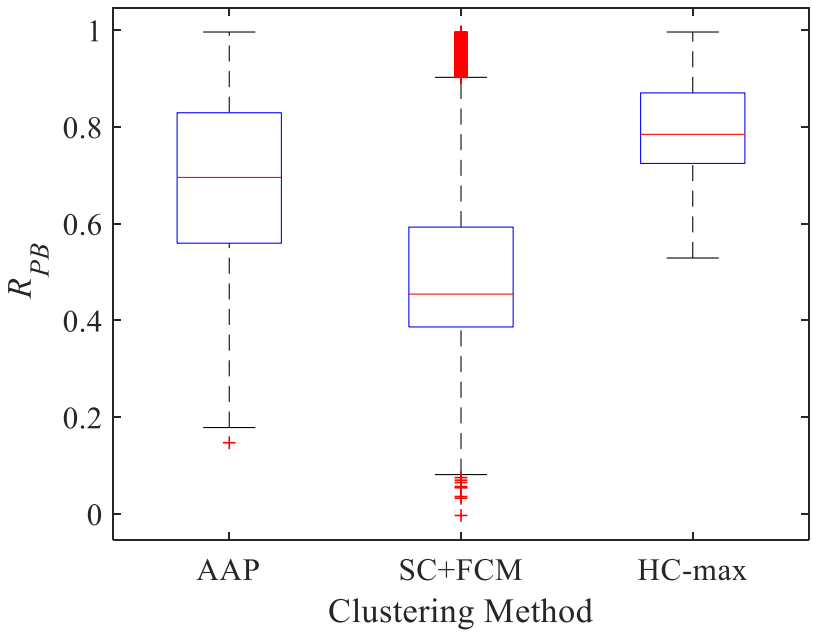

Fig. 7.2 Boxplots of point-biserial correlation coefficient for three methods.

Table 7.1 Parameters for three clustering methods.

Clustering Method	Parameter	Value/Method
AAP	Maximum number of iterations	5000
	Convergence condition	50
	Decreasing step of preferences	0.01
	Damping factor	0.55
SC+FCM	SC: Cluster influence range	0.3
	FCM: the number of FCM trials	300
	FCM: Exponent for fuzzy partition matrix	4.0
	FCM: Maximum number of iterations	100
	FCM: Maximum improvement in objective function between two consecutive iterations	1.0×10^{-5}
HC-max	Maximum number of cluster	6
	Linkage methods	Single, complete, unweighted/weighted average, unweighted/weighted centroid, ward

between R_{PB} = 0.870 and 0.724. On the other hand, the worst values of AAP and SC+FCM seem that no correlation is confirmed in terms of point-biserial correlation coefficient. Also, their data range of percentile are at least bigger and lower-located than HC-max. These results indicate that the area partition may be mistakenly performed. Since HC-max selects the clustering result which has the highest R_{PB} by changing the number of clusters and linkage methods, and others search the optimal clustering by their own evaluation functions without considering the relationship between the system and clustering result, HC-max is more accurate than two NHC methods.

To show how point-biserial correlation coefficient works, a case from MCS scenario is extracted, HC-max and SC+FCM are performed for the same scenario. Figures 7.3 and 7.5 show the clustering results by HC-max and SC+FCM, respectively. In the figures, the dimension is reduced from 39 to 2 by CMDS. Thus the data points are represented by 2 coordinates (first and second top components). It is obvious that the clustering by HC-max is correctly done. However, SC+FCM

does not really work, qualitatively observed from the figures. Figures 7.4 and 7.6 show the frequency deviation behavior with partitioned areas after the disturbance occurred, by HC-max and SC+FCM, respectively. For these results, in HC-max, R_{PB} = 0.890, in SC+FCM, R_{PB} = 0.291. Looking at Figures 7.3 and 7.4, the clustering input (bus frequency signals) is clearly partitioned three areas as well as the output (clustering result). Thus, there is a positive correlation between each

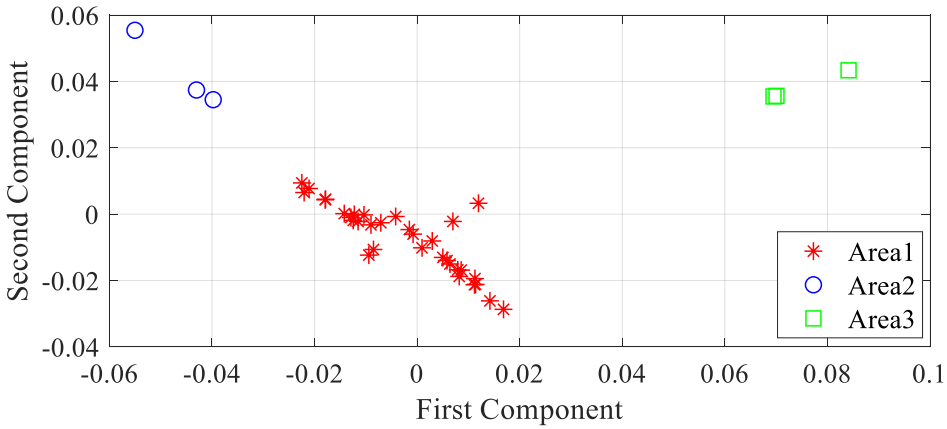

Fig. 7.3 Clustering result by HC-max.

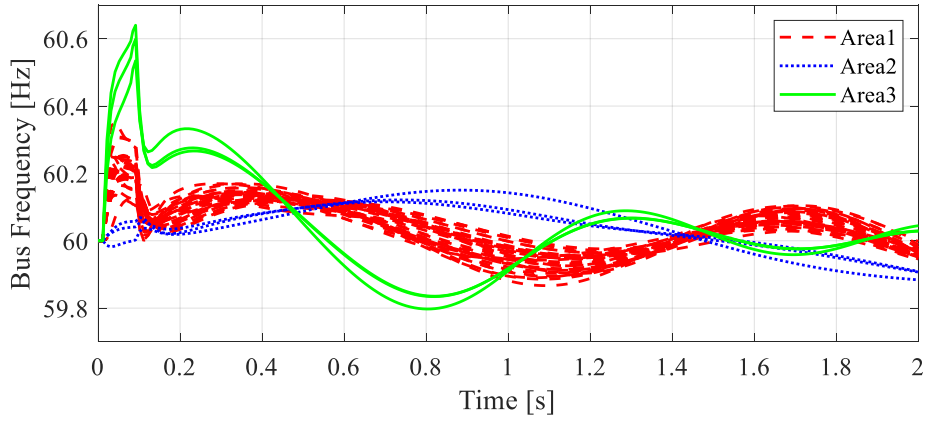

Fig. 7.4 Frequency deviation after a disturbance with fast coherent areas identified by HC-max.

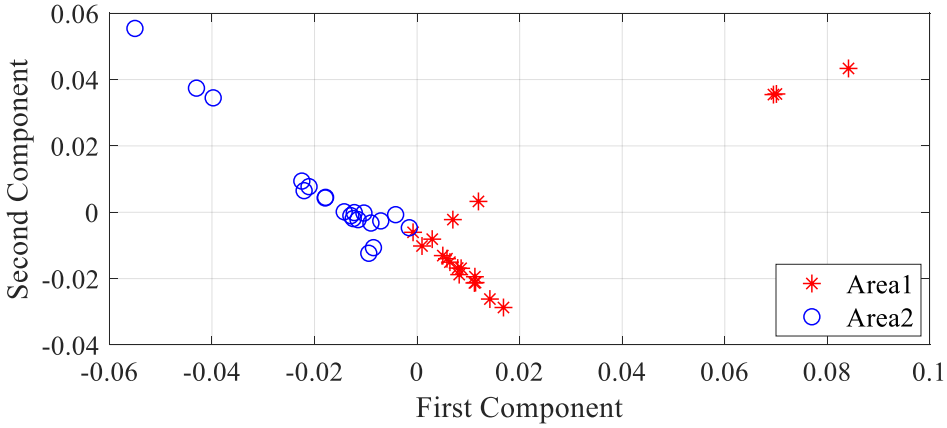

Fig. 7.5 Clustering result by SC+FCM.

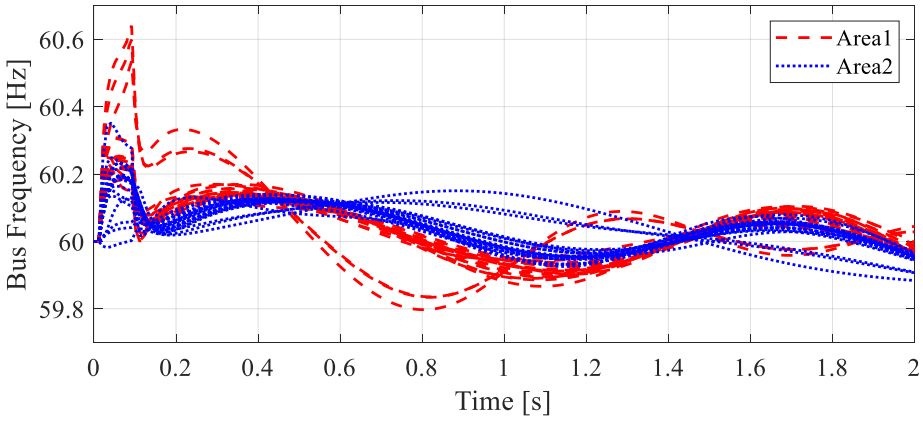

Fig. 7.6 Frequency deviation after a disturbance with fast coherent areas identified by SC+FCM.

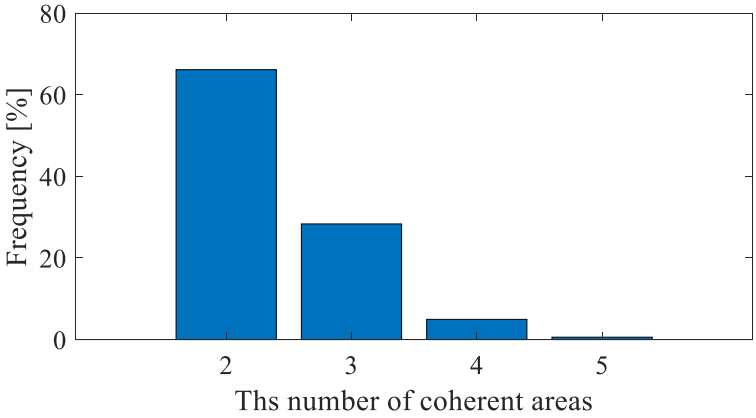

Fig. 7.7 Frequency histogram of the number of fast coherent areas in all scenarios.

other, the calculated R_{PB} indicates it. This happened because HC-max produces the optimal clustering by changing the number of clusters and linkage methods, in terms of the point-biserial correlation coefficient. However, looking at figures 7.5 and 7.6, the area partition falls into mess. This might happen because of performance of SC. If once SC cannot give an appropriate number of clusters to FCM, FCM cannot work properly. Also, it is obvious that the number parameters in NHC methods is bigger than HC-max. HC-max only has two simple parameters: the maximum number of clusters and linkage methods which can contribute to improve the clustering accuracy by increasing them. On the other hand, NHC methods have many more parameters which are complexly intertwined factors. As results of this subsection and discussion, HC-max is the parameter-less method and high accuracy method in terms of point-biserial correlation coefficient. By accurate clustering using HC-max, partitioned area is used in the next subsection.

7.4.3 DVA Index Calculation by Optimally Placed PMUs

After the clustering, optimal PMU placement is determined by OPP-DVA. Note that the all clustering results from this subsection are obtained by HC-max. A bar chart histogram shown in Fig. 7.7 means the frequency of the number of coherent areas. This indicates that the number of coherent areas is at most 5 in the scenario. Also, the areas separate into 2 at least. Therefore, the optimal PMU

placements are obtained in n_{PMU} = 2, 3, 4 and 5. The method to obtain the optimal placement is exhaustive method which enumerates all possible combinations. Note that the bus frequency is obtained by PMU direct measurement only. The pseudo measurement is not employed to estimate COI-based frequency in OPP-DVA.

Table 7.2 shows the optimal PMU placements obtained in OPP-DVA via exhaustive method. Fig. 7.8 illustrates the single connection diagram of NE 39-bus. The bus numbers on Fig. 7.8 and the second column of Table 7.2 are corresponding. The many more the number of PMU placement is, the higher evaluation value of OPP-DVA is. Also, all the placements of PMUs are at generator buses which have the highest dynamic observability. Table 7.3 shows a part of PMU placement ranking by z when n_{PMU} = 5. Since the optimal PMU placements are obtained by

Table 7.2 The optimal PMU placement buses and the evaluation value in OPP-DVA.

n_{PMU}	PMU placement bus	DVA evaluation value z	No.of Combinations
2	2, 6	10.25	741
3	1, 2, 7	4.69	9139
4	1, 2, 7, 9	1.03	82251
5	1, 2, 5, 7 ,9	0.55	575757

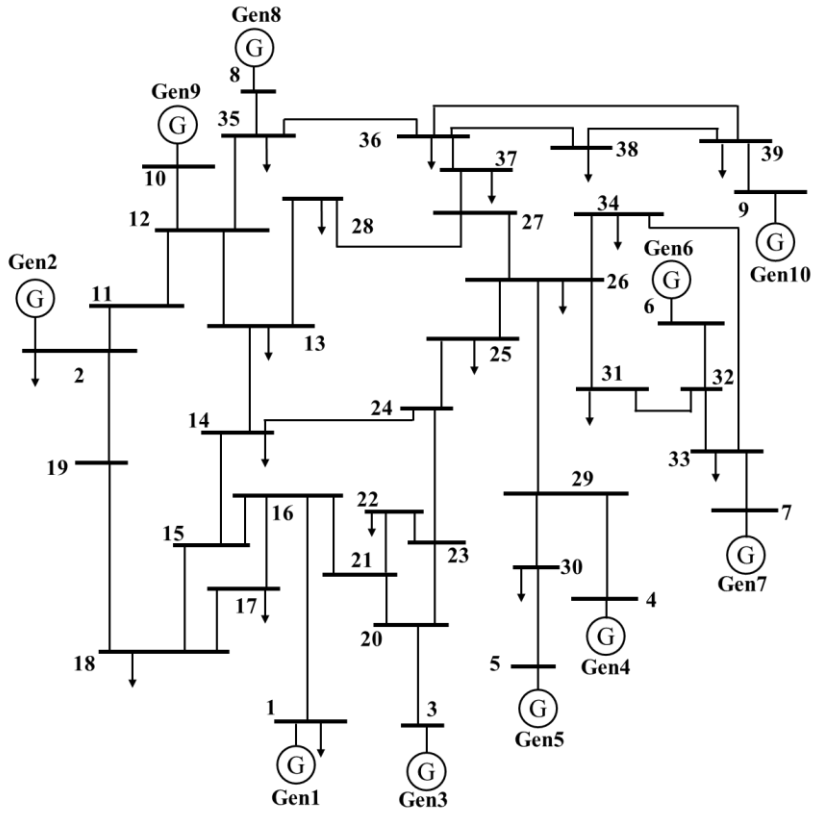

Fig. 7.8 IEEE NE 39-bus test system single line connection diagram.

the exhaustive method, all combinations ${}_{39}C_5 = 575757$ are tested. In the upper ranks, PMUs are placed at generator buses or the near buses and distributed. However, in the lower ranks, PMUs are placed at not generator bus and its placement is more concentrated. Especially, in the PMU placement of the worst z, all PMU placed buses are adjacent which indicate that it is difficult to observe the COI-based area frequency in each fast coherent area in many cases. Thus, DVA evaluation value z gets worse than any others.

To confirm how bus frequency signal estimates the COI based area frequency, two scenarios are picked up from MCS scenario set. Figures 7.9, 7.10, 7.11 are clustering behavior by HC-max, frequency signals and area partition on NE 39-bus with PMU placement when $n_{PMU} = 5$, respectively. In this case, 3-phase short circuit fault occurred at line 13-14 at 93.9 % of the length. Then, the power system is separated into 3 fast coherent areas identified by HC-max ($R_{PB} = 0.906$). Also, in CMDS, the dimension of dissimilarity matrix is reduced to 3. In each fast coherent area, there is at least one PMU is placed. In Fig. 7.10, solid lines indicate the COI based area frequency, dotted lines are bus frequency obtained by PMU placed at buses as in Fig. 7.11. It seems that PMU bus frequency signals well traces the COI based frequency signals in each area. In this case, the system is not vulnerable i.e. stable. Figures 7.12, 7.13 and 7.14 are clustering behavior by HC-max, frequency signals and area partition on NE 39-bus with PMU placement when $n_{PMU} = 5$, respectively, in another case as 3-phase short circuit fault occurred at line 26-34 at 91.0 % of the length. The system separated into 2 fast coherent areas identified by HC-max ($R_{PB} = 0.866$). In the process of clustering, the dimension of dissimilarity matrix is reduced to 2 by CMDS. There is at least one PMU in each area as well as

Table 7.3 A part of PMU placement ranking by z when $n_{PMU} = 5$.

Rank	PMU placement bus	z
1	1, 2, 5, 7, 9	0.555
30	2, 7, 18, 30, 39	0.593
287878	13, 23, 27, 30, 38	27.673
575757	1, 15, 16, 17, 18	38.554

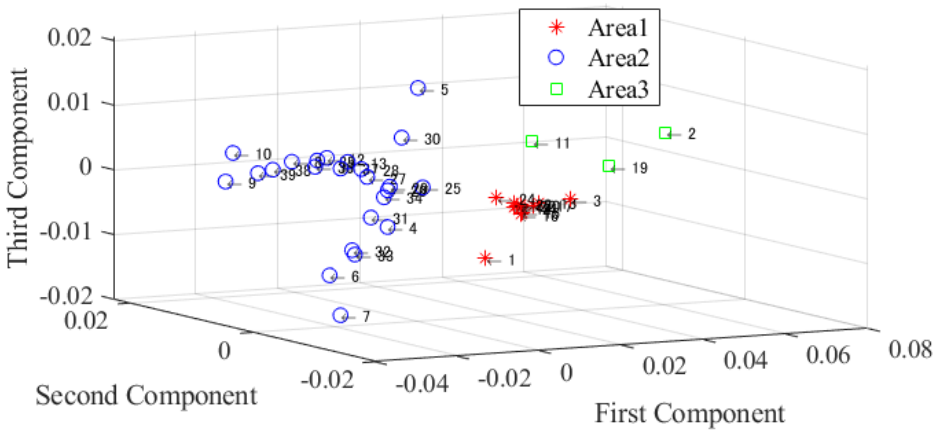

Fig. 7.9 Clustering result in the case: fault at line 13-14.

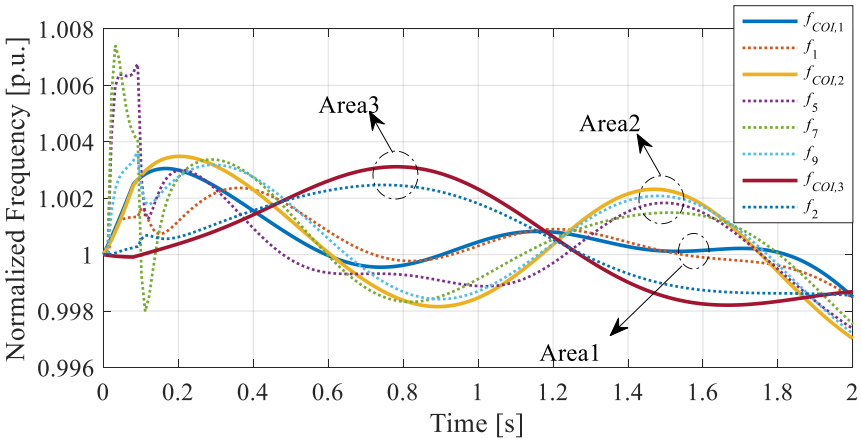

Fig. 7.10 Normalized COI based area/bus frequency after the fault on line 13-14.

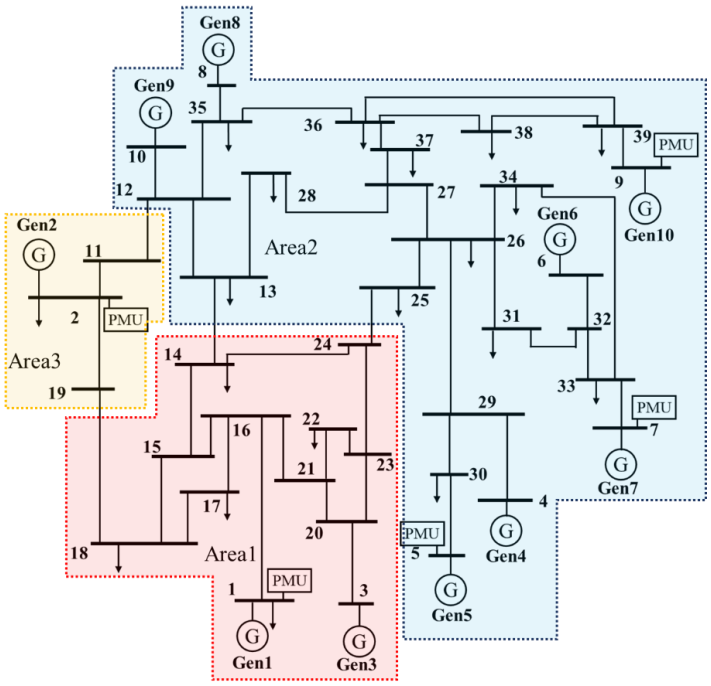

Fig. 7.11 IEEE NE 39-bus test system single line connection diagram in the case: fault on line 13-14.

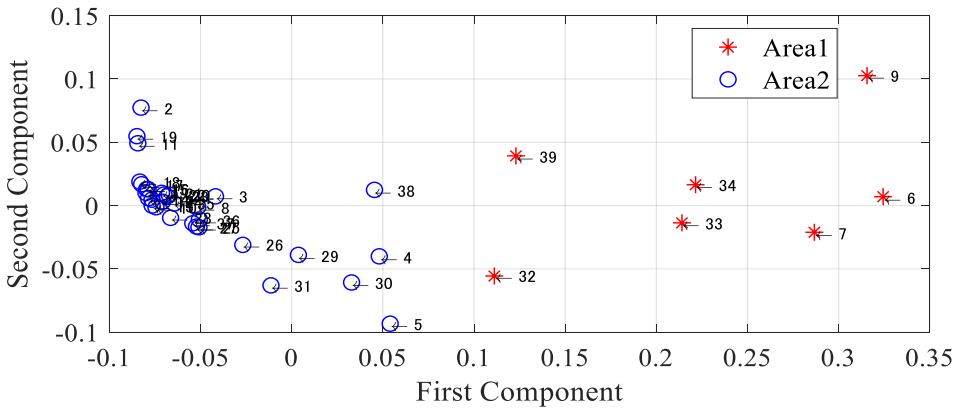

Fig. 7.12 Clustering result in the case: fault on line 26-34.

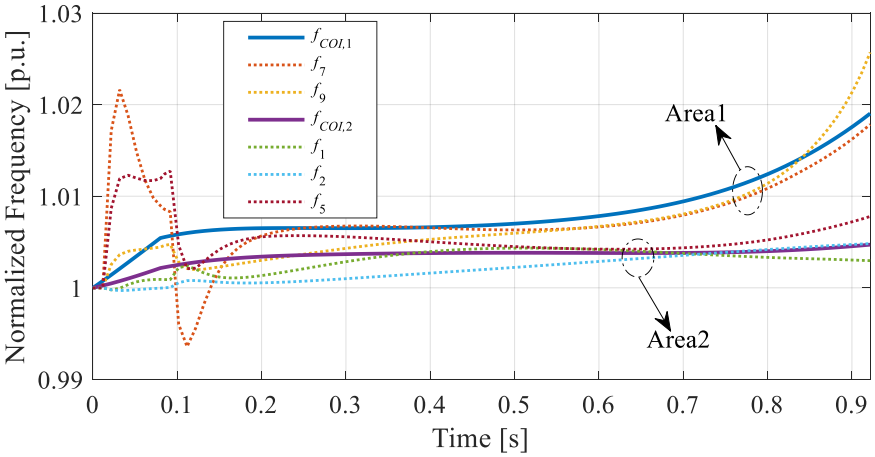

Fig. 7.13 Normalized COI based area/bus frequency after the fault on line 26-34.

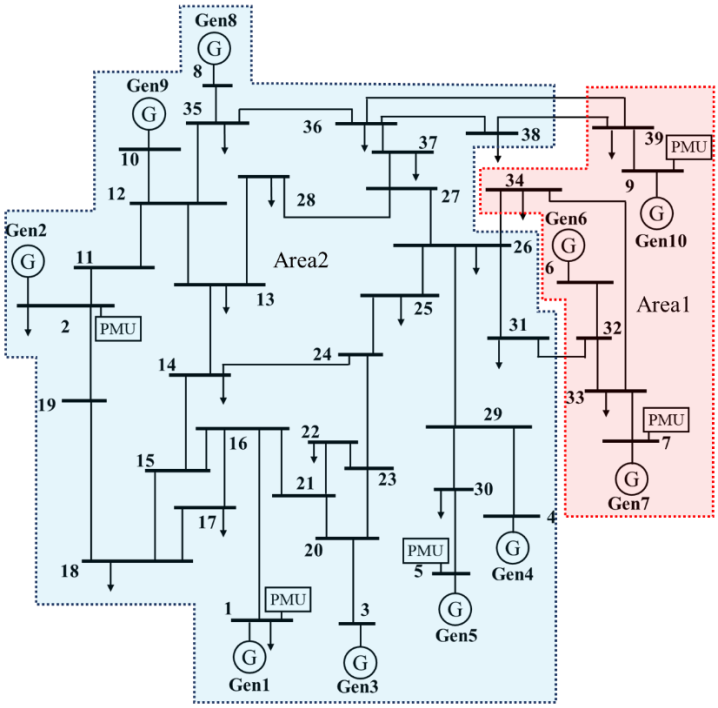

Fig. 7.14 IEEE NE 39-bus test system single line connection diagram in the case: fault on line 26-34.

the previous case. From the frequency signal plot, area 1 goes area out of step and it is detected by bus frequency signals obtained by PMUs at buses 7 and 9, reaching the over frequency deviation threshold 2.5% from the nominal value. Thus this area is identified as vulnerable. The time window finished at around 0.9 because following corrective control such as generators tripping in this area is initiated after this.

7.4.4 MOOPP Problem for Static and Dynamic Security Assessment

In chapters 4, 5 and 6, new types of MOOPP problems are proposed and the influence on following static security assessment is investigated. In this chapter so

far, OPP-DVA is proposed for dynamic security assessment. Both of static and dynamic security assessment scheme which give the evaluation of current security level to preventive and corrective security controls respectively are equally important, thus, enhancement of them should be targets of OPP. In this subsection, the possibility of OPP problem considering both the static and dynamic security assessment is shown. The proposed MOOPP problem is named CCS-MOOPP/U-S&D, formulated as follows:

$$\min_{\mathbf{y},\mathbf{D}} \ \{K_{VC}, TVE_{\max}\}, \tag{7.19}$$

subject to constraints:

$$\mathbf{y}\mathbf{y}^T > 0, \tag{7.20}$$

$$K_{VC} = w_V \mathbf{y}\mathbf{y}^T + w_C (\mathbf{C}^T\mathbf{b})^T \mathbf{b}, \tag{7.21}$$

$$\mathbf{b} = [1,...,1]^T, \tag{7.22}$$

$$TVE_{\max} = \max_{1\le j\le ns} \{TVE_j\}, \tag{7.23}$$

$$\left[\forall i \in \{1,2,...,nb\} \wedge \forall j \in \{1,2,...,ns\}\right] : \left(100\frac{\left|V^i - \hat{V}^i\right|}{\left|V^i\right|}\right)_j < E_{\max}^{mag}, \tag{7.24}$$

$$\left[\forall i \in \{1,2,...,nb\} \wedge \forall j \in \{1,2,...,ns\}\right] : \left(\left|\theta^i - \hat{\theta}^i\right|\right)_j < E_{\max}^{ang}, \tag{7.25}$$

$$z \le DVA_{\lim}, \tag{7.26}$$

where, $DVA_{\lim}$ is pre-determined upper bound for DVA evaluation value z calculated in (7.14). CCS-MOOPP/U-S&D basically focuses on the minimization of PMU device cost and the HSE error evaluated by TVE. As the result of OPP-DVA in the previous subsection 7.4.3, five of PMUs can cover all possible fast coherent area partition because the maximum number of area is 5 areas. The many more number of PMUs than five can also enhance DVA accuracy. However, increasing the number of PMUs more than five may not contribute very much to enhancement of DVA. Thus, the number of PMUs required in DVA as dynamic security assessment is less than the number of PMUs in static security assessment which needs to cover whole power system. By taking into account this, z is included in the constraints of the optimization problem in CCS-MOOPP/U-S&D. This problem could be three objective optimization problem, however, trade-off relationships between K_{VC} and z, $TVE_{\max}$ and z are supposed to be much weaker than K_{VC} and $TVE_{\max}$. Thus, this is still two-objective optimization problem. Here, considering the result of OPP-DVA according to Table 7.2, $DVA_{\lim}$ is set to 1 in order to ensure covering the maximum number of fast coherent areas with a certain quality of COI-based area frequency estimation. Figures 7.15 and 7.16 show the

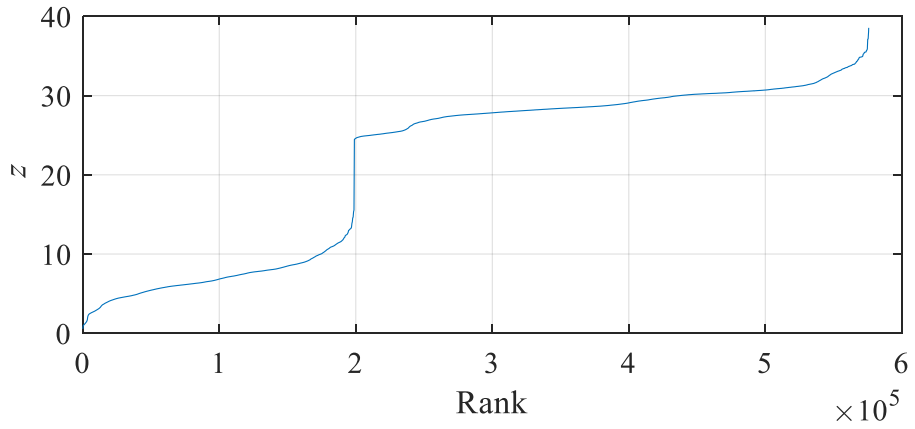

Fig. 7.15 PMU placement ranking in n_{PMU}=5.

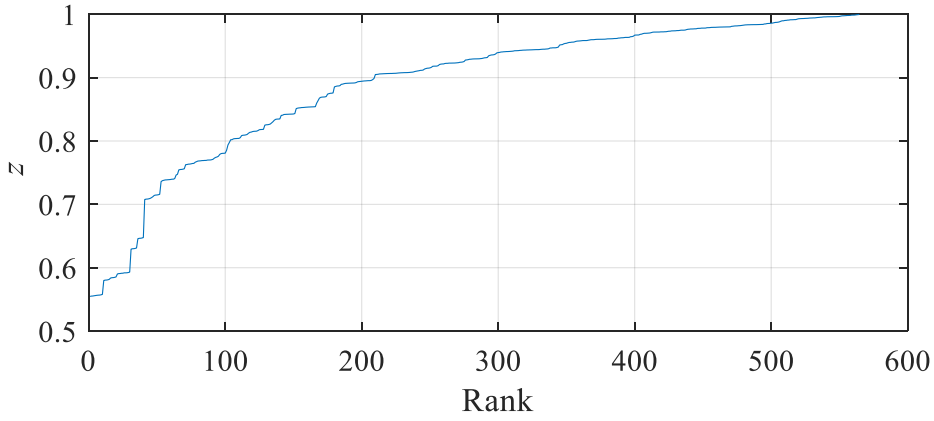

Fig. 7.16 PMU placement ranking in n_{PMU}=5 (zoomed).

ranking of PMU placement in n_{PMU}=5 lined up by ascending order and its zoomed one, respectively. From these figures, only about 1 % of all solutions in this case is below z=1. It indicates that it is perhaps very hard to keep value of z below 1 without considering it in the optimization process.

Table 7.4 lists the placement of RTU used for HSE. Fig. 7.17 shows the Pareto fronts obtained by CCS-MOOPP/U which only focuses on enhancement of HSE for static security assessment and CCS-MOOPP/U-S&D which considers to enhance both static and dynamic security assessment using NSGA-II. In the figure, the major difference between CCS-MOOPP/U and CCS-MOOPP/U-S&D is in lower PMU cost region. In this region, CCS-MOOPP/U is strongly dominating the Pareto front of CCS-MOOPP/U-S&D. This indicates that the CCS-MOOP/U has bigger degree of freedom for PMU placement. Fig. 7.18 shows 3-dimentional Pareto fronts which the DVA evaluation value is added. The flat surface is the upper bound of z: DVA_{lim}=1. In the figure, some Pareto solutions of CCS-MOOPP/U is significantly bigger in z than DVA_{lim}=1 which are dominating the Pareto front of CCS-MOOPP/U-S&D in terms of K_{VC} and TVE_{max}. The Pareto front of CCS-MOOPP/U-S&D in Fig. 7.18 is all settled within DVA_{lim}=1. This is obviously caused by no consideration of DVA indicator evaluation in CCS-MOOPP/U. Even though its minimum number of PMUs is 6 in the obtained Pareto front, it cannot satisfy DVA_{lim}=1 because of ignorance of capturing the dynamic characteristics in

Table 7.4 RTU placement in modified NE 39-bus.

Power injection meter	Power flow meter
1, 3, 4, 5, 6, 7, 8, 9, 10, 11, 12, 13, 14, 16, 18, 19, 22, 23, 25, 26, 29, 30, 32, 33, 34, 35, 36, 37, 38, 39	2-11, 26-29, 4-29, 5-30, 10-12, 12-13, 14-13, 28-13, 14-15, 16-15, 18-15, 18-17, 20-21, 14-24, 23-24, 25-24, 26-25, 26-27, 26-31, 26-34, 39-36, 35-36, 38-36, 39-38

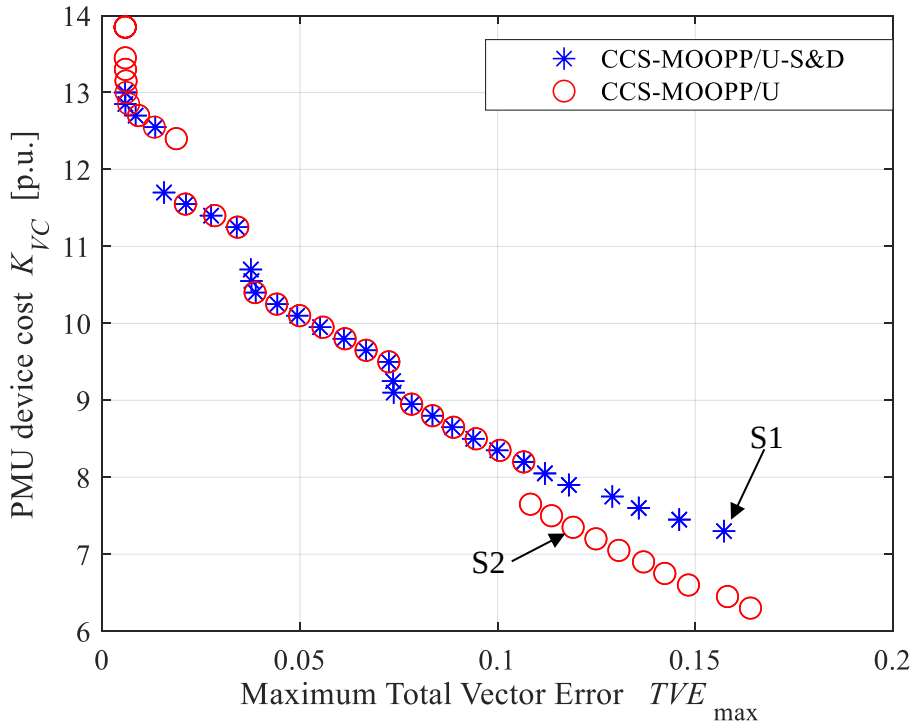

Fig. 7.17 Pareto front obtained by CCS-MOOPP/U and CCS-MOOPP/U-S&D: K_{VC} versus TVE_{max}.

the placement scheme.

In the low PMU cost region in the Pareto front, two solutions are compared in the similar K_{VC}: S1 and S2 highlighted on Fig. 7.17 by arrowed lines. The detailed information is listed in Table 7.5. Figures 7.19 and 7.20 show the histogram of Ω calculated by (7.15) i.e. the DVA index value in each scenario, for S1 and S2, respectively. By taking the average by all scenario for Ω, z can be obtained by (7.14). The distribution of Ω in each figure indicates that a lot of scenarios have huge Ω in S2 whereas Ω is settled in the small value in almost all scenarios in S1. Those high values of Ω in S2 are given by penalty value due to no PMU in fast coherent areas, according to (7.15). Equation (7.15) takes the minimum percentage error of the estimation result of COI-based area frequency by bus frequency information at PMU placed bus. If there is no PMU in an area, penalty value 100 is given to γ

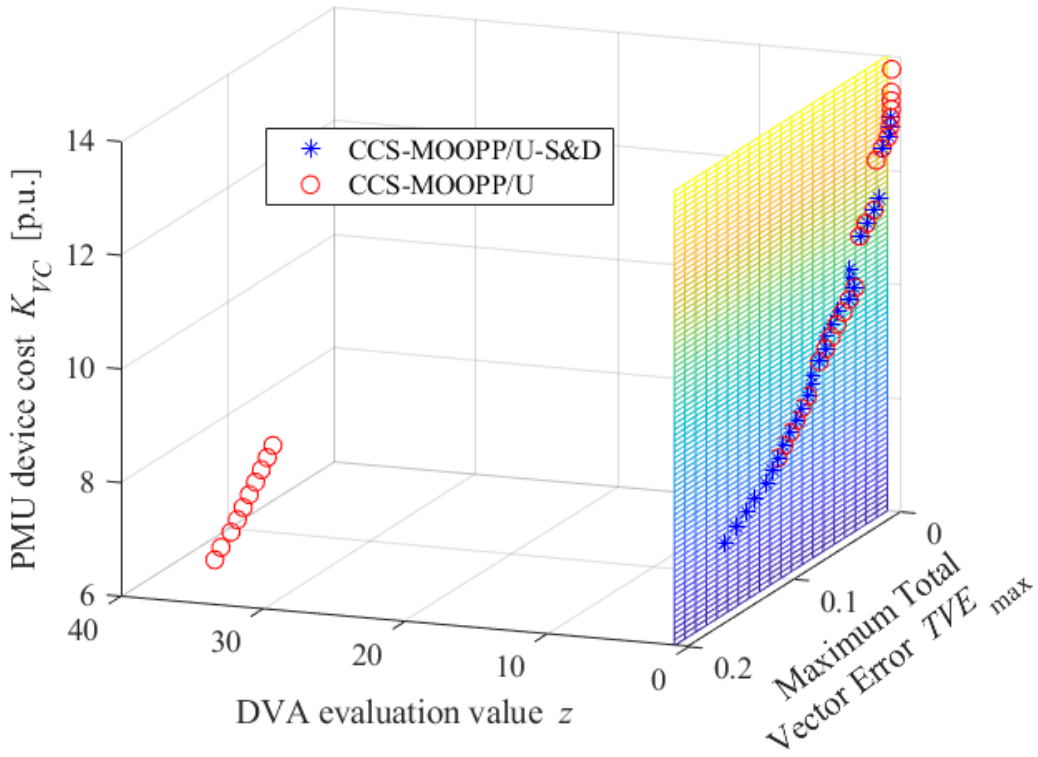

Fig. 7.18 Pareto front obtained by CCS-MOOPP/U and CCS-MOOPP/U-S&D: K_{VC} versus TVE_{max} versus z.

Table 7.5 Solution details.

Solu-tion	PMU placement bus	DVA evaluation value z	PMU placement cost K_{VC} [p.u.]	Maximum Total Vector Error TVE_{max}
S1	2, 3, 5, 8, 9, 31, 33	0.71	7.30	1.57×10^{-2}
S2	7, 8, 20, 30, 31, 39	36.17	7.35	1.19×10^{-2}

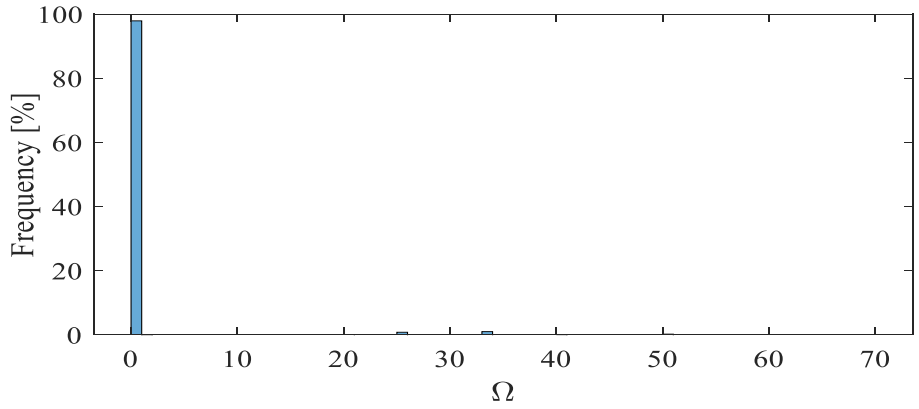

Fig. 7.19 Histogram of Ω in S1.

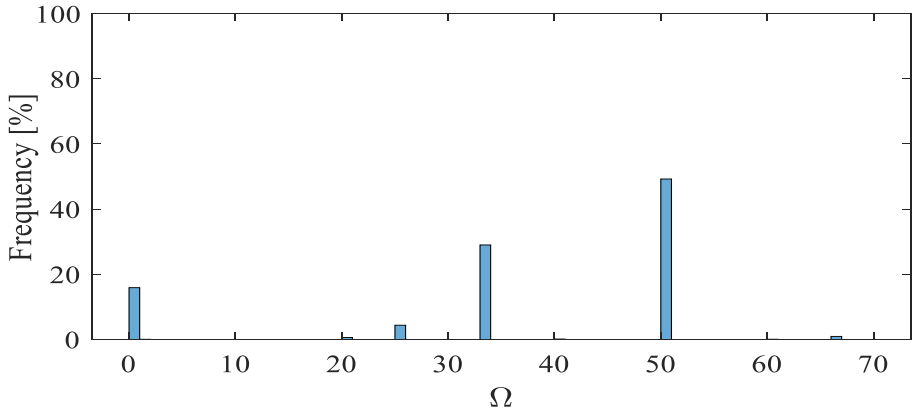

Fig. 7.20 Histogram of Ω in S2.

which makes Ω bigger. In Fig. 7.20, more than 80 % of scenarios are distributed above Ω = 20 which indicates that the PMU placement cannot cover all fast coherent area partition in those scenarios. Thus, *z* becomes bigger affected by huge value of Ω in low PMU cost region in Fig. 7.18 for Pareto solutions of CCS-MOOPP/U. When the number of PMUs is bigger, coverage of fast coherent area by PMUs gets higher. Therefore, concern of DVA in the high PMU cost region may not be significant compared to the low PMU cost region. By the numerical simulation results and discussions, consideration of dynamic security assessment while enhancing the accuracy of static security assessment in OPP problem is indispensable for whole power system security controls.

7.5 SUMMARY

This chapter proposed the novel clustering technique for power system fast coherent area partition and the novel formulation of OPP problem for DVA. Also, this chapter expanded CCS-MOOPP/U to CCS-MOOPP/U-S&D in order to consider both static and dynamic security assessment of power systems. For the fast coherent area partition, HC-max is introduced to improve accuracy of clustering by point-biserial correlation coefficient. As the result of numerical simulation, it is outstandingly accurate compared to SC+FCM and AAP as NHC methods. For the optimal PMU placement, the objective function is formulated to evaluate the estimation accuracy of COI-based area frequency by bus frequency signal obtained by placed PMUs. As the numerical simulation using area partition given by HC-max, optimal PMU placements are obtained via formulation and good estimation is shown by the optimally placed PMUs. To extend the range of security assessment of MOOPP considering minimization of PMU cost and HSE error, CCS-MOOPP/U-S&D considering minimization of PMU cost and HSE error bounded by DVA constraint is proposed. Comparing the obtained Pareto fronts by CCS-MOOPP/U and CCS-MOOPP/U-S&D, there is a significant difference of *z* in low PMU cost region. It is considered that this difference happened because of the natures of dynamic observability and static observability. By considering both of static and dynamic security assessment in PMU placement at the same time, it is possible to enhance the static/dynamic security assessment accuracy and following security control actions, eventually the whole system security level to avoid blackouts.

7.6 REFERENCES

[1] I. Kamwa, J. Béland, D. McNabb, PMU-based vulnerability assessment using wide-area severity indices and tracking modal analysis, *2006 IEEE PES Power Systems Conference and Exposition*, Atlanta, GA, USA, 2006.

[2] J. C. Cepeda and J. L. Rueda, *Introduction: The Role of Wide Area Monitoring Systems in Dynamic Vulnerability Assessment*, In *Dynamic Vulnerability Assessment and Intelligent Control: For Sustainable Power Systems*, J. L. Rueda-Torres and F. Gonzalez-Longatt (eds.), 1st ed., pp. 1-19, Wiley IEEE press, USA, 2018.

[3] J. C. Cepeda, J. L. Rueda, I. Erlich, and D. G. Colomé, Probabilistic approach-based PMU placement for real-time power system vulnerability assessment, *2012 IEEE PES 3rd Innovative Smart Grid Technologies Europe* (ISGT 2012), Berlin, Germany, 2012.

[4] J. C. Cepeda, and D. G. Colomé, Vulnerability assessment of electric power systems through identification and ranking of vulnerable areas, *International Journal of Emerging Electric Power Systems*, vol. 13, no. 1, pp. 1-21, 2012.

[5] J. C. Cepeda, J. L. Rueda, D. G. Colomé, and D. E. Echeverría, Real-time transient stability assessment based on center-of-inertia estimation from phasor measurement unit recodes, *IET Generation, Transmission and Distribution*, vol. 8, no. 8, pp. 1363-1376, 2014.

[6] K. Seethalekshmi, S. N. Singh, and S. C. Srivastava, WAMS assisted frequency and voltage stability based adaptive load shedding scheme, *2009 IEEE PES General Meeting*, Calgary, AB, Canada, 2009.

[7] IEEE Std C37.106: *IEEE Guide for Abnormal Frequency Protection for Power Generating Plants*, *IEEE*, New York, NY, USA, 2004.

[8] H. A. Alsafih and R. Dunn, Determination of coherent clusters in a multi-machine power system based on wide-area signal measurements, *IEEE PES General Meeting*, Providence, RI, USA, 2010.

[9] I. Kamwa, A. K. Pradhan, G. Joos, and S. R. Samantaray, Fuzzy partitioning of a real power system for dynamic vulnerability assessment, *IEEE Transactions on Power Systems*, vol. 24, no. 3, pp. 1356-1365, 2009.

[10] D. Sharma, K. Thulasiraman, D. Wu, and J. N. Jiang, A network science-based k-means++ clustering method for power systems network equivalence, *Computational Social Networks*, vol. 6, no. 4, 2019.

[11] C. Jin, W. Li, L. Liu, ping Li, and Xian Wu, A coherency identification method of active frequency response control based on support vector clustering for bulk power system, *Energies*, vol. 11, no. 16, pp. 3155-, 2019.

[12] J. Wang, *Geometric Structure of High-Dimensional Data and Dimensionality Reduction*, 1st ed., Springer, Berlin, Germany, Chapter 6, pp. 115-129, 2012.

[13] D. J. Sheskin, *Handbook of Parametric and Nonparametric Statistical Procedures*, 3rd ed., pp.990-997, Boca Raton, FL: CRC press, USA, 2004.

[14] S. Chui, Fuzzy model identification based on cluster estimation, *Journal of Intelligent and Fuzzy Systems*, vol. 2, no. 3, pp. 267-278, 1994.

[15] J. C. Bezdek, R. Ehrlich, and W. Full, FCM: The fuzzy c-means clustering algorithm, *Computers and Geosciences*, vol. 10, no. 2-3, pp. 191-203, 1984.

[16] K. Wang, J, Zhang, D. Li, X. Zhang, and T. Guo, Adaptive affinity propagation clustering, *Acta Automata Sinica*, vol. 33, no. 12, pp. 1242-1246, 2007.

8 Conclusions

In this research work, the study on the multi objective optimal PMU placement for enhancing power system security assessment has been conducted. For the purpose of preventing a huge blackout in recent uncertain and complicated power systems using PMU, the author has attempted to bridge a gap between OPP problem and actual static/dynamic security assessment. In order to build the MOOPP problem considering PMU device cost minimization, SE accuracy maximization for static security assessment and enhancement of dynamic security assessment, each chapter has been unfolded. The proposals of this research work are summarized below:

1. Because of the trade-off relationship between PMU cost and SE accuracy, MOOPP considering minimizing PMU cost and SE error is formulated. For SE error evaluation, MCS-based statistical assessment is employed to consider load variability whereas most of the OPP problem has not considered actual SE. For PMU cost reduction, current channel selectability has been proposed to reduce unnecessarily redundant current channel which may affect the total PMU device cost, inspired by hierarchical structure representation. This type of problem is called CCS-MOOPP.

2. In SE, measurement uncertainty propagation which may make SE error bigger occurs in pseudo measurement when a measurement is obtained by using other measurements. Since most of OPP problem has not considered it whereas it has been considered in SE research, CCS-MOOPP/U evaluates SE error considering measurement uncertainty propagation by the classical uncertainty propagation theory has been proposed.

3. As the analysis after PMUs are optimally placed, static voltage stability assessment via CBI using estimated state vector has been investigated in the mixed measurement situation by HSE. This research work confirmed deterioration of CBI in case of use of voltage phasors at both ends of a line which are estimated via different estimator. By discarding PMU value in such case and setting same type of estimator for voltage phasors, the deterioration can be mitigated.

4. Also focusing on the power system dynamic security assessment after the fault for corrective security controls, OPP problem for DVA is proposed. For DVA, the fast coherent area partition is necessary, the novel clustering method called HC-max has been applied for area partition. Based on the divided areas by HC-max, OPP-DVA minimizes the estimation error of COI-based area frequency as the DVA indicator by placed PMU and lets PMUs cover variable areas as many scenarios as possible.

5. As seen in previous chapters, static and dynamic characteristics of power systems are different, thus PMU placement methodology is different. Also, there are trade off relationships between PMU cost and static SE accuracy, between PMU cost and

DVA accuracy. However, the relationship between SE and DVA accuracy is much weaker than others because placing PMU can enhance both of them at least. Additionally, capturing dynamic signature needs less PMUs than static signature. Therefore, to enhance the accuracy of both of static and dynamic security assessment, CCS-MOOPP/U-S&D has been proposed to minimize the PMU device cost by current channel selectability and SE error considering measurement uncertainty propagation via evaluation by MCS, bounded by DVA constraint. Proposed method not only connotes the current channel selectability and measurement uncertainty propagation but also confines DVA evaluation value within a certain range to keep dynamic security assessment accuracy.

By above those novelties, this research can contribute to the power system security assessment:

1. By proposals of PMU current channel selectivity and including measurement uncertainty propagation in PMU: CCS-MOOPP/U, a better Pareto front can be obtained using multi-objective optimization algorithm. The better Pareto front indicates much more effective in the PMU device cost and accurate in SE. Therefore, those proposals in PMU placement are able to contribute to enhance the static security assessment accuracy by its accurate SE while mitigating the power system planning cost.

2. Since mixed measurement based HSE includes RTU and PMU simultaneously, the deterioration of CBI as VSI has been concerned. By this research work's analysis as calculation of CBI using estimated state vector obtained by RTUs and optimally placed PMUs, mixed measurement situation may make the CBI calculation error bigger because of subtraction of estimates of phase angle having different error order. Hence, this research work can contribute to show how SE error influences the following static security assessments, eventually resulting in improving preventive security control actions.

3. By extending the range of OPP target to dynamic region like OPP-DVA and CCS-MOOPP/U-S&D, several contributions have been presented. Firstly, by inventing HC-max and its application to fast coherent area partition, a certain level of clustering accuracy has been ensured. This may avoid the misrecognition of fast coherent areas in power systems. Second, by OPP-DVA, optimal PMU placement can be obtained for estimating COI-based area frequency which is significant DVA indicator. Finally, CCS-MOOPP/U-S&D has optimally placed PMUs considering enhancement of both of static and dynamic security assessment accuracy.

Those proposed methods and the performed analyses in this research work are important for accurate understanding of the system state using PMU. By placing PMUs in accordance with CCS-MOOPP/U-S&D, it is possible to make power systems father from the whole power system blackout by enhanced static/dynamic security assessments and following security controls, in recent uncertain and unpredictable power system condition.

Appendix A: Test Systems Parameters

The detailed parameters of employed test power system models are appended here: IEEE WCSS 9-bus test system, IEEE NE 39-bus test system, modified IEEE NE 39-bus test system and IEEE 57-bus test system. Reference capacity is 100 MVA for all test systems. Nominal frequency is 50 Hz for 9-bus and 57-bus systems, 60 Hz for modified NE 39-bus and NE 39-bus system. Power and voltage set points for bus are same in modified NE 39-bus and NE-39 bus. Line parameters in NE 39-bus is obtained by eliminating lines 3-18, 12-26, 13-25, 26-38, 29-24 and 29-31 from modified NE 39-bus.

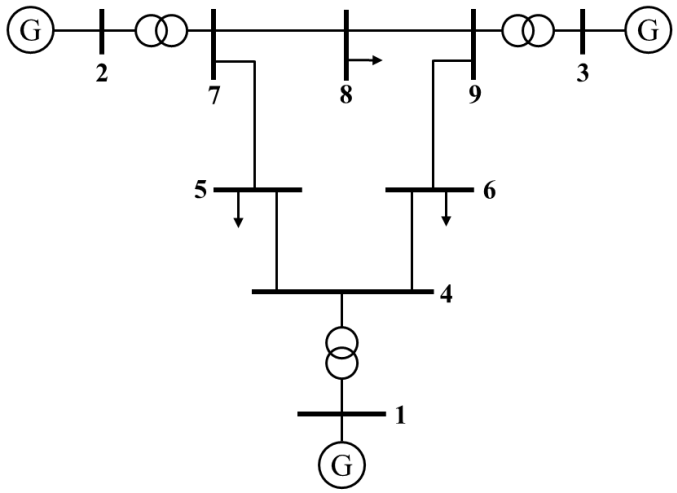

app.Fig. A.1 IEEE WSCC 9-bus test system single line connection diagram.

app.Table A.1 Power and voltage set points in IEEE WSCC 9-bus test system.

Bus No.	Bus type	Voltage magnitude [p.u.]	P generation [p.u.]	P load [p.u.]	Q load [p.u.]
1	Slack	1.04	-	0.0	0.0
2	PV	1.025	1.63	0.0	0.0
3	PV	1.025	0.85	0.0	0.0
4	PQ	-	0.0	0.0	0.0
5	PQ	-	0.0	1.25	0.5
6	PQ	-	0.0	0.9	0.3
7	PQ	-	0.0	0.0	0.0
8	PQ	-	0.0	1.0	0.35
9	PQ	-	0.0	0.0	0.0

app.Table A.2 Line parameters in IEEE WSCC 9-bus test system.

Bus From	Bus to	R [p.u.]	X [p.u.]	B/2 [p.u.]	Tr tap [p.u.]
1	4	0.0000	0.0576	0.0000	1.0000
2	7	0.0000	0.0625	0.0000	1.0000
3	9	0.0000	0.0586	0.0000	1.0000
4	5	0.0100	0.0850	0.0880	1.0000
4	6	0.0170	0.0920	0.0790	1.0000
5	7	0.0320	0.1610	0.1530	1.0000
6	9	0.0390	0.1700	0.1790	1.0000
7	8	0.0085	0.0720	0.0745	1.0000
8	9	0.0119	0.1008	0.1045	1.0000

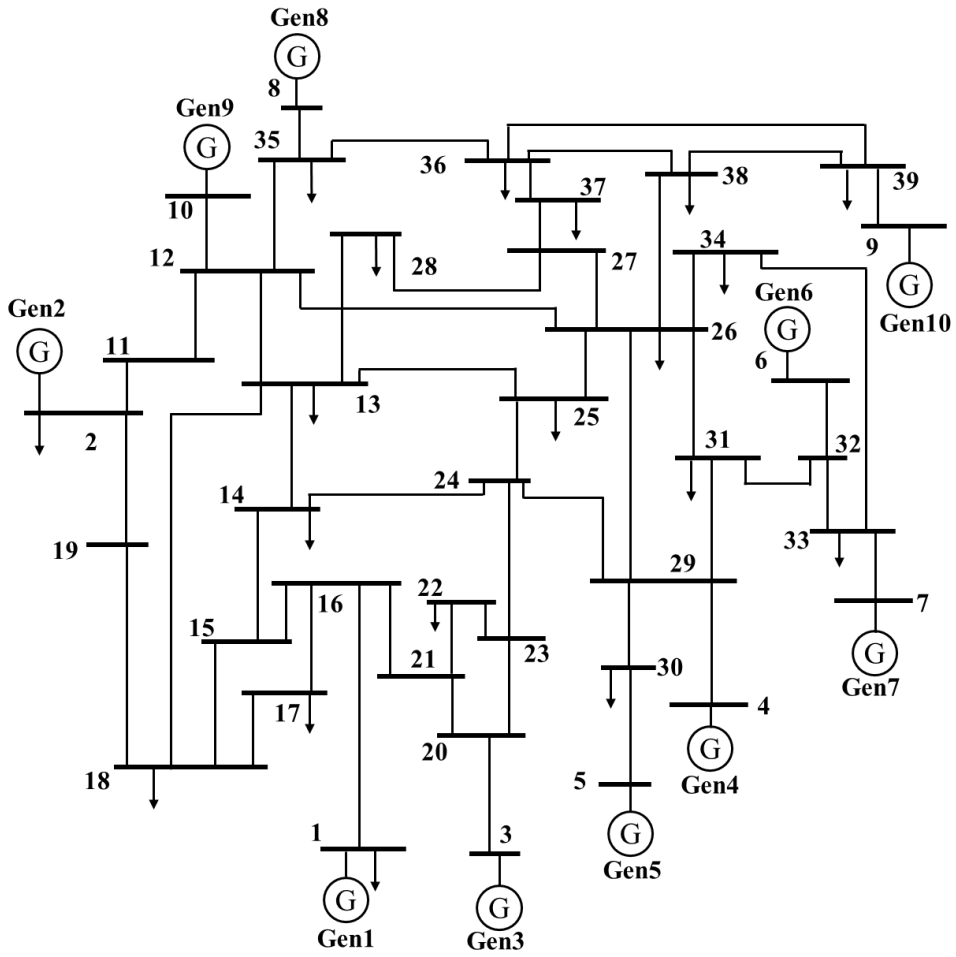

app.Fig. A.2 IEEE modified NE 39-bus test system single line connection diagram.

app.Table A.3 Power and voltage set points in IEEE modified NE 39-bus test system.

Bus No.	Bus type	Voltage magnitude [p.u.]	P generation [p.u.]	P load [p.u.]	Q load [p.u.]
1	Slack	0.982	-	0.092	0.046
2	PV	1.03	10	11.04	2.5
3	PV	0.9831	6.5	0.0	0.0
4	PV	0.9972	6.32	0.0	0.0
5	PV	1.0123	5.08	0.0	0.0
6	PV	1.0493	6.5	0.0	0.0
7	PV	1.0635	5.6	0.0	0.0
8	PV	1.0278	5.4	0.0	0.0
9	PV	1.0265	8.3	0.0	0.0
10	PV	1.0475	2.5	0.0	0.0
11	PQ	-	0.0	0.0	0.0
12	PQ	-	0.0	0.0	0.0
13	PQ	-	0.0	3.22	0.024
14	PQ	-	0.0	5	1.84
15	PQ	-	0.0	0.0	0.0
16	PQ	-	0.0	0.0	0.0
17	PQ	-	0.0	2.338	0.84
18	PQ	-	0.0	5.22	1.76
19	PQ	-	0.0	0.0	0.0
20	PQ	-	0.0	0.0	0.0
21	PQ	-	0.0	0.0	0.0
22	PQ	-	0.0	0.075	0.88
23	PQ	-	0.0	0.0	0.0
24	PQ	-	0.0	0.0	0.0
25	PQ	-	0.0	3.2	1.53
26	PQ	-	0.0	3.294	0.323
27	PQ	-	0.0	0.0	0.0
28	PQ	-	0.0	1.58	0.3

app.Table A.4 Power and voltage set points in IEEE modified NE 39-bus test system (continued).

Bus No.	Bus type	Voltage magnitude [p.u.]	P generation [p.u.]	P load [p.u.]	Q load [p.u.]
29	PQ	-	0.0	0.0	0.0
30	PQ	-	10	6.28	1.03
31	PQ	-	6.5	2.74	1.15
32	PQ	-	6.32	0	0
33	PQ	-	5.08	2.475	0.846
34	PQ	-	6.5	3.086	-0.922
35	PQ	-	5.6	2.24	0.472
36	PQ	-	5.4	1.39	0.17
37	PQ	-	8.3	2.81	0.755
38	PQ	-	2.5	2.06	0.276
39	PQ	-	0.0	2.835	0.269

app.Table A.5 Line parameters in IEEE modified NE 39-bus test system.

Bus From	Bus to	R [p.u.]	X [p.u.]	B/2 [p.u.]	Tr tap [p.u.]
2	11	0.0010	0.025	0.375	1.0000
11	12	0.0035	0.0411	0.34935	1.0000
12	13	0.0013	0.0151	0.1286	1.0000
12	35	0.0070	0.0086	0.073	1.0000
12	26	0.0035	0.0411	0.34935	1.0000
13	14	0.0013	0.0213	0.1107	1.0000
13	18	0.0008	0.0129	0.0691	1.0000
13	25	0.0033	0.0613	0.7902	1.0000
13	28	0.0011	0.0133	0.1069	1.0000
14	15	0.0008	0.0128	0.0671	1.0000
14	24	0.0008	0.0129	0.0691	1.0000
15	16	0.0002	0.0026	0.0217	1.0000
15	18	0.0008	0.0112	0.0738	1.0000
16	17	0.0006	0.0092	0.0565	1.0000

app.Table A.6 Line parameters in IEEE modified NE 39-bus test system (continued, 1st).

Bus From	Bus to	R [p.u.]	X [p.u.]	B/2 [p.u.]	Tr tap [p.u.]
16	21	0.0007	0.0082	6.9450×10^{-2}	1.0000
17	18	0.0004	0.0046	0.0390	1.0000
18	19	0.0023	0.0363	0.1902	1.0000
19	2	0.0010	0.025	0.6000	1.0000
20	21	0.0004	0.0043	3.6450×10^{-2}	1.0000
20	23	0.0004	0.0043	3.6450×10^{-2}	1.0000
23	24	0.0009	0.0101	8.6150×10^{-2}	1.0000
24	25	0.0018	0.0217	0.1830	1.0000
25	26	0.0009	0.0094	0.0855	1.0000
26	27	0.0007	0.0089	0.0671	1.0000
26	29	0.0016	0.0195	0.1520	1.0000
26	31	0.0008	0.0135	0.1274	1.0000
26	34	0.0003	0.0059	0.0340	1.0000
26	38	0.0020	0.0262	0.2279	1.0000
27	28	0.0007	0.0082	6.5950×10^{-2}	1.0000
27	37	0.0013	0.0173	0.1608	1.0000
29	24	0.0013	0.0213	0.1107	1.0000
29	31	0.0006	0.0096	0.0923	1.0000
31	32	0.0008	0.014	0.1283	1.0000
32	33	0.0006	0.0096	0.0923	1.0000
33	34	0.0022	0.035	0.1805	1.0000
35	36	0.0032	0.0323	0.2565	1.0000
36	37	0.0014	0.0147	0.1198	1.0000
36	38	0.0043	0.0474	0.3901	1.0000
36	39	0.0057	0.0625	0.5145	1.0000
38	39	0.0014	0.0151	0.1245	1.0000
22	21	0.0016	0.0435	0	1.0060
22	23	0.0016	0.0435	0	1.0060
16	1	0.0000	0.025	0	1.0700
20	3	0.0000	0.02	0	1.0700

app.Table A.7 Line parameters in IEEE modified NE 39-bus test system (continued, 2nd).

Bus From	Bus to	R [p.u.]	X [p.u.]	B/2 [p.u.]	Tr tap [p.u.]
29	4	0.0007	0.0142	0.0000	1.0700
30	5	0.0009	0.0180	0.0000	1.0090
32	6	0.0000	0.0143	0.0000	1.0250
33	7	0.0005	0.0272	0.0000	1.0000
35	8	0.0006	0.0232	0.0000	1.0250
12	10	0.0000	0.0181	0.0000	1.0250
39	9	0.0008	0.0156	0.0000	1.0250
29	30	0.0007	0.0138	0.0000	1.0600
29	4	0.0007	0.0142	0.0000	1.0700
30	5	0.0009	0.0180	0.0000	1.0090
32	6	0.0000	0.0143	0.0000	1.0250

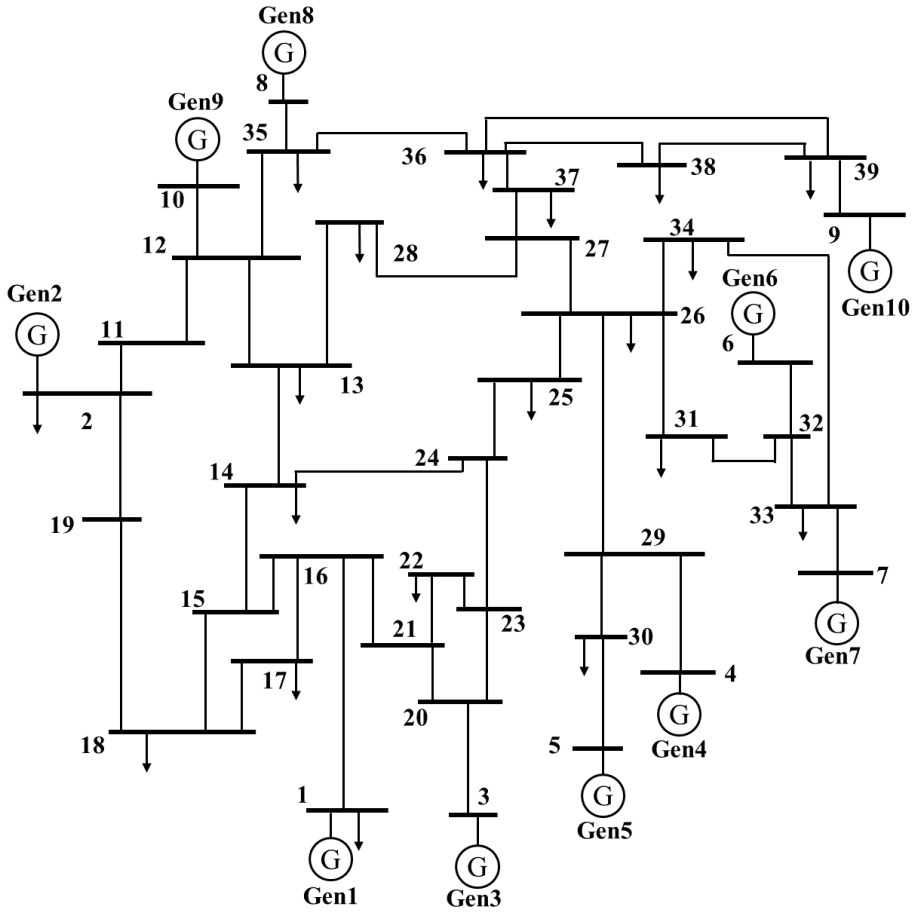

app.Fig. A.3 IEEE NE 39-bus test system single line connection diagram.

app.Table A.8 Dynamic Parameters in NE 39-bus.

Unit No.	Plant category	Apparent power [MVA]	Inertia constant [s]	*xd* [p.u.]	*xd′* [p.u.]	*xd″* [p.u.]	*xl* [p.u.]
1	Nuclear	700	4.329	2.605	0.4879	0.350	0.035
2	Aggrega-ted Gen.	10000	5.000	2.000	0.600	0.400	0.003
3	Nuclear	800	4.475	1.996	0.4248	0.360	0.0304
4	Coal	800	3.375	2.069	0.3488	0.280	0.0295
5	Coal	300	4.333	2.010	0.396	0.267	0.054
6	Nuclear	800	4.350	2.032	0.400	0.320	0.0224
7	Coal	700	3.771	2.065	0.343	0.308	0.0322
8	Nuclear	700	3.471	2.030	0.399	0.315	0.028
9	Nuclear	1000	3.450	2.106	0.570	0.450	0.0298
10	Hydro	1000	4.200	1.000	0.310	0.250	0.0125

app.Table A.9 Dynamic Parameters in NE 39-bus (continued).

Unit No.	*xq* [p.u.]	*xq′* [p.u.]	*xq″* [p.u.]	*Td*0′ [s]	*Td*0″ [s]	*Tq*0′ [s]	*Tq*0″ [s]	*R* [p.u.]
1	1.974	1.190	0.350	6.560	0.050	1.500	0.035	0.000
2	1.900	0.800	0.400	7.000	0.050	0.700	0.035	0.000
3	1.896	0.7008	0.360	5.700	0.050	1.500	0.035	0.000
4	2.064	1.328	0.280	5.690	0.050	1.500	0.035	0.000
5	1.860	0.498	0.267	5.400	0.050	0.440	0.035	0.000
6	1.928	0.6512	0.320	7.300	0.050	0.400	0.035	0.000
7	2.044	1.302	0.308	5.660	0.050	1.500	0.035	0.000
8	1.960	0.6377	0.315	6.700	0.050	0.410	0.035	0.000
9	2.050	0.587	0.450	4.790	0.050	1.960	0.035	0.000
10	0.690	0.500	0.250	10.200	0.050	0.000	0.035	0.000

app.Table A.10 Type of dynamic controllers in NE 39-bus.

Unit No.	GOV	AVR	PSS
1	IEEEG1	IEEET1	$\Delta\omega$-Type
3	IEEEG1	IEEET1	$\Delta\omega$-Type
4	IEEEG1	IEEET1	$\Delta\omega$-Type
5	IEEEG1	IEEET1	$\Delta\omega$-Type
6	IEEEG1	IEEET1	$\Delta\omega$-Type
7	IEEEG1	IEEET1	$\Delta\omega$-Type
8	IEEEG1	IEEET1	$\Delta\omega$-Type
9	IEEEG1	IEEET1	$\Delta\omega$-Type
10	IEEEG3	IEEET1	$\Delta\omega$-Type

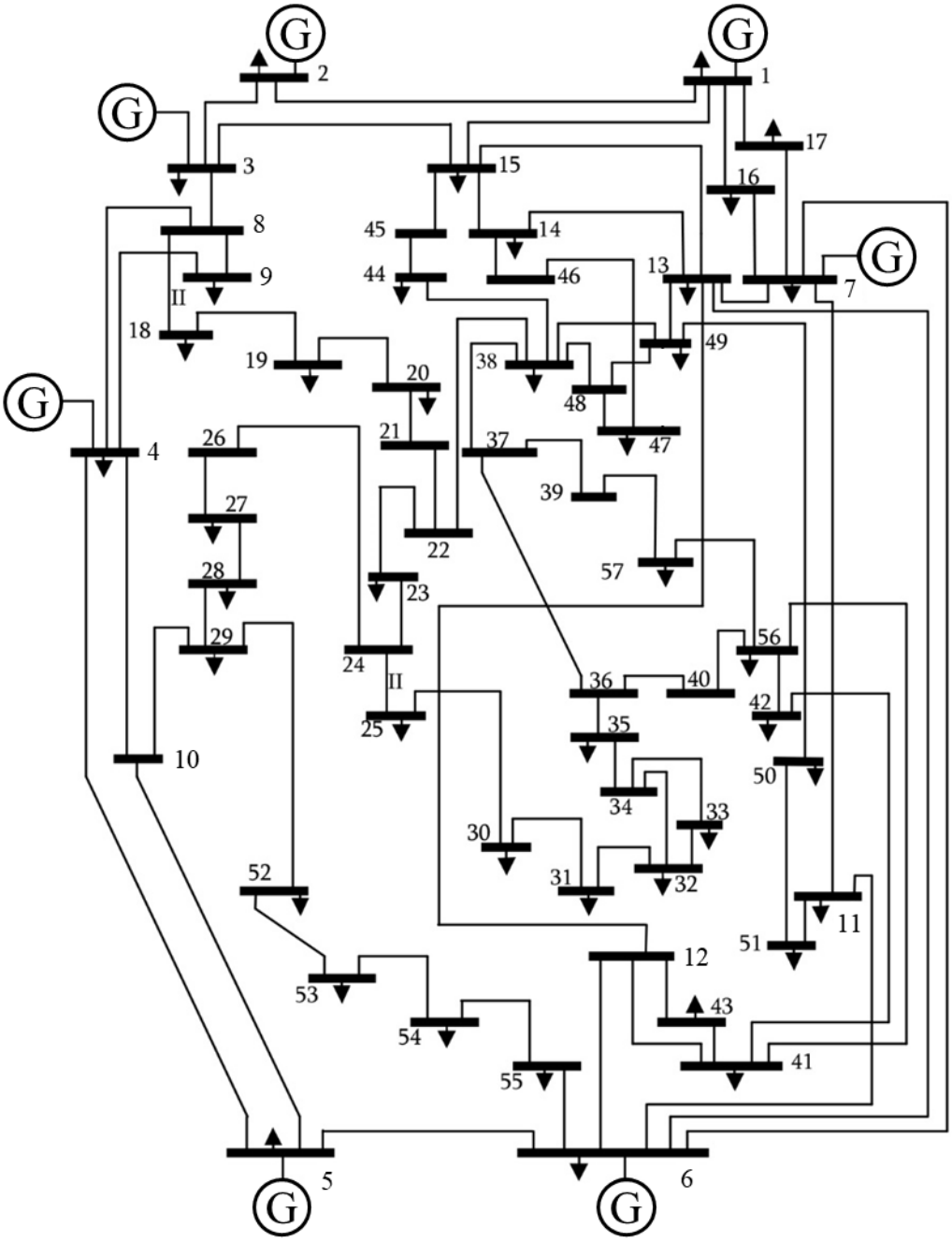

app.Fig. A.4 IEEE 57-bus test system single line connection diagram.

app.Table A.11 Power and voltage set points in IEEE 57-bus test system.

Bus No.	Bus type	Voltage magnitude [p.u.]	P generation [p.u.]	P load [p.u.]	Q load [p.u.]
1	Slack	1.04	-	0.55	0.17
2	PV	1.01	0	0.03	0.88
3	PV	0.985	0.4	0.41	0.21
4	PV	0.98	0	0.75	0.02
5	PV	1.005	4.5	1.5	0.22
6	PV	0.98	0	1.21	0.26
7	PV	1.015	3.1	3.77	0.24
8	PQ	-	0.0	0.0	0.0
9	PQ	-	0.0	0.13	0.04
10	PQ	-	0.0	0.0	0.0
11	PQ	-	0.0	0.05	0.02
12	PQ	-	0.0	0.0	0.0
13	PQ	-	0.0	0.18	0.023
14	PQ	-	0.0	0.105	0.053
15	PQ	-	0.0	0.22	0.05
16	PQ	-	0.0	0.43	0.03
17	PQ	-	0.0	0.42	0.08
18	PQ	-	0.0	0.272	0.098
19	PQ	-	0.0	0.033	0.06
20	PQ	-	0.0	0.023	0.01
21	PQ	-	0.0	0.0	0.0
22	PQ	-	0.0	0.0	0.0
23	PQ	-	0.0	0.063	0.021
24	PQ	-	0.0	0.0	0.0
25	PQ	-	0.0	0.063	0.032
26	PQ	-	0.0	0.0	0.0
27	PQ	-	0.0	0.093	0.005
28	PQ	-	0.0	0.046	0.023
29	PQ	-	0.0	0.17	0.026

app.Table A.12 Power and voltage set points in IEEE 57-bus test system (continued).

Bus No.	Bus type	Voltage magnitude [p.u.]	P generation [p.u.]	P load [p.u.]	Q load [p.u.]
30	PQ	-	0.0	0.063	0.018
31	PQ	-	0.0	0.058	0.029
32	PQ	-	0.0	0.016	0.008
33	PQ	-	0.0	0.038	0.019
34	PQ	-	0.0	0.0	0.0
35	PQ	-	0.0	0.06	0.03
36	PQ	-	0.0	0.0	0.0
37	PQ	-	0.0	0.0	0.0
38	PQ	-	0.0	0.14	0.07
39	PQ	-	0.0	0.0	0.0
40	PQ	-	0.0	0.0	0.0
41	PQ	-	0.0	0.063	0.03
42	PQ	-	0.0	0.071	0.044
43	PQ	-	0.0	0.02	0.01
44	PQ	-	0.0	0.12	0.018
45	PQ	-	0.0	0.0	0.0
46	PQ	-	0.0	0.0	0.0
47	PQ	-	0.0	0.297	0.116
48	PQ	-	0.0	0.0	0.0
49	PQ	-	0.0	0.18	0.085
50	PQ	-	0.0	0.21	0.105
51	PQ	-	0.0	0.18	0.053
52	PQ	-	0.0	0.049	0.022
53	PQ	-	0.0	0.2	0.1
54	PQ	-	0.0	0.041	0.014
55	PQ	-	0.0	0.068	0.034
56	PQ	-	0.0	0.076	0.022
57	PQ	-	0.0	0.067	0.02

app.Table A.13 Line parameters in IEEE 57-bus test system.

Bus From	Bus to	R [p.u.]	X [p.u.]	B/2 [p.u.]	Tr tap [p.u.]
1	2	0.0083	0.0280	0.0645	1.0000
2	3	0.0298	0.0850	0.0409	1.0000
3	8	0.0112	0.0366	0.0190	1.0000
8	9	0.0625	0.1320	0.0129	1.0000
8	4	0.0430	0.1480	0.0174	1.0000
4	10	0.0200	0.1020	0.0138	1.0000
4	5	0.0339	0.1730	0.0235	1.0000
5	6	0.0099	0.0505	0.0274	1.0000
6	11	0.0369	0.1679	0.0220	1.0000
6	12	0.0258	0.0848	0.0109	1.0000
6	7	0.0648	0.2950	0.0386	1.0000
6	13	0.0481	0.1580	0.0203	1.0000
13	14	0.0132	0.0434	0.0055	1.0000
13	15	0.0269	0.0869	0.0115	1.0000
1	15	0.0178	0.0910	0.0494	1.0000
1	16	0.0454	0.2060	0.0273	1.0000
1	17	0.0238	0.1080	0.0143	1.0000
3	15	0.0162	0.0530	0.0272	1.0000
8	18	0.0000	0.2423	0.0000	1.0225
9	4	0.0302	0.0641	0.0062	1.0000
10	5	0.0139	0.0712	0.0097	1.0000
11	7	0.0277	0.1262	0.0164	1.0000
12	13	0.0223	0.0732	0.0094	1.0000
7	13	0.0178	0.0580	0.0302	1.0000
7	16	0.0180	0.0813	0.0108	1.0000
7	17	0.0397	0.1790	0.0238	1.0000
14	15	0.0171	0.0547	0.0074	1.0000
18	19	0.4610	0.6850	0.0000	1.0000
19	20	0.2830	0.4340	0.0000	1.0000
21	20	0.0000	0.7767	0.0000	0.9588

app.Table A.14 Line parameters in IEEE 57-bus test system (continued, 1st).

Bus From	Bus to	R [p.u.]	X [p.u.]	B/2 [p.u.]	Tr tap [p.u.]
21	22	0.0736	0.1170	0.0000	1.0000
22	23	0.0099	0.0152	0.0000	1.0000
23	24	0.1660	0.2560	0.0042	1.0000
24	25	0.0000	0.6028	0.0000	1.0000
24	26	0.0000	0.0473	0.0000	0.9588
26	27	0.1650	0.2540	0.0000	1.0000
27	28	0.0618	0.0954	0.0000	1.0000
28	29	0.0418	0.0587	0.0000	1.0000
10	29	0.0000	0.0648	0.0000	1.0341
25	30	0.1350	0.2020	0.0000	1.0000
30	31	0.3260	0.4970	0.0000	1.0000
31	32	0.5070	0.7550	0.0000	1.0000
32	33	0.0392	0.0360	0.0000	1.0000
34	32	0.0000	0.9530	0.0000	1.0256
34	35	0.0520	0.0780	0.0016	1.0000
35	36	0.0430	0.0537	0.0008	1.0000
36	37	0.0290	0.0366	0.0000	1.0000
37	38	0.0651	0.1009	0.001	1.0000
37	39	0.0239	0.0379	0.0000	1.0000
36	40	0.0300	0.0466	0.0000	1.0000
22	38	0.0192	0.0295	0.0000	1.0000
12	41	0.0000	0.7490	0.0000	1.0471
41	42	0.2070	0.3520	0.0000	1.0000
41	43	0.0000	0.4120	0.0000	1.0000
38	44	0.0289	0.0585	0.0010	1.0000
15	45	0.0000	0.1042	0.0000	1.0471
14	46	0.0000	0.0735	0.0000	1.1111
46	47	0.0230	0.0680	0.0016	1.0000
47	48	0.0182	0.0233	0.0000	1.0000
48	49	0.0834	0.1290	0.0024	1.0000

app.Table A.15 Line parameters in IEEE 57-bus test system (continued, 2nd).

Bus From	Bus to	R [p.u.]	X [p.u.]	B/2 [p.u.]	Tr tap [p.u.]
49	50	0.0801	0.1280	0.0000	1.0000
50	51	0.1386	0.2200	0.0000	1.0000
11	51	0.0000	0.0712	0.0000	1.0753
13	49	0.0000	0.1910	0.0000	1.1173
29	52	0.1442	0.1870	0.0000	1.0000
52	53	0.0762	0.0984	0.0000	1.0000
53	54	0.1878	0.2320	0.0000	1.0000
54	55	0.1732	0.2265	0.0000	1.0000
12	43	0.0000	0.1530	0.0000	1.0438
44	45	0.0624	0.1242	0.0020	1.0000
40	56	0.0000	1.1950	0.0000	1.0438
56	41	0.5530	0.5490	0.0000	1.0000
56	42	0.2125	0.3540	0.0000	1.0000
39	57	0.0000	1.3550	0.0000	1.0204
57	56	0.1740	0.2600	0.0000	1.0000
38	49	0.1150	0.1770	0.0015	1.0000
38	48	0.0312	0.0482	0.0000	1.0000
6	55	0.0000	0.1205	0.0000	1.0638

Appendix B: Hardware, Software and Computation Time

Machine performance of the computer used in this research is shown in app.Table B.1. Also, computing software used in the numerical experiments is listed in app.Table B.2. App.Table B.3 shows computation time in hour taken for each OPP and MOOPP problem.

app.Table B.1 Machine performance.

CPU	Intel Core-i7-8700 3.20 GHz
Main Memory	32.0 GB
OS	Windows 10 Education 64 bit

app.Table B.2 Software information.

Type of software	Purpose
Matlab 2018a/2019a	Implementing optimization algorithm (NSGA-II), state estimation algorithm (SCADA SE, HSE) and clustering algorithm (HC-max, SC+FCM, AAP), processing data and graphical support
DigSILENT PowerFactory 2018	Dynamic simulation and modeling of test power systems

app.Table B.3 Computation time.

Method	Test system	Average computation time [h]
MOOPP	Modified NE 39-bus	3.08
	57-bus	16.29
CCS-MOOPP	Modified NE 39-bus	3.04
	57-bus	13.99
CCS-MOOPP/U	Modified NE 39-bus	16.35
OPP-DVA (n_{PMU} =2)	NE 39-bus	3.69×10^{-2}
OPP-DVA (n_{PMU} =3)	NE 39-bus	0.46
OPP-DVA (n_{PMU} =4)	NE 39-bus	4.64
OPP-DVA (n_{PMU} =5)	NE 39-bus	18.49
CCS-MOOPP/U-S&D	NE 39-bus	37.15

List of Publications by the Author

TECHNICAL JOURNALS AND TRANSACTIONS

I. **Y. Matsukawa**, J. Terashi, M. Watanabe, and Y. Mitani, Power systems inertia evaluation associated with PV installation by frequency analysis of inter-area oscillation based on phasor measurements, *Journal of International Council on Electrical Engineering*, vol. 7, no. 1, pp.153-158, 2017.

II. **Y. Matsukawa**, M. L. Othman, M. Watanabe, and Y. Mitani, Reliably optimal PMU placement using disparity evolution-based genetic algorithm, *Pertanika Journal of Science and Technology*, vol. 25, pp.103-110, 2017.

III. A. A. Kadhem, N. I. A. Wahab, I. Aris, J. Jasni, A. N. Abdalla, **Y. Matsukawa**, Reliability assessment of generating systems with wind power penetration via BPSO, *International Journal on Advanced Science, Engineering and Information Technology*, vol. 7, no. 4, pp.1248-1254, 2017.

IV. **Y. Matsukawa**, M. Watanabe, Y. Mitani, and M. L. Othman, Multi-objective PMU placement optimization considering the placement cost including the current channel allocation and state estimation accuracy, *Electrical Engineering in Japan (English translation of Denki Gakkai Ronbunshi)*, vol. 207, no. 2, pp.20-27, 2019. (Translated from: 松川 義明, 渡邊 政幸, 三谷 康範, Mohammad Lutfi Othman, 電流チャネル配置コストと状態推定精度を考慮した多目的 PMU 配置最適化, 電気学会論文誌 B, 139 巻, 2 号, 頁 84-90, 2019 年)

V. **Y. Matsukawa**, M. Watanabe, N. I. A. Wahab, and M. L. Othman, Voltage stability index calculation by hybrid state estimation based on multi objective optimal phasor measurement unit placement, *Energies*, vol. 12, no. 4, pp.2688-, 2019.

CONFERENCE PROCEEDINGS (REVIEWED)

I. **Y. Matsukawa**, J. Terashi, M. Watanabe, and Y. Mitani, Power systems inertia evaluation associated with PV installation by frequency analysis of inter-area oscillation based on phasor measurements, *The International Conference on Electrical Engineering* 2016 (ICEE 2016), Okinawa, Japan, 2016.

II. **Y. Matsukawa**, M. L. Othman, M. Watanabe, and Y. Mitani, Reliably optimal PMU placement using disparity evolution-based genetic algorithm, *International Conference on Electrical and Electronic Technology 2016* (ICEETech 2016), Oral presentation, Selangor, Malaysia, 2016.

III. **Y. Matsukawa**, M. Watanabe, Y. Mitani, and M. L. Othman, Two-phase optimization of phasor measurement unit placement based on reliability of observability, *International Conference on Electrical Engineering* (ICEE 2017), Oral presentation, Weihai, China, 2017.

IV. **Y. Matsukawa**, M. Watanabe, H. Takahashi, and Y. Mitani, Optimal design of power system stabilizer using remote signal considering the transport delay, *IFAC Symposium on Control of Power and Energy Systems* (IFAC CPES 2018), Oral presentation, Tokyo, Japan, 2018.

V. **Y. Matsukawa**, M. Watanabe, H. Takahashi, and Y. Mitani, Optimal placement and tuning approach for design of power system stabilizers and wide area damping controllers, *IFAC Workshop on Control Applications of Optimization* (IFAC CAO 2018), Oral presentation, Yekaterinburg, Russia, 2018.

VI. **Y. Matsukawa**, M. Watanabe, Y. Mitani, and M. L. Othman, Influence of measurement uncertainty propagation in current-channel-selectable multi objective optimal phasor measurement unit placement problem, *IEEE PES Grand International Conference and Exposition Asia*, (IEEE GTD Asia 2019), Oral presentation, Bangkok, Thailand, 2019.

VII. **Y. Matsukawa**, M. Watanabe, Fast coherent area-based phasor measurement unit placement for power system dynamic vulnerability assessment via hierarchical clustering, *IEEE Innovative Smart Grid Technologies North America*, (IEEE ISGT NA 2020), Poster presentation, Washington DC, USA, 2020.

VIII. T. Kerdphol, **Y. Matsukawa**, M. Watanabe, and Y. Mitani, Monitoring large-scale PV generation infeed on grid frequency using synchrophasor measurement: recent perspective from Kyushu Island, *IEEE PES Transmission and Distribution Conference and Exposition*, (IEEE T&D 2020), Oral presentation, Chicago, IL, USA, 2020. (Accepted, to be presented)

CONFERENCE PROCEEDINGS (UNREVIEWED)

I. **松川 義明**, 渡邊 政幸, 三谷 康範, 同期位相情報に基づく電力系統における同期化力余裕の評価, 平成 27 年電気・情報関係学会九州支部連合大会, 口頭発表, 福岡, 2015 年

II. **Y. Matsukawa**, M. Watanabe, Y. Mitani, Margin level evaluation of the synchronizing power in power systems based on phasor measurements, *3rd International Symposium on Applied Engineering and Sciences* (SAES 2015), Oral presentation, Selangor, Malaysia, 2015.

III. **松川 義明**, 渡邊 政幸, 三谷 康範, 同期位相情報に基づく広域動揺の周波数解析による電力系統の慣性の評価, 平成 28 年電気学会全国大会, 口頭発表, 宮城, 2016 年

IV. **松川 義明**, 渡邊 政幸, 三谷 康範, Mohammad Lutfi Othman, 可観測信頼性に基づく PMU 配置最適化, 平成 28 年電気学会電力技術・電力系統技術合同研究会, 口頭発表, 福井, 2016 年

V. **Y. Matsukawa**, M. Watanabe, Y. Mitani, and M. L. Othman, Reliable and optimal PMU placement in power systems using disparity evolution-type genetic algorithm, *4th International Symposium on Applied Engineering and Sciences* (SAES 2016), Oral presentation, Kitakyushu, Japan, 2016.

VI. **松川 義明**, 渡邊 政幸, 三谷 康範, Mohammad Lutfi Othman, N－1 想定事故を考慮した可観測信頼性に基づく PMU 最適配置, 平成 29 年電気学会全国大会, 口頭発表, 富山, 2017 年

VII. **松川 義明**, 渡邊 政幸, 三谷 康範, Mohammad Lutfi Othman, 二段階最適化手法による N－1 想定事故を考慮した PMU 最適配置とその評価, 平成 29 年電気学会電力・エネルギー部門大会, ポスター発表(論文 II), 東京, 2017 年

VIII. **Y. Matsukawa**, M. Watanabe, Y. Mitani, and M. L. Othman, Two-phase optimal PMU placement considering complete topological observability level for single contingency, *5th International Symposium on Applied Engineering and Sciences* (SAES 2017), Oral presentation, Selangor, Malaysia, 2017.

IX. **松川 義明**, 渡邊 政幸, 三谷 康範, Mohammad Lutfi Othman, 電流チャネル配置コストと状態推定精度を考慮した多目的 PMU 配置最適化, 平成 30 年電気学会電力・エネルギー部門大会, 口頭発表兼ポスター発表(論文 I), 徳島, 2018 年

X. 中村 好秀, **松川 義明**, 渡邊 政幸, 三谷 康範, 動揺周期に着目した二段階最適化による系統安定化装置設計, 平成 31 年電気学会全国大会, 口頭発表, 北海道, 2019 年

XI. 中村 好秀, **松川 義明**, 渡邊 政幸, 三谷 康範, 時間解析評価を導入した二段階最適化による系統安定化装置設計, 平成 31 年電気学会電力技術・電力系統技術合同研究会, 口頭発表, 沖縄, 2019 年

XII. **Y. Matsukawa**, M. Watanabe, Optimal phasor measurement unit placement for power system dynamic vulnerability assessment based on fast coherent area, 2019 年電気・情報関係学会九州支部連合大会, 口頭発表, 福岡, 2019 年

XIII. 中村 好秀, **松川 義明**, 渡邊 政幸, 三谷 康範, 固有値および時間解析に基づく二段階最適化による系統安定化装置設計, 2019 年電気・情報関係学会九州支部連合大会, 口頭発表, 福岡, 2019 年

Biography of the Author

Yoshiaki Matsukawa was born on May 5, 1992 in Yamaguchi prefecture. After high school, he enrolled to Hiroshima Institute of Technology (HIT) in 2011. During the undergraduate, he learned electrical engineering and graduated with top score of GPA in department of electrical system engineering. He studied on power system outage planning problem using immune genetic algorithm supervised by Prof. Dr. Koji Kawahara, as the bachelor thesis. After graduating bachelor degree in HIT, He attended a master degree at electrical and electronic engineering at Kyushu Institute of Technology (Kyutech) in 2015. Under supervised by Assoc. Prof. Dr. Masayuki Watanabe and Prof. Dr. Yasunori Mitani in Kyutech and collaborated with Assoc. Prof. Ir. Dr. Mohammad Lutfi Othman in Universiti Putra Malaysia (UPM), he studied on synchrophasor technology with PMU for power system stability analysis, oscillation control, state estimation and vulnerability assessment. He graduated the master degree, and entered to the doctoral course of electrical and electronic engineering at Kyutech. During that time, he was hired to work as a research assistant at Watanabe laboratory until the doctoral graduation. In his research on PMU, he received several awards: the encouraging prize in IEEJ Power and Energy Society (PES) conference on power and energy systems in 2016, Young Poster Competition (YPC) the best poster award in IEEJ PES annual conference in 2017 and young author award in IFAC CAO in 2018. He was also awarded the power academy research grant for PhD students from 2018 to 2019. His research area includes power system state estimation, stability analysis, oscillation control, continuous/discrete optimization and unsupervised machine learning in power systems. He is the members of the IEEJ and IEEE.